AN ABSTRACT OF THE THESIS OF

Todd C. Feeley for the degree of __Master of Science__ in Geology presented on __June 2, 1989.__

Title:__The Egan Range Volcanic Complex: Implications for the Evolution of a Mid-Tertiary Synextensional Volcanic System.__

Abstract approved:_____

Dr. Anita L. Grunder

The Egan Range volcanic complex (ERVC), located approximately 30 km northwest of Ely, Nevada, lies astride a boundary separating a zone of high crustal extension (approximately 300% extension) to the east, including the Snake Range metamorphic core complex, and a relatively unextended domain (approximately 15% extension) to the west, including the Butte Mountains. The volcanic and minor sedimentary rocks of the ERVC have been divided into three stratigraphic groups: the early, middle, and late groups. Two new ^{40}Ar-^{39}Ar age determinations indicate that the volcanic rocks were erupted approximately 35 Ma ago and were coeval with other mid-Tertiary volcanic rocks in east-central Nevada.

Volcanic rocks of the early group range from basaltic andesite (54% SiO_2) to rhyodacite (70% SiO_2), although the bulk of the lavas are two-pyroxene andesites and dacites. Apparent compositional gaps are present at 56 to 58% SiO_2 and 66 to 68% SiO2, although these may be an artifact of

incomplete sampling. Textural evidence, including plagioclase with sieved cores mantled by normally and reversely zoned rims, olivine coexisting with quartz surrounded by augite coronas, and quenched inclusions of basaltic andesite, suggest that these magmas represent incomplete mixtures of mafic and silicic magmas.

Volcanic rocks of the middle group are exposed in a northwest trending belt of outcrops in the north-eastern to central-western region of the study area. In contrast to the large compositional diversity of the early group, rocks of the middle group are relatively homogeneous biotite, hornblende, pyroxene dacites. With respect to bulk composition, rocks of the middle group range from 65.7 to 68.5 wt.% SiO_2 and fall in the upper gap in SiO_2 content defined by the early group.

During the late cycle of magmatism a bimodal suite of fine-grained andesite and petrographically and compositionally homogeneous biotite rhyodacites was erupted.

The total volume of volcanic rocks in the ERVC is approximately 40 km^3. Dacites and rhyodacites comprise greater then 95% of the volume of erupted products. Volumes of mafic lavas (basaltic andesites and andesites) are greatest in the early group, absent in the middle group, and minor in the late group. The volume of silicic rocks dramatically increases upsection.

Two generations of high-angle normal faulting are observed in the ERVC; an older set of N30-60°E, N30-40°W, and roughly east-west trending faults, and a younger set of approximately north-south trending faults. At the present level of exposure, faults of the older set appear to have small displacements, although some may have vertical offsets as great as 600 m. Apparent vertical separation on faults of the younger set are as great as

500 m. An angular unconformity developed between unit of the middle group and N40°E alignment of middle group vent loci suggest that the older set was most active during eruption of the early and middle groups. The age of initiation of movement on the younger faults is not known, although they probably postdate the volcanic rocks.

Early and middle group andesites and dacites have elevated Cr (280-10 ppm), Sc (26-7 ppm), and Rb (60-180 ppm) concentrations and define linear trends indicating mixing between contaminated mantle-derived magmas and crustal melts. Isotope data are consistent with intermediate lavas containing a large crustal component. Chemical models require fractionation of minor amounts of cpx (< 3.5%) and accessory phases (<1%) prior to or during mixing. Cross- over patterns on REE plots (La/Lu$_n$ = 9.9$_{mafic}$ to 26.7$_{silicic}$) preclude significant fractional crystallization or assimilation-fractional crystallization to produce the compositional spectrum. Low Ni concentrations (<25 ppm) and Mg# (<45) in basaltic andesites indicate fractionation of olivine prior to mixing.

Major- and trace-element variations within the late group may be explained by up to 90% crystal fractionation of the observed phenocryst assemblage. Slightly depleted HREE concentrations and constant LREE and Zr concentrations in dacites relative to andesites suggest that amphibole fractionated in proportions greater than in the mode. Crystal fractionation cannot, however, account for elevated Rb, Th, and U in the dacites and thus, moderate amounts of assimilation are required.

The sequence of magma types in the ERVC are explained by a model where mantle-derived magmas are repeatedly injected into the crust. The early group records the initial injections of basaltic magma, production of

silicic crustal melts, and wholescale mixing of these magmas. The middle group records further heating and melting of the crust and, thus, an increase in the volume of silicic magma in the system. The volume of silicic magma in the system during the middle group was large enough to prevent wholescale mixing of basalt and silicic crustal melt, although newly generated crustal melts mixed with resident intermediate hybrid magmas. The switch to crystal fractionation in the late group indicates a decrease in the rate of supply of new basaltic magma to the system. As a result, thermal gradients and, therefore, convective velocities began to decline and crystallization and fractionation followed.

The Egan Range Volcanic
Complex: Implications
For the Evolution of a Mid-Tertiary
Synextensional Volcanic System

by

Todd C. Feeley

A THESIS

submitted to

Oregon State University

in partial fulfillment of
the requirements for the
degree of

Master of Science

Completed June 2, 1989

Commencement June 1990

APPROVED:

Redacted for Privacy

Assistant Professor of Geology in charge of major

Redacted for Privacy

Head of Department of Geology

Redacted for Privacy

Dean of Graduate School

Date thesis is presented___June 2, 1989

Acknowledgements

I feel fortunate to have been associated with so many helpful and inspiring people during the last three years. Their encouragement and support not only enabled me to complete this thesis, but also begin my study of Geology. I owe the bulk of my thanks to Anita Grunder. Her guidance on matters both scientific and personal were invaluable. I thank my committee members John Dilles and Roman Schmitt. Their thorough reviews significantly improved the thesis and my ability to think critically. Roger Nielsen offered helpful advice on petrologic modeling.

Although I thank everyone in the Geology Department, I want to particularly acknowledge Jeff Marso for stimulating petrologic discussions, computer help, and friendship. I thank all the members of the Journal Club, including Reed Lewis, Gary Davidson, Britt Hill, and George Moore for provocative Friday afternoon discussions. Zhang Ning, cofounder of the Expanding Earth Society, deserves special credit for his rational, collected thinking in the face of adversary. Office mates Phyllis Camilleri and Bill Gallahan displayed admirable patience during often difficult times. I am indebted to Therese Belden for her generosity and help in administrative matters.

I am particularly grateful to Phil Gans for very helpful discussions on volcanic stratigraphy and structure during a visit to the field, and for age determinations. Thanks go to Bob Walker for analytical support and enlightening discussions on Tertiary magmatism. Mike Conrady supplied his expertise on matters pertaining to reduction of the INAA data. The unsung hero award goes to the Albuquerque Dukes for providing many exciting moments during two, often lonely field seasons.

TABLE OF CONTENTS

LIST OF FIGURES

LIST OF TABLES

LIST OF PLATES

THE EGAN RANGE VOLCANIC COMPLEX: IMPLICATIONS FOR THE EVOLUTION OF A MID-TERTIARY SYNEXTENSIONAL VOLCANIC SYSTEM

CHAPTER ONE: INTRODUCTION

The mid-Tertiary magmatism of east-central Nevada is recorded in thousands of km^3 of basaltic andesite to high-silica rhyolite lavas and ash-flow tuffs whose eruption was synchronous with large scale (approximately 250%) west-northwest extension 38 to 34 Ma (Gans and Miller, 1983). The association of these rocks with crustal attenuation is unusual because the composition and style of volcanism resembles neither the "bimodal" alkali basalt-rhyolite suite characteristic of Basin and Range faulting during the late Tertiary (e.g., Christiansen and Lipman, 1972; Stewart and Carlson, 1978), nor the alkalic silica-undersaturated volcanism associated with extension in the African rift systems. Overall, the high-K, calcalkaline character of the mid-Tertiary volcanic rocks is identical to the composition of volcanic rocks generated in a continental arc environment. Petrographic and geochemical work by Gans et al. (1989) indicates that volcanism associated with the early stages of extension (38 to 36 Ma) was heterogeneous and crudely bimodal, consisting of silicic andesite to high-silica rhyolite; rhyodacites and rhyolites are rare. As extension

continued the composition of the contemporaneous volcanism
(35 to 34 Ma) became more homogeneous and consisted mainly
of rhyodacites to rhyolites (Gans et al., 1989).

This work investigates a suite of mid-Tertiary
synextensional volcanic rocks in the Egan Range volcanic
complex of White Pine County, Nevada. This suite is
particularly important because mid-Tertiary volcanic rocks
of the northern Egan Range coincided with the onset of
faulting in the region (Gans, 1982). Geologic mapping
(1:24,000; plate 1) complemented by two ^{40}Ar-^{39}Ar age
determinations have established a time framework for this
geochemical and petrologic study. Samples collected
during field study were analyzed for petrographic,
geochemical, and isotopic data in order to evaluate the
following points:

1. Possible sources of the volcanic rocks,
   and the role of contamination and/or magma
   mixing.

2. The extent and type of mineral fractionation
   involved in different units.

3. The petrologic evolution of the volcanic rocks
   as extension proceeded.

4. The volume of new mantle magma added to the
   crustal column during extension.

This study is part of a regional petrologic study on the mid-Tertiary magmatism of east-central Nevada by A.L. Grunder, and a supplement to studies by Gans, Miller, and Mahood on the interplay between magmatism and crustal extension in east-central Nevada during the mid-Tertiary (Gans and Miller, 1983; Gans et al. 1989; Gans and Mahood, 1989).

Location and Physiography

The Egan Range volcanic complex is located on the
western flank of the northern Egan Range approximately 30
km northwest of Ely (Figure 1). Access to the western,
northern, and eastern boundaries of the area is excellent
via the Thirty mile and Bothwick graded dirt roads (Plate
1). U.S. Highway 50 marks the southern boundary of the
study area (Plate 1). Elevation ranges between 2000 m
above sea level in the Butte Valley, to more then 2700 m
on the highest ridge. The geology is moderately exposed
on lower slopes due to sparse forests of juniper, pinion
pine, and mountain mahogany. Bedrock is locally covered
by landslide deposits and talus.

Mid-Tertiary volcanic rocks

Mesozoic and Cenozoic intrusive rocks

Paleozoic sedimentary rocks
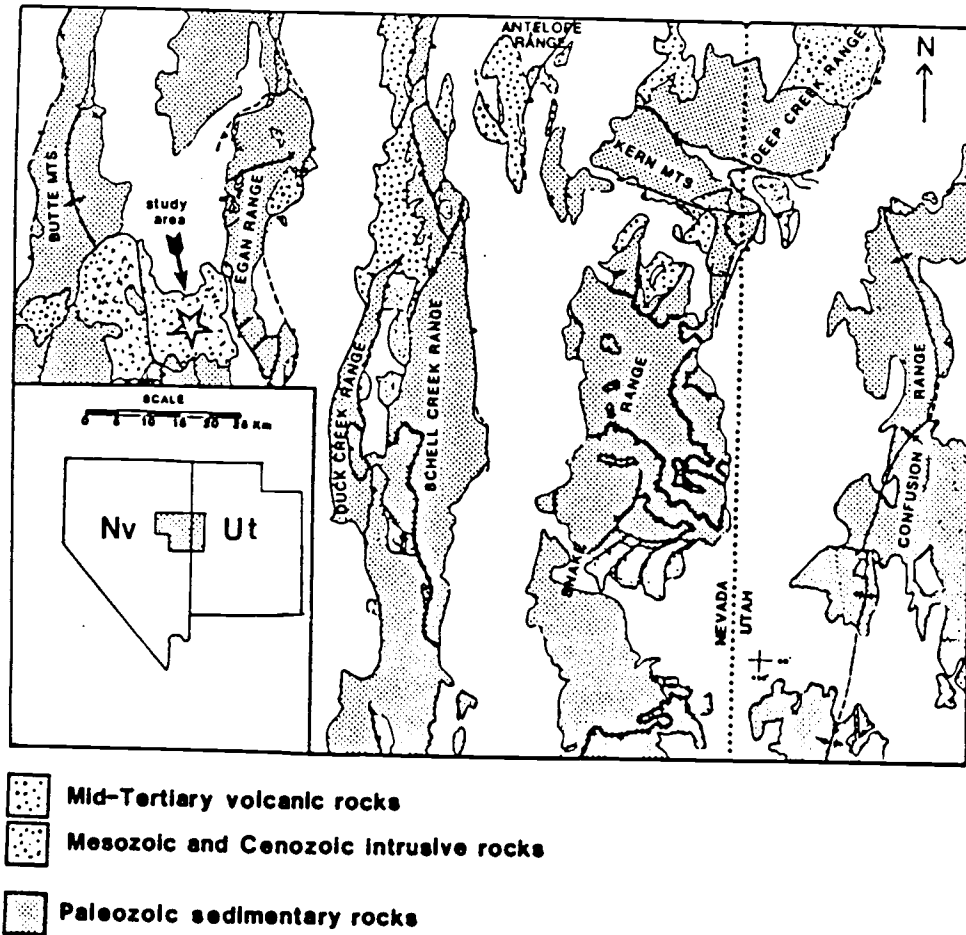
Figure 1.   Regional location and geologic setting of the Egan Range
            volcanic complex. Star indicates Egan Range volcanic
            complex. (After Gans et al., 1989).

Previous Work and Geologic Setting

The mid-Tertiary volcanic rocks of east-central
Nevada are part of a broad, roughly east-west trending
belt of volcanic rocks that extends from Nevada to central
Utah (Figure 2). Previous studies concerning the Tertiary
in central Nevada through central Utah have mainly focused
on the structural and tectonic evolution of the region
(e.g., Misch, 1960; Fritz, 1960; Armstrong, 1972; Coney,
1974; Gans and Miller, 1983; Gans et al., 1985; Gans,
1987). Notable exceptions include Gans (1982) and Gans et
al. (1989). The first analytical dating of volcanic rocks
in east-central Nevada (Armstrong, 1970) indicated that
the principal eruptions occurred approximately 35 Ma ago.
Subsequent dating by McKee et al. (1976) and Gans et al.
(1989) indicate a wider interval of volcanism from
approximately 39 to 34 Ma ago.

Early regional overviews of volcanism in White Pine
County by Blake et al. (1969) and Hose and Blake (1976)
indicated that the southern parts of White Pine County are
dominated by aerially extensive ash-flow sheets, whereas
the northern and northwestern parts of the county are
dominated by locally derived lavas and tuffs. On the
basis of composition and eruptive style, the volcanic
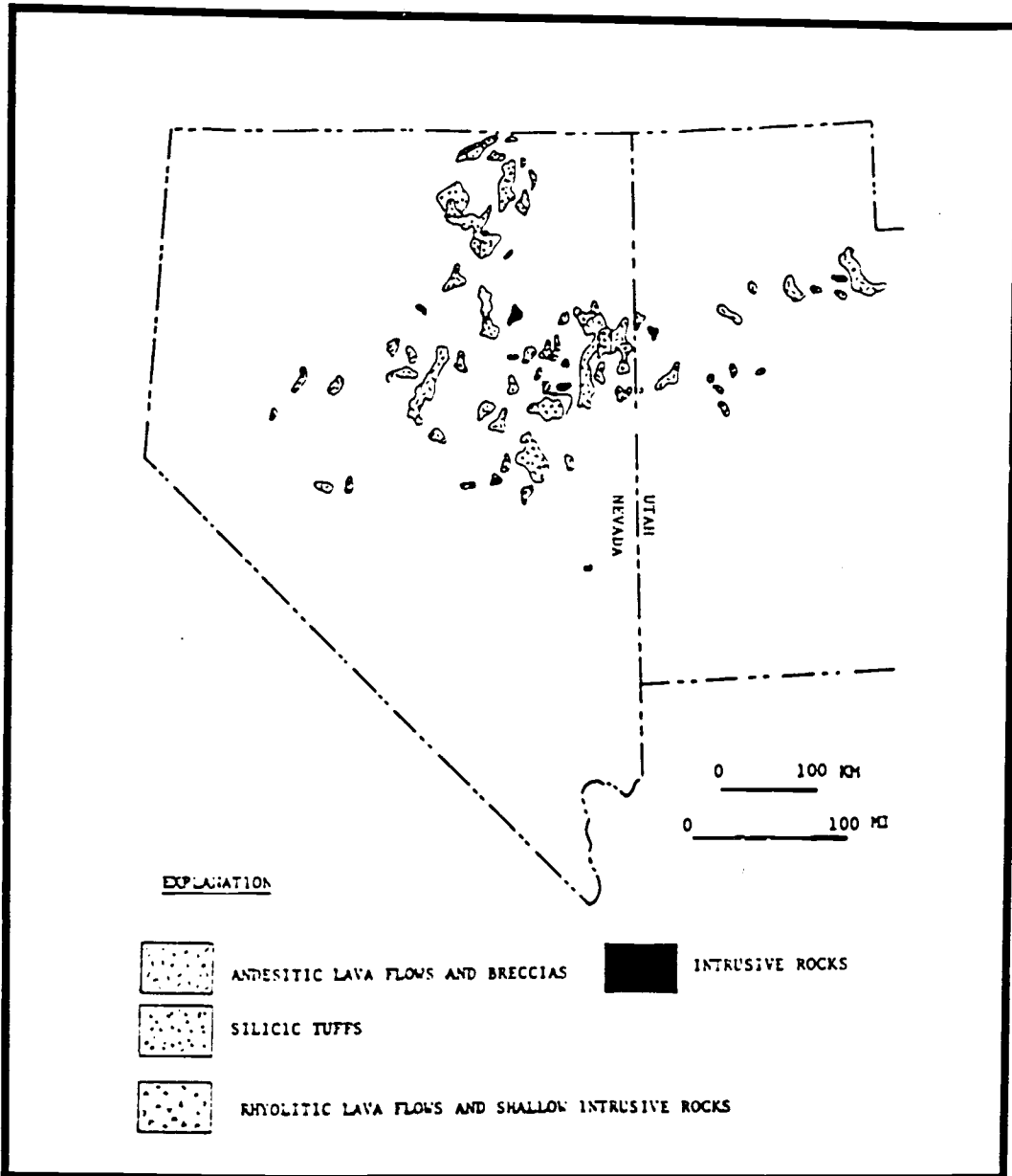
Figure 2. Map of Nevada and western Utah showing generalized
distribution of 43 to 34 Ma old igneous rocks.
(After Stewart and Poole, 1974).

rocks were divided into two main groups: (1) the early
volcanic rocks (39-35 Ma) including two pyroxene, high-
silica andesite to dacite and biotite high-silica rhyolite
erupted from scattered vents, and (2) the Kalamazoo tuff
and younger volcanic rocks (35-34 Ma) including
hornblende-biotite dacite to low-silica rhyolite erupted
as large volume, regionally extensive units (Grunder et
al., 1987; Gans et al., 1989). This study includes rocks
from both the early and late groups.

On the basis of regional isotopic studies of plutonic
rocks, Farmer and DePaolo (1983) and Lee and Christiansen
(1983) presented a model for magmatism in eastern Nevada
requiring no contribution of the Tertiary mantle; magmas
are a product of lower to mid-crustal melting. In
contrast, Schermer and Gans (1985) and Gans et al. (1989)
have argued, on the basis of regional isotopic and trace
element studies, that magmas represent mixing between an
enriched mantle component and up to 65% of upper
continental crust. This volume estimate is in agreement
with the observation by Gans (1987) that the present
crustal thickness in the eastern Great Basin is remarkably
uniform even across highly extended and little extended
domains (Figure 3). This lack of relief on the Moho
requires lateral flow of lower crustal material from less
extended domains into highly extended domains, and
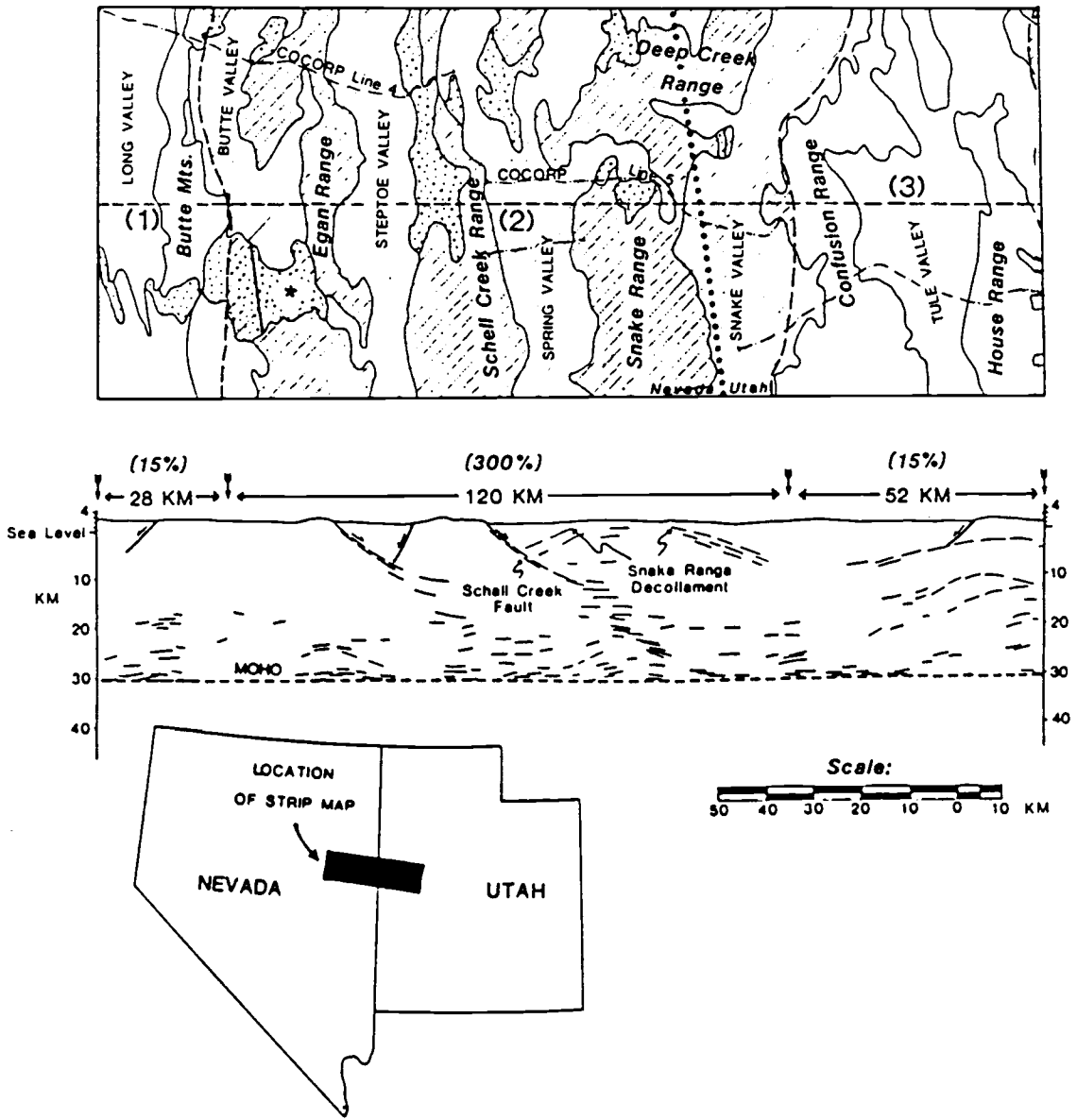
Figure 3. Geologic strip map and generalized cross section from east-central Nevada and west-central Utah. Lined area gives highly extended domain. Study area indicated by stippled area marked by an asterisk (*). (After Gans, 1987)

significant additions of mantle-derived magmas to areas of greatest supracrustal strain to balance extreme thinning of the upper crust in these regions (Gans, 1987). These magmas possibly interacted extensively with subsequent crustal melts.

The Tertiary volcanic and sedimentary section of east-central Nevada unconformably overlies a regionally extensive section of Precambrian to Triassic miogeoclinal sandstones, shales, and carbonates with an aggregate thickness in excess of 13 km (Stewart and Poole, 1974; Hose and Blake, 1976). The observation that Mississippian or younger strata usually underlie the Tertiary section indicates that the unconformity had little relief at the onset of Tertiary extension (Armstrong, 1972; Gans and Miller, 1983).

The Egan Range is part of a highly extended domain (approximately 300% extension) including the Duck Creek, Schell Creek, Antelope, Snake, and Deep Creek Ranges (Figure 3; Gans and Miller, 1983; Gans et al., 1985). Adjacent to this highly extended domain are relatively unextended domains (approximately 15% extension), including the Butte Mountains and the Confusion Range, where most of the extension occurs on major range-front faults. Deformation within the highly extended domain is associated with extension in the N. Snake Range

metamorphic core complex and is similar to other .
Cordilleran metamorphic core complexes (e.g., Crittendon
et al., 1980 and references therein) in that extension in
the unmetamorphosed or weakly metamorphosed upper crust is
manifested in brittle normal faults and is separated from
a strongly ductile, metamorphosed and penetratively
deformed mid- to lower crust by a decollement (Gans and
Miller, 1983; Bartley and Wernicke, 1984). The nature of
the surface of detachment and the mechanism by which
extension proceeded in the N. Snake Range is a
controversial topic (c.f. Gans and Miller, 1985; Bartley
and Wernicke, 1985). While not a direct concern of this
study, estimates of heatflow relevant to models of
extension and kinematic interpretations of the N. Snake
Range decollement will be critically constrained by
thorough petrologic studies.

CHAPTER TWO: STRATIGRAPHY AND LITHOLOGIC CHARACTER OF MAP

UNITS

North-south trending high-angle normal faults have cut all of the volcanic units in the Egan Range thereby exposing a record of three phases of mid-Tertiary volcanism. Rocks exposed in the footwalls of these faults include a variety of basaltic andesite to rhyolite lavas, domes, volcanic breccias, ash-flow tuffs, and volcaniclastic sedimentary rocks. In this study basaltic andesites range from 52-57 wt.% SiO_2; andesites from 57% to 63%; dacites from 63% to 68%; rhyodacites from 68% to 72%; and rhyolites above 72% (see Figure 4). A chemical classification scheme is necessary because petrographic and field evidence indicate that mafic magmas came into direct physical contact with more silicic compositions within the magmatic system. Thus, many intermediate composition magmas exhibit extreme mineralogic disequilibrium rendering modal classification schemes unsuitable. However, modal characteristics, such as conspicuous large quartz phenocrysts, proved useful for mapping purposes.

The volcanic stratigrahpy, field descriptions, and generalized petrologic character of mapped units are
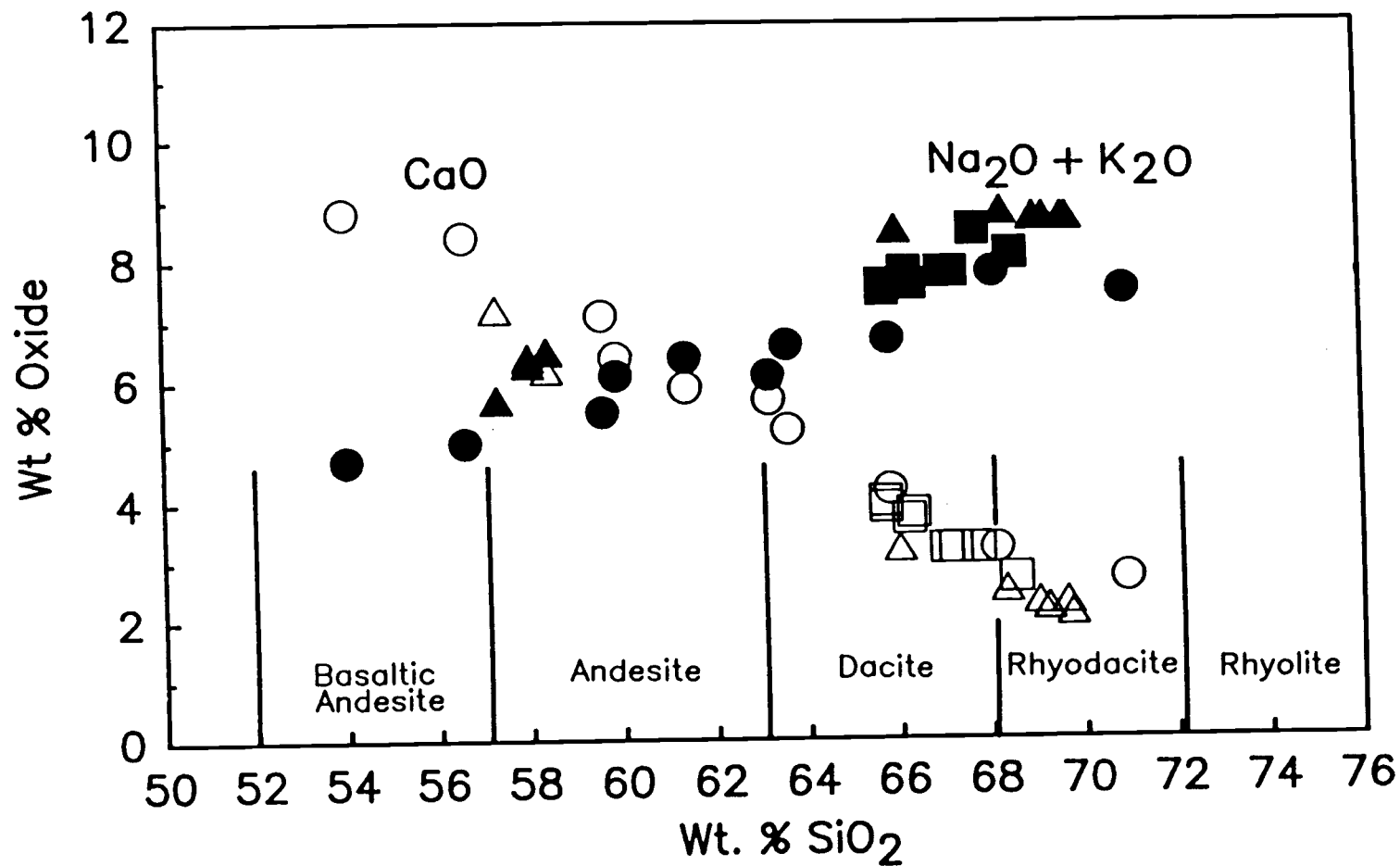
Figure 4. Alkali-lime variation diagram for the Egan Range
volcanic complex suite. Early group, middle group, and
late group shown as circles, squares, and triangles,
respectively. Classification scheme used here is
represented at the bottom of the figure. Data are
normalized to 100% anhydrous.

Table 1a: Major-element compositions of early group volcanic rocks

Sample #	Mt8749	Mt879	Mt8787	Mt8789	Mt8760	Mt8763	Mt8711	Mt872	Mt8786	Mt876	Mt8735
Type:	MI	MI	DL	DL	DL	DL	DL	DL	VL	DL	P
Strat. Unit	Tvl1	Tvl1	Tves	Tves	Tvl1	Tvl1	Tvl1	Tvl1	Tvl1	Tvl1	Tvesa
XRF Analysis											
SiO_2	54.0	56.6	59.6	59.9	61.4	63.2	63.6	65.8	68.1	70.9	70.1
Al_2O_3	15.3	15.4	15.0	16.0	15.8	15.1	15.7	15.3	15.5	14.4	16.0
FeO^*	9.0	7.6	6.5	6.3	6.1	5.4	5.6	5.0	3.6	3.2	2.6
MgO	6.4	5.4	4.9	3.9	3.2	3.3	2.1	2.0	1.0	0.7	1.7
CaO	8.8	8.4	7.1	6.4	5.9	5.7	5.2	4.2	3.2	2.7	3.3
Na_2O	2.0	2.1	2.3	2.5	2.7	2.6	2.8	2.8	3.0	3.0	2.4
K_2O	2.7	2.9	3.2	3.6	3.7	3.5	3.8	3.9	4.8	4.5	3.3
TiO_2	1.20	1.10	0.88	0.93	0.85	0.79	0.83	0.76	0.56	0.48	0.42
P_2O_5	0.42	0.31	0.28	0.30	0.36	0.25	0.26	0.22	0.19	0.16	0.09
MnO	0.15	0.13	0.12	0.11	0.10	0.09	0.10	0.08	0.06	0.06	0.10
Age (Ma):											35.6 +/- 0.1

Data normalized to 100% anhydrous.

Rock types: MI = magmatic inclusion, DL = devitrified lava, VL = vitrophyric lava, P = pumice.

40Ar-39Ar age determination; error is one sigma.

FeO* as ferrous iron.

Table 1b: Major-element compositions of middle group volcanic rocks

Sample#	Mt871a	Mt8712	Mt8717	Mt8734	Mt8720	Mt8737	Mt8743	Mt8778
Type:	VC	VL	VL	VL	DL	DL	DL	DL
Strat. Unit	Tvm1	Tvm1	Tvm1	Tvm1	Tvm2	Tvm3	Tvm3	Tvm3
XRF Analysis								
SiO2	65.7	66.3	65.7	66.2	68.5	67.0	67.2	67.7
Al2O3	16.1	15.9	16.1	16.0	15.5	15.9	15.8	15.7
FeO*	4.3	4.2	4.4	4.1	3.5	4.0	3.9	4.0
MgO	1.4	1.3	1.3	1.2	0.8	1.2	1.2	0.9
CaO	4.0	3.8	3.9	3.7	2.7	3.2	3.2	3.2
Na2O	2.9	3.1	3.2	3.1	3.3	3.2	3.2	3.4
K2O	4.7	4.5	4.3	4.7	4.8	4.6	4.6	5.1
TiO2	0.65	0.65	0.69	0.65	0.54	0.63	0.62	0.61
P2O5	0.21	0.21	0.23	0.23	0.20	0.20	0.21	0.21
MnO	0.07	0.07	0.07	0.07	0.06	0.05	0.06	0.04

Data normalized to 100% anhydrous.

Rock types: VC = vitrophyric clast, VL = vitrophyric lava, DL = devitrified lava

FeO* as ferrous iron.

Table 1c: Major-element compositions of late group volcanic rocks

Sample#	Mt8781	Tf872	Mt8764	Mt8759	Mt8765	Mt8775	Mt8791b	Mt8791c	Mt8791d
Type:	L	L	L	D	VL	DL	DL	DL	DL
Strat. Unit	Tvl1	Tvl2	Tvl2	Tvl2	Tvl3	Tvl3	Tvl3	Tvl3	Tvl3
XRF Analyses									
SiO2	66.0	58.4	58.0	57.3	69.6	68.3	69.7	69.2	69.0
Al2O3	16.5	17.1	17.0	16.5	15.5	15.8	15.5	15.5	15.6
FeO*	4.1	7.6	7.6	7.8	2.8	3.3	2.8	3.2	3.2
MgO	0.9	2.6	3.0	3.8	0.5	0.5	0.5	0.4	0.5
CaO	3.2	6.2	6.4	7.2	2.3	2.5	2.1	2.2	2.3
Na2O	3.4	2.9	2.9	2.6	3.1	3.5	3.3	3.4	3.4
K2O	5.1	3.6	3.4	3.1	5.6	5.3	5.4	5.4	5.3
TiO2	0.70	1.18	1.17	1.18	0.45	0.51	0.46	0.48	0.49
P2O5	0.21	0.45	0.43	0.38	0.11	0.15	0.12	0.15	0.14
MnO	0.04	0.11	0.12	0.11	0.06	0.07	0.03	0.06	0.07

Data normalized to 100% anhydrous.

Rock types: L = glassy lava, D = dike, VL = vitrophyric lava, OL = devitrified lava

FeO* as ferrous iron.

presented in ascending stratigraphic order. Sample locations are on Plate 1 and formal petrographic descriptions of all analyzed samples are in Appendix 1. Major-element compositions are in Table 1. Detailed major- and trace-element compositions are discussed in Chapter 4.

The volcanic section is divided into three age and compositional groups: the early, middle, and late groups. Table 2, a schematic stratigraphic column for the Egan Range volcanic complex, summarizes the lithology, modal characteristics, and compositions of the three groups. The division between the early and middle groups is chosen to lie below the map unit that is similar in age and lithologic character to the Kalamazoo tuff and associated lavas. The voluminous (>350 km^3) Kalamazoo tuff forms the regional division between the early and middle suites in east-central Nevada (Grunder, 1989).

Table 2. Modal analyses of Egan Range Volcanic Complex lavas (vol. percent)

Rock Type	Unit	Sample	Ol	Plag	Cpx	Opx	Amph	Bio	Qtz	San	Ox	Gmass+Mph	n
Late Group													
Drd	Tvl3	MI8791d	-	10.5	0.5	tr	-	4.7	tr	-	0.3	84.0	1019
Vrd	Tvl3	MI876S	-	9.0	0.3	0.1	-	3.8	-	-	0.2	76.6	1170
Aa	Tvl2	MI8764	tr	0.4	0.1	0.1	-	-	-	-	tr	99.4	1202
Dd	Tvl1	MI8814	-	4.7	0.9	0.3	0.3	1.3	-	-	0.9	91.6	1221
Middle Group													
Dd	Tvm3	MI8743	-	15.2	0.2	2.1	0.8	0.9	tr	-	0.5	80.3	1172
Drd	Tvm2	MI8720	-	11.8	0.5	2.5	3.2	4.7	0.2	tr	tr	77.1	1218
Vd	Tvm1	MI8715	-	15.9	tr	1.5	1.8	2.8	tr	-	1.0	77.1	1118
Vd	Tvm1	MI8717	-	24.8	1.2	3.4	2.9	2.9	tr	-	1.2	63.6	1018
Vd	Tvm1	MI8712	-	19.6	0.7	2.3	4.3	6.4	tr	-	1.0	65.7	1212
Early Group													
Vrd	Tve1	MI8786	-	17.7	-	tr	4.9	5.6	2.7	1.4	tr	67.7	1028
MIba	Tve1	MI8819a	-	40.9	2.0	11.1	-	-	-	-	4.4	41.6[1]	812
Dd	Tve1	MI8819b	-	18.4	3.1	3.6	3.2	2.4	tr	-	0.8	68.5	745
MIba	Tve1	MI879	-	35.1	38.9[2]		6.1	1.5	2.1	-	-	16.3[1]	1114
Da	Tve1	MI8763	-	7.9	3.4	4.3	1.9	0.3	4.1	-	0.7	77.4	1110
Da	Tves	MI8787	1.4	5.8	12.0	6.1	tr	-	0.6	-	3.0	71.1	1263
Vr	Tves	MI8816a	-	22.0	-	-	-	2.8	1.3	2.8	-	71.1	1218
AFd	Tvesa	MI8735	-	7.6	tr	tr	tr	2.2	9.5	3.1	0.3	77.3	880

1. Including approximately 15% vesicles
2. Cpx + Opx combined (Opx > Cpx)

Abbreviations for rock types are as follows:
D = devitrified lava
V = vitrophyric lava
A = aphyric lava
MI = magmatic inclusion
AF = ash flow tuff

r = rhyolite
rd = rhyodacite
d = dacite
a = andesite
ba = basaltic andesite

n = number of points counted
tr = trace amount

Early Group

Rocks of the early group are exposed as a series of west- and east-dipping sections of lacustrine limestones, tuffaceous sediments, volcaniclastic sediments (Tves), a dacitic ash flow tuff (Tvesa), and crystal-rich lavas (Tve_1).

Lower Clastic and Pyroclastic Unit (Tves)

This unit is the oldest unit in the Egan Range volcanic complex. Where the base is exposed it overlies the Permian Arcturus Formation (Hose and Blake, 1976) which marks the top of the Paleozoic miogeoclinal sequence in east-central Nevada. This relationship is similar to other areas in east-central Nevada where the mid-Tertiary unconformity is exposed; the mid-Tertiary volcanic section consistently overlies Mississippian or younger basement rocks (Gans and Miller, 1983). Tves is composed of discontinuous, isolated outcrops of lacustrine limestones, tuffaceous sediments, calcareous pebble conglomerates, a dacitic ash-flow tuff, and a volcaniclastic debris flow. The discontinuous nature of Tves outcrops precludes precise correlation of individual exposures. Thus, outcrop localities will be described individually and all rock types are considered stratigraphic equivalents.

Near Jones Canyon in the south central region of the study area (Plate 1), Tves occurs as a 19-23 m thick section of extensively channelized, reworked tuffaceous sediments with impressive sweeping crossbeds. These appear to be interbedded with thin (0.5 m thick) beds of white tuffaceous, poorly laminated limestone containing ooliths and detrital grains of biotite and quartz. Near the base of this exposure, lenses of brown to grey, recrystallized lacustrine limestone, 5-7 m thick, containing occasional grains of biotite and smokey quartz are interstratified with the tuffaceous sediments. Near Gleason Creek (Plate 1), a thick accumulation of the tuffaceous sediments is present without limestone intervals. The abrupt thickening of the sediments here suggests that this area may have been a local topographic low at the time of deposition.

Overlying the tuffaceous sediments and lacustrine limestones are at least two ash-flow tuffs. A distinctive and apparently widespread tuff, informally referred to as the "Uhalde tuff", has been mapped separately (map unit Tvesa) because it is a good stratigraphic marker. Outcrops of the early tuffs are discontinuous because their poorly welded nature causes them to be easily eroded or buried by colluvium. Each early tuff, excluding the

Uhalde tuff, is exposed at only one locality, suggesting that they are small and locally derived.

Near Jones Canyon (Plate 1), an approximately 3 m-thick ash-flow tuff is in uncertain stratigraphic relationship with the Uhalde tuff. This tuff is a fine-grained, lapilli ash-flow tuff containing approximately 12% phenocrysts of plagioclase, biotite, sanidine, and quartz. Pumice lapilli account for approximately 10% of the rock.

The Uhalde tuff (sample Mt8735) is a poorly welded to non-welded, salmon to white, lapilli ash-flow tuff. Pumice separated from the Uhalde tuff is biotite rhyodacite (Table 1). It is the most distinctive and widespread ash-flow tuff in the Egan Range volcanic complex. It averages between 9 and 10 m in thickness and is exposed in a discontinuous belt of outcrops that trends crudely west-northwest (Plate 1). The phenocryst assemblage is quartz > plagioclase > sanidine > biotite > opaques, plus trace amounts of amphibole, clinopyroxene, orthopyroxene, and accessory allanite, sphene, and zircon (Table 2). Quartz grains are characteristically smokey and euhedral, often with bipyramidal terminations. Whole rock phenocryst content is approximately 23% (Table 2) although the phenocryst content of the pumice is half this amount. The matrix contains 1% sandstone and carbonate

lithic clasts typically as large as 1 cm across, and in some exposures northwest of the study area (Thirty mile Ranch area), the matrix contains black, rounded inclusions that average about 1.5-2.0 cm in diameter and appear to be composed of carbonaceous organic matter. Pumice lapilli are slightly elongate suggesting some welding. In thin section, however, glass shards appear undeformed indicating that the pumice lapilli were stretched prior to emplacement of the tuff. Vapor phase alteration is variable giving the rock a punky, friable texture.

New $^{40}Ar-^{39}Ar$ age determinations and the petrographic character suggest that the Uhalde tuff may be correlative with the Charcoal Ovens Tuff in the southern Egan Range (Table 1). The Uhalde tuff yielded a preliminary $^{40}Ar-^{39}Ar$-sanidine age of 35.6 ± 0.5 (two sigma) in fair agreement with a new weighted average $^{40}Ar-^{39}Ar$-sanidine age of 35.33 ± 0.06 Ma (Deino and Best, pers. comm. 1988) obtained from the Charcoal Ovens Tuff. Macroscopically, the Charcoal Ovens Tuff is a moderately welded ash flow tuff lacking pumice and containing 35% phenocrysts of large, euhedral smokey quartz, sanidine, plagioclase, biotite, and rare sphene. The age determinations, the distinctive smokey nature of the quartz phenocrysts, the presence of rare sphene, and the occurrence of biotite as the dominant mafic phase together suggest that the tuffs

may be correlative. However, the absence of pumice in the
Charcoal Ovens Tuff at its type locality is problematic
and requires a very efficient mechanism to separate pumice
and matrix. If the tuffs are correlative the Uhalde tuff
represents a more distal facies. The Charcoal Ovens Tuff
attains a thickness of approximately 130 m at its type
locality near Ward Charcoal Ovens State Park on the east
side of the Egan Range (Hose and Blake, 1976). However,
the presence of accidental lithic clasts within the Uhalde
tuff argues against it being a distal facies because
lithic fragments are typically concentrated in the
proximal regions of an ash-flow tuff (Sheridan, 1981). In
any case, two very similar ash-flow tuffs were erupted
close in time, although their sources are as yet unknown.

South of Piscevich Summit (Plate 1) the base of Tves
is defined by a poorly exposed outcrop of well-lithified
calcareous pebble conglomerate in fault contact with
younger lavas. Calcareous sandstone clasts within this
unit are angular to subrounded, average about 2 cm in
diameter, and are set in a pink, fine-grained sandy
limestone matrix. These clasts resemble lithologies in
the Permian Arcturus Formation (Hose and Blake, 1976). A
distinctive brick-red soil is developed on top of this
rock type. Similar Tertiary pebble conglomerates have
been noted overlying the Arcturus Formation in the Egan

Range (Woodward, 1962). Young (1960) describes
discontinuous intervals of limestone conglomerate
containing Pennsylvanian (?) and Permian clasts overlain
by lacustrine limestones and tuffaceous sediments
collectively known as the Kinsey Canyon Formation in the
northern Schell Creek Range. Taken together then, Tves
can be correlated with the Kinsey Canyon Formation.
Furthermore, Young (1960) correlated the Kinsey Canyon
Formation with the late Paleocene to Eocene Sheep Pass
Formation in the southern Egan Range. Kleinhampl and
Ziony (1985) note, however, that the Sheep Pass Formation
contains no volcanic detritus in its type section in Sheep
Pass Canyon apparently reflecting the small volume and
local character of the early volcanism in east-central
Nevada (Grunder et al., 1987; Gans et al., in press).

The dominant lithology of Tves is a faintly
stratified volcanic debris flow (terminology of Smith,
1986) which overlies the limestone pebble conglomerate
south of Piscevich Summit (Plate 1). This unit ranges
from 0 to 15 m thick and contains clasts ranging from
approximately 0.5 cm to boulders rarely as much as 1.5 m
across. Clasts make up approximately 30% of the unit on
the average but range from 10% to 45%. The unit is poorly
exposed but does not appear to size graded or sorted.

Clasts are supported by a fine-grained, muddy sandstone matrix.

Volcanic clasts within this deposit record the earliest magmatic activity in the Egan Range volcanic complex. They include clasts of andesite and rhyolite and their vesiculated equivalents. Additionally, pebbles and blocks of fine-grained, slightly calcareous sandstone, possibly derived from the Arcturus Formation, are present and occur throughout the unit. Whole-rock, major oxide compositions of two dense andesite clasts (Mt8787, Mt8789) are in Table 1.

Black, quartz- and olivine-bearing two-pyroxene andesite is the most common volcanic clast type and is present through out the unit. These andesites are seriate, glomeroporphyritic with approximately 30% phenocrysts of clinopyroxene > orthopyroxene $\geq$ plagioclase > opaques > olivine; plus trace xenocrystic quartz and amphibole and accessory zircon (Table 2). Clinopyroxene dominates the mode (12%) occurring as single grains or in clusters that may contain Fe-Ti oxides. These clusters are often quite large and may be of cumulate origin. Plagioclase phenocrysts have a bimodal compositional distribution which is mirrored by grain morphologies. A distinct population of grains has sieved, calcic (An80) cores that are slightly zoned. Another variety has fresh

sodic cores (An35) surrounded by cloudy resorbed rims. These textures are common in rocks that are presumed to have a hybrid origin (Ussler and Glazner, 1989). Rare olivine phenocrysts are subhedral to anhedral and are commonly completely altered to fibrous, yellow-green bowlingite. These grains may be relics of early crystallizing phenocrysts as suggested by their resorbed outlines and absence as a groundmass phase. No compositional data are available for olivine, although lack of pleochroism in fresh phenocryst cores indicates that they are a MgO rich variety. Rounded, embayed quartz xenocrysts are typically armored by radiating augite coronas (Figure 5). The rounded, resorbed nature of the quartz grains and the clinopyroxene coronas are consistent with a xenocrystic origin for the quartz.

Quartz in basalts and basaltic andesites bearing magnesian olivine has been interpreted to result from assimilation of crustal material or mixing with silicic magmas (Sato, 1975; Eichelberger and Gooley, 1977; Feeley and Mullen, 1986). This interpretation is consistent with the xenocrystic nature of the quartz described above. The quartz is not the result of high-pressure fractionation product of a silica-rich magma (Nicholls et al., 1971) because Helz (1976) and Bender et al. (1978) have
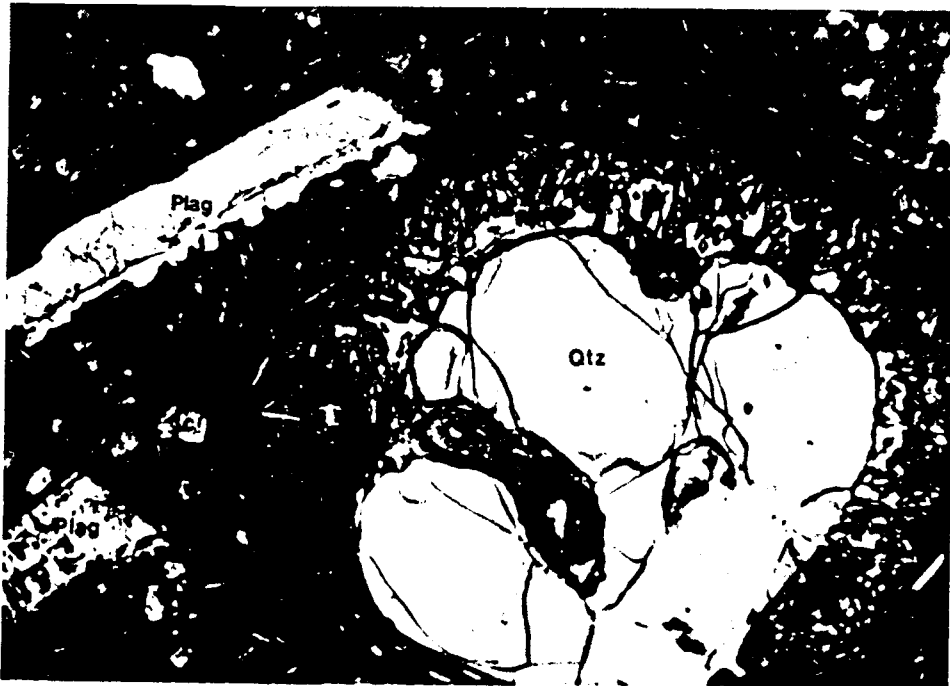
Figure 5. Augite corona surrounding quartz xenocryst
(Qtz) in olivine-bearing andesite sample
Mt8787. Note the resorbed edge of the
plagioclase phenocryst (plag) to the
northwest of the quartz. Gl = silicate
glass. Width of field = 3.0 mm. Plane
light.

demonstrated that quartz is not an equilibrium-near-liquidus phase in basalts at high pressure.

The origin of augite coronas on quartz has been investigated by Sato (1975) and Ussler and Glazner (1987). These investigations indicate that the growth of the augite is a diffusion controlled process involving the diffusion of alkalis against concentration gradients because no reaction relationship exists between a silica polymorph and mafic liquid in published phase equilibria in the system forsterite-diopside-silica (Sato, 1975; Ussler and Glazner, 1987).

Silicic clasts are present in lower exposures of Tves and are represented by dense hypohyaline rhyolite blocks with 29% phenocrysts of plagioclase > sanidine = biotite > quartz plus accessory allanite, zircon, and apatite (Table 2).

Euhedral sodic plagioclase (An35) as large as 4 mm across dominates the assemblage. Most crystals are unzoned, although some grains may show weak oscillatory zoning. Euhedral quartz, sanidine, and biotite are present in roughly equal proportions. Quartz is of the smokey variety and may indicate high concentrations of radioactive U, Th, and K in the host rock.[1]

---

[1]. Nassau and Prescott (1975) performed irradiation and heating experiments on natural and synthetic quartz. The results of their studies indicate that the smokey

One of the silicic clasts was found to contain a rounded granitic xenolith containing plagioclase and alkali feldspar and quartz in graphic intergrowth. This xenolith may indicate a crustal source for the rhyolite, although except perhaps for rounding, it does not appear to have melted.

The debris flow probably represents mass flow of water-saturated, volcanic debris during or immediately after an eruption (Smith, 1986). Debris flows may extend 100 km or more from their sources in high-volume volcanic regions (Crandell, 1971; Janda et al., 1981). However, the small size and local occurrence of the Tves debris flow argues that it represents a near-source deposit. Stratigraphically equivalent units and probable source rocks for the debris flow occur in the White Pine Range

---

color in quartz results from production of a spectral absorption band at 2.90 eV upon irradiation. The absorption band is attributed to Al3+ replacing Si4+ with a missing electron at one of the neighboring oxygens coupled with a charge compensating alkali ion (Griffiths et al., 1979). Upon heating of the irradiated quartz, the smokey color disappears due to annealing of the absorption band. The published annealing temperature is approximately 390°C (Nassau and Prescott, 1977). My own experiments suggest that this temperature may be as low as 350°. Because the annealing temperature is well below magmatic temperatures, the smokey color in the quartz grains must be imparted insitu after crystallization. It follows that the smokey color in quartz grains may be an indication of high concentrations of radioactive U, Th, and K in the host rock and that the presence of smokey quartz may be used as a geochemical fingerprint in the field.

where mafic flows are interbedded with silicic volcaniclastic rocks (Gans, pers. comm. 1988).

Lavas Bearing Magmatic Inclusions (Tve$_1$)

The oldest sequence of lavas in the thesis area is exposed in the northwest corner of the study area in several west-dipping fault blocks. Thickest exposures are approximately 500 m thick although most sections range from 50 to 100 m in thickness. Tve$_1$ is estimated to represent approximately 1.8 km^3 of magma. This is a minimum because in the thickest sections either the base or the top or neither are exposed. Most exposures of Tve$_1$ are massive, rounded outcrops making determination of structural attitudes difficult. The unit is easily recognized in the field because it contains ubiquitous large, rounded quartz grains often in polycrystalline clusters, and fine-grained vesiculated magmatic inclusions in all exposures. Quartz may be smokey. Extensive devitrification and oxidation have imparted a reddish-purple color to most rocks, although south of Piscevich Summit (Plate 1) Tve$_1$ rhyodacites are hydrated vitrophyres.

Compositions of Tve$_1$ range from basaltic andesite through rhyodacite, although the bulk of the lavas are two-pyroxene andesites and dacites (Table 1). Poor

exposure and structural disruption do not permit elucidation of stratigraphic relations amongst individual flows within Tve_1. There is a paucity of magmas with SiO_2 contents between 56.5 to 61 and 65.8 and 68.1 percent (Figure 4), although these "compositional gaps" may simply reflect incomplete sampling. Andesites are seriate, glomeroporphyritic and contain up to 32% phenocrysts of plagioclase > orthopyroxene $\geq$ clinopyroxene = quartz > amphibole > Fe-Ti oxides $\pm$ biotite and accessory zircon and apatite (Table 2). Dacites are petrographically similar to the andesites except that they contain more modal amphibole and biotite and less orthopyroxene and clinopyroxene (Table 2). Rhyodacites are distinct mineralogically in that they contain sanidine and sphene while pyroxenes are absent in general (Table 2).

Clinopyroxene grains are anhedral to subhedral and are seriate ranging in size from 1.5 mm to 0.3 mm. They occur as a groundmass phase along with Fe-Ti oxides and microlites of sodic plagioclase. Plagioclase phenocrysts occur in two distinct morphologies in all compositions: (1) as euhedral megacrysts, as large as 2 cm across in some units, or euhedral grains with sieved cores (An 80-60) that contain irregularly shaped melt inclusions and are mantled by normally zoned inclusion free rims (An 50-30), and (2) as smaller (up to 5mm) subhedral to euhedral,

reversely zoned, fresh grains (An 35-30; Figure 6). Based on the criteria of Dungan and Rhodes (1978) the melt inclusions are interpreted to reflect corrosion of the plagioclase phenocrysts by disequilibrium with the enclosing liquid. Quartz grains (up to 1 cm across) are characteristically rounded and embayed. Embayments are filled with clear silicate glass. Larger grains are often in polycrystalline clusters. In andesites, quartz grains may be surrounded by augite reaction coronas.

The sodic plagioclase grains and quartz xenocrysts are presumed remnants of silicic material that was mixed into, or assimilated by, more mafic magma. Glazner et al. (1988) studied the effects induced by incorporation of granitic minerals into mafic magmas. They found that quartz and sodic plagioclase regularly occur as xenocrysts while alkali feldspar is conspicuously absent; quartz and plagioclase react rapidly with the liquid to form protective overgrowths while alkali feldspar readily dissolves. This is consistent with the absence of alkali feldspar in rocks containing quartz xenocrysts. An important implication of this study is that the alkali feldspar component of a granitic partial melt is preferentially incorporated into the hybrid melt.

All lavas of Tve_1 contain vesiculated inclusions of
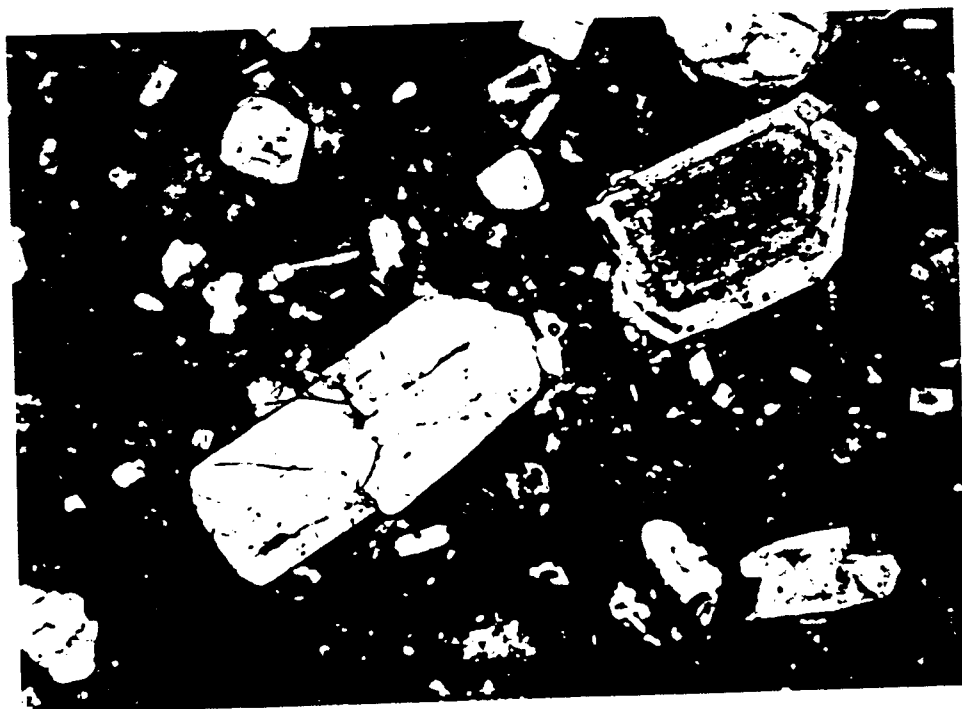
Figure 6. Two plagioclase populations in rhyodacite
sample Mt876. Plagioclase at right is
normally zoned with An74 sieved core;
clear, euhedral rim is An48. Euhedral,
clear plagioclase at left is An31 with a
thin rim of An34. Width of field = 6.0
mm. Plane light.

basaltic andesite (Table 1). In outcrop, inclusions rarely make up more than 2% of the total exposure, are ellipsoidal, and range in size from microscopic to 13 cm in long. The phenocryst assemblage is plagioclase > orthopyroxene > clinopyroxene > opaques plus accessory apatite and zircon (Table 2). Quartz, amphibole, and biotite may occur as xenocrysts in some inclusions (Appendix 1). Quartz xenocrysts are typically resorbed, embayed, and armored by clinopyroxene coronas. Fe-Ti oxides and rims of orthopyroxene grains have been extensively oxidized to hematite imparting a red color to most inclusions.

Textural evidence, including high groundmass vesicularity, concentric zoning of vesicles with size increasing toward the core of the inclusion, glassy rims, and acicular laths of plagioclase and orthopyroxene (aspect ratios of approximately 15) often in radiating fans or randomly oriented (Figure 7), indicates that these inclusions represent quenched blobs of mafic magma cooled at moderate degrees of undercooling in more silicic hosts (Bacon and Metz, 1984; Bacon, 1986; Lofgren, 1974; Mathis, 1988). Many clinopyroxene grains are equant and prismatic, however, clearly indicating an earlier generation of crystal growth. Borders of inclusions are
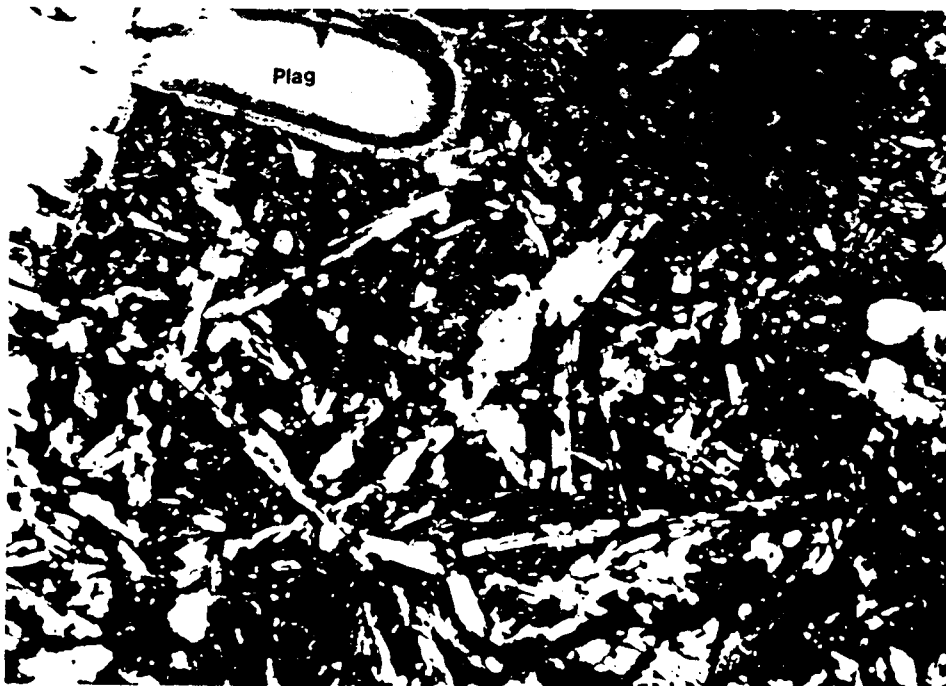
Figure 7.   Radiating fan splay of plagioclase (bright
            laths; center of photo) in magmatic
            inclusion sample Mt879. Larger
            plagioclase grain (Plag) and biotite grain
            (Bio) at the top of the photo are
            xenocrystic. Width of field = 3.0 mm.
            Crossed nichols.
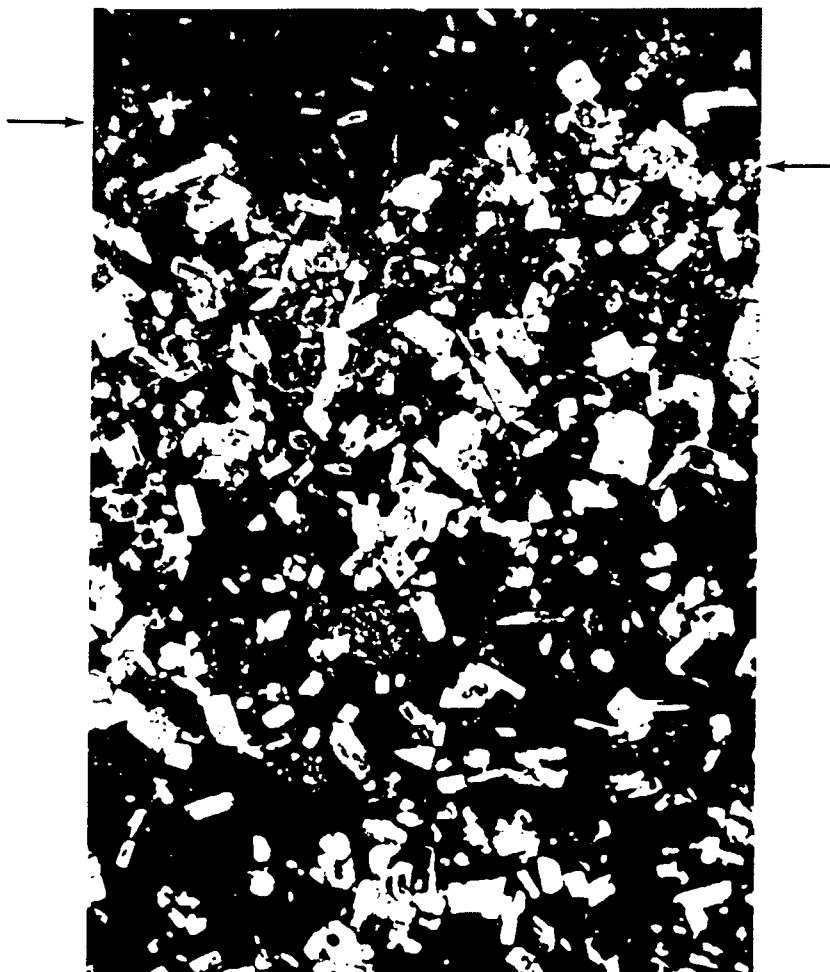
Figure 8. Detail of border between magmatic
inclusion (Mt8819a) and host (Mt8819b).
Magmatic inclusion is in
lower four-fifths of photomicrograph
(below arrows). Note the increase in the
size and volume of vesicles (dark areas)
towards the interior of the inclusion and
the crenulated margin of the inclusion.
Width of field = 6.0 mm. Crossed Nichols.

crenulated and convex toward the host on a microscopic scale (Figure 8).

There appears to be a general inverse correlation between the size and abundance of magmatic inclusions and the silica concentration of their hosts. Rhyodacites (samples Mt-87-86 and Mt-87-6; Table 1) contain small, rare inclusions whereas andesites and dacites contain the largest size and greatest abundance of inclusions. Although many of the smaller inclusions appear partially disaggregated, no other evidence is seen for mixing between inclusions and hosts.

Discussion of the Early Group

Rocks of the Early Group have been separated into two distinct units. The base of the lowest unit, Tves, is marked by isolated exposures of tuffaceous volcaniclastic sediments and calcareous pebble conglomerates. These rocks are overlain either by a volcaniclastic debris flow or by a dacitic ash-flow tuff (Tvesa). There is some evidence to suggest that the ash-flow tuff was erupted from a vent outside the Egan Range volcanic complex. Volcanic clasts within the debris flow provide the record of earliest magmatism in the Egan Range volcanic complex. These clasts indicate that the earliest volcanic activity was bimodal in composition.

Lavas of the Tve_1 indicate that magmatism became much more voluminous and compositionally diverse with time. While magmas of Tve_1 do not cover a complete compositional spectrum, there is extensive petrographic and field evidence in the form of disequilibrium phenocryst textures and assemblages and mafic magmatic inclusions to suggest that these magmas represent incomplete mixtures of mafic and silicic magmas. Suggested origins for the formation and dispersion of mafic inclusions in more silicic hosts are diverse and will be discussed below (Chapter 4). Whatever the suggested mechanism for the origin of the mafic inclusions, it must be compatible with petrographic and chemical evidence (Chapter 4) which indicate that both the inclusions and hosts are hybrid rocks.

Middle Group

Rocks of the middle group are those that most closely resemble the Kalamazoo volcanic rocks of east-central Nevada in composition, mineralogy and age (Young, 1960; Gans et al., 1989). Gans et al. (1989) have divided the Kalamazoo volcanic rocks into three members. In ascending order these are: the Kalamazoo tuff, hornblende dacite lavas, and the tuff of North Creek and related lavas. Rocks correlative to the tuff of North Creek are classified as the late group in this study. Age dates by Gans et al. (1989) and McKee et al. (1976) indicate that the Kalamazoo volcanic rocks erupted over a very short time span, approximately 35 Ma ago[2]. Hornblende from a biotite-hornblende bearing dacite vitrophyre near the base of the middle group in this study yielded a preliminary ^{40}Ar-^{39}Ar age determination of 35.1 Ma. No error is attached to this age estimate because of unquantified large flux gradients during sample irradiation, although it is likely to be about 0.5 Ma. The age determination signifies, however, that these rocks are contemporaneous

---

[2]Biotite from the Kalamazoo tuff yielded a new weighted mean ^{40}Ar-^{39}Ar age of 35.2 $\pm$ 0.1 Ma (Gans, 1988 pers. comm.). Existing geochronology for the hornblende dacite lavas yields a weighted mean age of 34.9 $\pm$ 0.8 Ma (Gans et al., 1989; McKee et al., 1976).

with other synextensional volcanic rocks erupted in east-central Nevada during the mid-Tertiary.

Rocks of the middle group are exposed in the northeastern to central-western region of the study area (Plate 1). These rocks represent a significant change in the character of magmatism in the Egan Range volcanic complex. In contrast to the large compositional diversity of the early group, the middle group is relatively homogeneous compositionally and petrographically. With respect to bulk composition, the middle group lavas fill in the upper gap in silica content defined by Tve1 (Table 1).

Kalamazoo Tuff (Tkt)

The Kalamazoo tuff is the most distinctive and widespread ash-flow tuff in east-central Nevada. Complete sections are up to 350 m thick in the Schell Creek Range and thin toward the Butte Mountains and the Confusion Range (Gans et al., 1989). Gans et al. (1989) subdivide the tuff into four members informally named A,B,C, and D. Unit B is the most widespread member and occurs in all sections of the tuff. On the basis of field appearance, petrography, and geochemistry, outcrops of a densely welded rhyolitic ash-flow tuff in the Egan Range volcanic complex are correlated with the basal to middle part of unit B.

Thin, discontinuous exposures of the Kalamazoo tuff are present in Jones Canyon and in the vicinity of Coombs Creek in the northeast region of the area (Plate 1; map unit Tkt). Thickness of the tuff in both localities is approximately 20 m. Flattened pumice lapilli range from 1 cm to 30 cm in diameter, but typically are about 3 cm. These fiamme contain approximately 3% to 4% phenocrysts of plagioclase > biotite > sanidine > amphibole = Fe-Ti oxides ± pyroxenes plus accessory zircon and allanite. Lithic fragments include carbonate, sandstone, and clays and constitute 2% on the tuff matrix. These lithic fragments preferentially weather out of the matrix leaving distinct white pockmarks on outcrop surfaces; this feature is distinctive of member B (Gans et al., 1989).

Rare-earth element (REE) abundances of pumice separated from the Kalamazoo tuff at both localities (Appendix III) are nearly identical or slightly lower than those of fiamme from the basal part of unit B in the Schell Creek Range (Gans et al., 1989; Grunder pers. comm., 1989). Based on the REE abundances, field appearance of the unit, and the regional distribution of the Kalamazoo tuff in east-central Nevada, it is likely that these exposures represent distal facies of the basal to middle part of member B.

Autoclastic Dacites (Tvm$_1$)

Tvm$_1$ lavas, vitric breccias, and block and ash flows were mapped as a single unit because they have nearly identical mineral modes and major-element concentrations (Table 1). These rocks probably represent a continuum of autoclastic deposits associated with growth and collapse of a dacitic dome located between the Robinson and Miller Ranches (Plate 1). Maximum thickness of the unit is approximately 380 m and total volume is estimated at $\geq$ 0.5 km^3, which represents a minimum value because some of the unit has been stripped by erosion. Samples taken at different stratigraphic levels are analytically indistinguishable dacites (Mt8712; Mt8717; Mt8734; and Mt871a; Table 1).

Lavas at the base of the section are vitroclastic, megascopically glomeroporphyritic with 34% phenocrysts of plagioclase > biotite $\geq$ amphibole > orthopyroxene > clinopyroxene > Fe-Ti oxides > quartz plus accessory zircon and apatite (Table 2). Glomerocrysts of plagioclase and clinopyroxene, and plagioclase and biotite are common. Phenocrysts are sub- to euhedral and range up to 0.7 cm across. Interiors of plagioclase grains commonly are strongly sieved and contain abundant brown glass melt inclusions and have fresh overgrowths. A subordinate population of plagioclase grains, however, is

extremely fresh and euhedral and appears to be in equilibrium with the melt. These morphologies suggest that the sieved grains may represent relict phenocrysts that survived an early disequilibrium event while the fresh grains may have grown subsequent to this event (Wyborn and Chappell, 1986). Orthopyroxene commonly occurs in glomerocrysts with plagioclase and opaque oxides. These grains are all riddled with opaque oxide inclusions. Clinopyroxene occurs as clusters of small phenocrysts; rarely with opaque oxides, as isolated phenocrysts, and as intergrowths with orthopyroxene. The groundmass is composed of both brown and clear discontinuously laminated glass suggesting that this rock represents a mixed lithology (Figure 9).

The lavas of Tvm_1 grade continuously into a thick, wedge-shaped, sequence of vitric breccias that thin markedly to the east suggesting a westward source area. These breccias are crudely stratified and are in clast support. The matrix is composed of laminated glass containing abundant, granulated phenocrysts. Clast size ranges from lapilli to blocks commonly as large as 1 m in diameter. Clasts are variably flattened. Modal mineralogy of clasts are identical to lower, dense lavas except that the phenocryst content is less; approximately 23% (Table 2). Compositions are, however,

Figure 9.   Mixed glass in dacite sample Mt8715. Note large, sieved plagioclase phenocryst with euhedral overgrowth in northwest corner of photo. P = plagioclase, O = orthopyroxene, B = biotite, A = amphibole. Width of field = 6.0 mm. Plane light.

analytically indistinguishable (Table 1).

Depositionally overlying Tve_1, in the northeast corner of the study area is a well-bedded block and ash flow containing small (≤ 1 cm) undeformed pumice lapilli and vitrophyric blocks (up to 0.5 m across). This unit probably represents a more distal facies of Tvm_1 because the vitrophyric clasts (Mt871a) are petrographically and compositionally indistinguishable from lavas and vitric breccias described above (Table 1). Total thickness of the block and ash flow is approximately 10 m. Vitrophyric blocks are dispersed throughout the deposit, although they are more abundant in a reversely graded, inclusion rich basal horizon. Blocks account for approximately 5-10% of the total deposit.

Smokey Quartz-Bearing Rhyodacite (Tvm_2)

The lavas of Tvm_2 are pink to white devitrified rhyodacites (Mt8720; Table 1) conformably overlying Tvm_1. The unit is easily recognized in the field by the presence of large, jet-black quartz grains. While smokey quartz bearing lavas are also present in the early unit, Tvm_2 lavas are distinguished because they lack magmatic inclusions. Similarly, the presence of rare sanidine distinguishes them from underlying Tvm_1 and overlying Tvm_3. The unit is locally exposed in the northeastern

corner of the study area where it attains a maximum thickness of 70 m (Plate 1).

Rhyodacites of Tvm_2 contain approximately 23% phenocrysts of plagioclase > biotite > amphibole > orthopyroxene > clinopyroxene > quartz > sanidine = Fe-Ti oxides plus accessory zircon and apatite in an extensively devitrified groundmass devoid of crystals (Table 2). Biotite and amphibole are oxidized to opaque oxides. As in other middle group lithologies, plagioclase textures are complex. Many grains have extremely sieved cores, with oscillatory zonation, that range in An content from An20 to An35. A subordinate population of grains (An35) are fresh and relatively unzoned. Again, these relationships suggest that the sieved grains are relict phenocrysts which survived an early disequilibrium event, whereas fresh grains grew subsequent to this event (Wyborn and Chappell, 1986). Glomerocrysts of amphibole and plagioclase are common. Extremely rounded, jet-black quartz grains, which are interpreted as xenocrysts, account for approximately 1% of the mode. Often they occur as elongate polycrystalline "stringers" as long as 1.5 cm.

Glomeroporphyritic Dacites (Tvm₃)

Tvm_3 is primarily exposed as a spectacular, 280 m-
thick, mesa of dacite located in the north-central region
of the area (Plate 1). This exposure is interpreted as
another large dacitic dome complex centered between the
Robinson and Miller Ranches. Total volume of Tvm_3 is
estimated at 1 km^3.

In outcrop the unit is blocky to platy, devitrified
lavas with very contorted flow banding. Variable
oxidation and vapor-phase alteration have imparted a red
to maroon color to the lavas. The flow banding is defined
by alternating centimeter to meter scale crystal-poor and
crystal-rich bands and by alignment of biotite and
hornblende phenocrysts. At the flat top of the dome
complex, flow banding is continuous from the devitrified
lavas into a dark vitrophyre which forms the upper margin
of the unit. Elsewhere, a similar dark vitrophyre usually
marks the top of Tvm3 and serves as an excellent
stratigraphic marker. A prominent feature of the dome
complex is well-developed jointing parallel to flow
foliation that steepens from subhorizontal at the base to
subvertical at the top of the dome. These joints are
often on a large scale (hundreds of meters) and may
represent large flow ramping structures.

Dacites of Tvm_3 are also well exposed as a few small inliers surrounded by Quaternary alluvium, and as two prominent buttes located directly east of Robinson Ranch (Plate 1). These exposures may represent subvolcanic intrusions; they have the same mode as the flow banded lavas but are massive in outcrop.

Northeast alignment of the inliers suggests that eruptive centers for Tvm_3 were strongly controlled by the regional stress field. Indeed, the entire aerial distribution of Tvm_3 lavas forms a crude east-northeast trending belt of outcrops (Plate 1). Furthermore, the contact between Tvm_2 and Tvm_3 lavas has an angular discordance of approximately $20°$ between the Miller and Robinson Ranches, suggesting that these units were erupted during active faulting and tilting (Chapter 3). This study and previous work in the Hunter District of the northern Egan Range (Gans, 1982) indicate that the earliest set of Tertiary normal faults in the region trend northeast and east-west. Gans (1982) has demonstrated in the Hunter District that movement on these faults occurred synchronously with the earliest episode of magmatic activity and that they guided many of the feeder dikes for associated volcanic rocks. Although volcanic rocks in the Hunter District are slightly older, the relations described above suggest that the same regional stress

field probably controlled vent loci of Tvm3 lavas. This will be discussed further in Chapter 3 and placed in a structural context.

Petrographically, the dacites of Tvm_3 are strongly glomeroporphyritic both in hand sample and thin section. They contain 20% phenocrysts of plagioclase > orthopyroxene > biotite = amphibole > Fe-Ti oxide > clinopyroxene > quartz with accessory zircon and apatite set in a devitrified groundmass (Table 2). Glomerocrysts of orthopyroxene, plagioclase, plus opaques are abundant (Figure 10), whereas glomerocrysts of plagioclase plus amphibole; and orthopyroxene, clinopyroxene, opaques, plus plagioclase are less common. Stewart (1975 a,b) and Boettcher (1977) suggested that plagioclase-two pyroxene-magnetite glomerocrysts may represent the low pressure breakdown products of amphibole crystallized at high pressure. The hypidiomorphic granular texture of the glomerocrysts argues that they are, however, not amphibole breakdown products (Garcia and Jacobson, 1979); they may represent relics of an earlier crystallizing assemblage. Furthermore, amphibole present in Tvm_3 lavas are subhedral to euhedral and do not appear to be in reaction relationship with the liquid. Plagioclase phenocrysts (up to 1.3 cm across) occur as two distinct groups: (1) as larger grains with sieved cores and fresh, slightly

Figure 10. Plagioclase (P) - orthopyroxene (O) -
Fe-Ti oxide (F) glomerocryst in dacite
sample Mt8743. Width of field = 0.6 mm.
Plane light.

reversely zoned rims; and (2) as somewhat smaller fresh, subhedral to euhedral grains that are either unzoned or normally zoned. Amphibole and biotite phenocrysts are predominantly replaced by a very fine aggregate of minute opaque oxide minerals. This reaction product may result from dehydration and oxidation during extrusion caused by increased fugacity of O_2 relative to H_2 and decreased fugacity of H_2O (Kuno, 1950). Orthopyroxene and clinopyroxene occur primarily as glomerocrysts with plagioclase and Fe-Ti oxides, although a few larger isolated grains are present.

Discussion of the Middle Group

Following eruption of the mafic to silicic magmas of the early group, relatively homogeneous dacites and rhyodacites were erupted in the northern region of the Egan Range volcanic complex. All of the vents of the middle group appear to have been localized along an east-northeast trending lineament although extensive cover by younger lavas and difficulty in identifying definitive vent facies indicators (e.g. wide-spread fumarolic alteration or vent breccias) make this conclusion speculative. However, the association of wedge-shaped collapse breccias, block and ash flows, subvolcanic intrusions, and related lavas are typical of near-vent

facies (Fisher and Schmincke, 1984). Such deposits commonly form constructional topographic features of considerable relief which was probably the case between the Robinson and Miller Ranches where two large dome complexes were constructed (Plate 1).

Age relations discussed above and general petrologic similarities suggest that the middle group correlates with the hornblende dacite lavas of Gans et al. (1989). Inferred vent complexes of these dacites have been identified at widely scattered localities throughout east-central Nevada. Grunder (1989) has suggested that eruption of over 2500 km^3 of monotonous dacite from these vents signifies the development of a batholith beneath east-central Nevada 35 Ma ago. The regional extent of these lavas and the parallels in timing and eruptive products argue that similar processes operated over a very large area.

Late Group

The late group contains a monotonous assemblage of rock types which are dominantly biotite rhyodacites. This youngest cycle, the most voluminous of the three (approximately 35 km^3), resulted in numerous flows and domes that are exposed at the structurally highest elevations. In a regional sense, however, rocks correlative to the late group are volumetrically subordinate to middle group correlative rocks (Grunder, pers. comm., 1989). Typical exposures in the Egan Range volcanic complex are 350 m thick and a few sections attain thicknesses of 375 m. These lavas are extremely uniform in petrographic and field appearance with the exception of an andesite flow (Tvl$_2$; Plate 1) which forms a regional marker unit. In areas of poor exposure where this unit is not present in the stratigraphy, it is not possible to locate the contact between the upper and lower members of the late group. In these cases, the late group is undifferentiated (Tvlu; Plate 1).

Age determinations were not obtained for lavas in the late group resulting in some uncertainty of the stratigraphic relationship of the lowest member (Tvl$_1$) with respect to the middle group. At its base, Tvl$_1$ conformably overlies the Uhalde tuff which is older than the middle group lavas based on new ^{40}Ar-^{39}Ar age

determinations (this study). Where exposed, the tops of both the middle group and Tvl1 are in sharp contact with the middle member of the late group (Tvl$_2$). Thus, on the basis of stratigraphic relations, Tvl$_1$ and the intermediate group are age equivalents. Several lines of evidence, however, suggest that Tvl$_1$ lavas are products of a later cycle of magmatism: (1) lavas of the late group, including Tvl$_1$, represent the first, and only, volcanic products of widespread extent, whereas earlier units are only locally exposed; (2) the shift from local to widespread magmatism coincides with a change from crystal rich, biotite-hornblende-two pyroxene lavas to crystal poor, biotite dominated lavas; and (3) chemically, Tvl$_1$ lavas are more akin to late group lavas (e.g.: elevated K2O, Rb, and Zr; Chapter 4). Dacites of Tvl$_1$ are therefore stratigraphically equivalent to the middle group but are considered to be part of a younger cycle of magmatism and are thus assigned to the late group.

Major element compositions of representative samples of the late group are presented in Table 1. Detailed petrographic descriptions of analyzed samples are in Appendix 1.

Dacite Lavas (Tvl$_1$)

This unit is exposed principally in the southern region of the map area where it conformably overlies the Uhalde tuff (Plate 1). Where the Uhalde tuff thins and pinches out, Tvl$_1$ conformably overlies the Permian Arcturus Formation (Hose and Blake, 1976). Nowhere is it observed to overlie rocks younger then the Uhalde Tuff. The unit also occurs in the northwestern region of the area although poor exposure and the absence of Tvl$_2$ made it impossible to locate the contact between it and overlying lavas of Tvl$_3$.

Tvl$_1$ has a black, 4 m-thick basal member which typically consists of multiple thin dacite flows or flow lobes. Different flows are defined by dense lavas grading into vesiculated tops. Some exposures are massive, however, and appear to represent a single, thicker flow. Overlying this basal member is a thick section (up to 125 m) of dacite lavas with well-developed platy jointing. Jointing occurs at a scale of a few centimeters to less then one centimeter. Where jointing is strongly developed the unit forms characteristic steep slopes covered by coarse, angular talus. On a fresh surface Tvl$_1$ is dark grey with lighter spots where the glass has begun to devitrify.

Petrographically, Tvl₁ lavas are porphyritic with approximately 8% modal phenocrysts set in a very finely crystalline hyalopilitic groundmass (Figure 11). Phenocrysts typically display well-developed trachytic alignment presumably due to flowage. The phenocryst assemblage is plagioclase > biotite > clinopyroxene = Fe-Ti oxides > orthopyroxene = amphibole (Table 2). The plagioclase grains are normally zoned from An55 to An45 and are extremely fresh. Biotite is fresh; amphibole often has pitted cores and is always surrounded by rims of Fe-Ti oxides. Clinopyroxene grains (0.3-0.4 mm) have euhedral outlines although their outer margins are cloudy and do not appear to be in equilibrium with the host liquid. A few glomeroporphyritic clots (approximately 1 mm in diameter) of plagioclase + clinopyroxene + Fe-Ti oxides are present, as well as very rare, strongly resorbed, irregular quartz xenocrysts with thick reaction rims of augite.

Locally overlying the platy dacites is a black, 5 to 6 m-thick, biotite dacite flow. Although this flow strongly resembles the basal member of Tvll, it can usually be distinguished in the field on the basis of stratigraphic position and a slightly greater abundance of biotite. Excepting the greater biotite content, this unit is petrographically identical to the
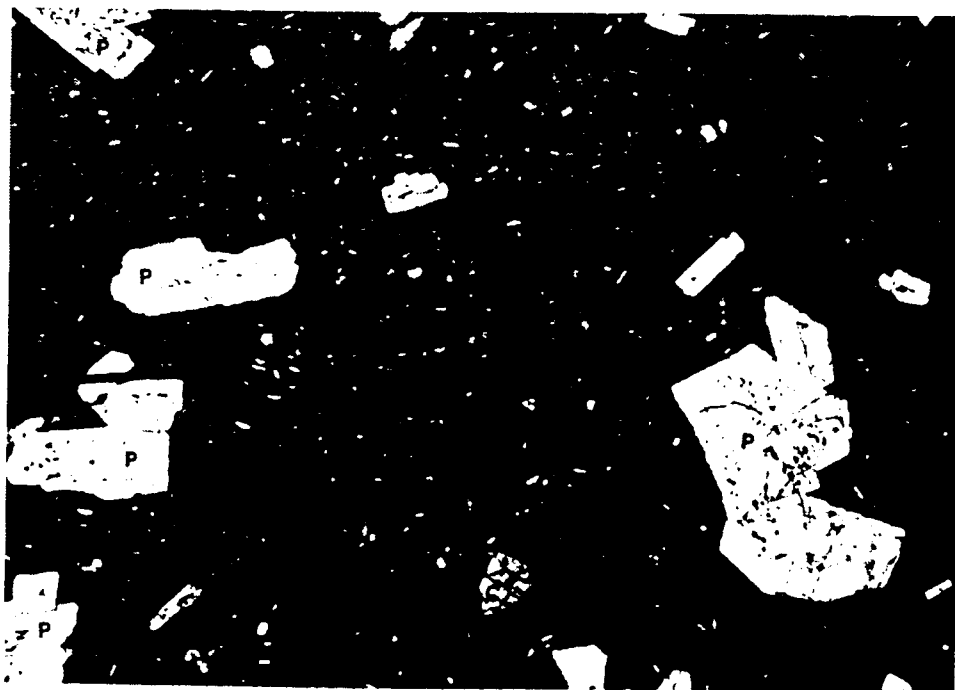
Figure 11. Porphyritic - hyalopilitic texture of
dacite sample Mt8781. Note the clear,
euhedral nature of the plagioclase (P)
phenocrysts, and the reaction rim on the
clinopyroxene (C) phenocryst. A =
amphibole. Width of field = 3.0 mm.
Plane light.

underlying dacites of Tvl$_1$.

Aphyric Andesite Lava (Tvl$_2$)

Tvl$_2$ crops out throughout the study area except in the northwest quadrant (Plate 1). It is composed of platy, virtually aphyric andesite lava (Table 1; Tf872, Mt8764) that is easily distinguished in the field. Strong resistance to erosion and burial, and regionally consistent field appearance makes Tvl$_2$ an excellent stratigraphic marker unit. This lava averages 1.5 m in thickness suggesting that it represents a single flow. Because the unit is commonly too thin to properly illustrate on the map, contacts on Plate 1 are approximated and are intended to emphasize the distribution of outcrops. Additionally, Tvl$_2$ is particularly prone to erosion by, and incorporation into, overlying basal flows of Tvl$_3$, such that many exposures of Tvl$_2$ are actually clasts within Tvl$_3$. Locally Tvl$_2$ may considerably thicken (up to 5-6 m) over short distances suggesting the flow was filling modest topographic relief.

In outcrop the andesite is greyish-green to black. In thin section, Tvl$_2$ contains approximately 1% phenocrysts of plagioclase (An45) > clinopyroxene $\geq$ orthopyroxene set in an extremely fine-grained pilotaxitic groundmass of plagioclase, pyroxenes, and Fe-Ti oxides

(Table 2; Figure 12). Rare quartz xenocrysts surrounded by augite reaction coronas are observed in some sections and one section contains a single rounded olivine phenocryst.

Near Bradley Canyon (Plate 1) a thin, north-northwest trending vesiculated olivine andesite dike intrudes Tve_1 (Table 1; Mt8759). Chemical similarity (e.g. elevated TiO_2, with respect to SiO_2 content) suggests this dike is probably correlative with the andesite of Tvl_2. However, the possibility that it is younger cannot be ruled out because middle Miocene (20.2 Ma) alkaline olivine basalts associated with the initiation of north-south trending Basin and Range normal faulting are present in small volume throughout White Pine County (Hose and Blake, 1976). The dominance of olivine as the principal ferromagnesian phase in the dike andesite is more reminiscent of the Miocene rocks although, as indicated above, rare olivine is found in Tvl_2 andesites.

Rhyodacite Lavas (Tvl_3)

Lavas of Tvl_3 are the most voluminous and monotonous in the Egan Range volcanic complex. Typical sections are 100 m thick, and the thickest section is slightly over 300 m thick, assuming there is no repetition of the section by
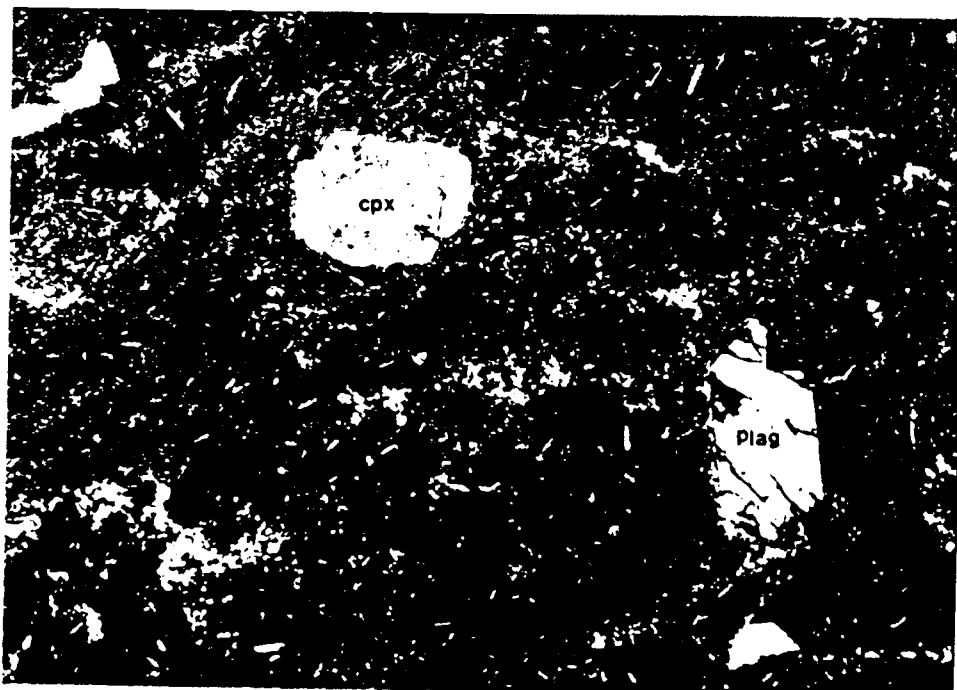
Figure 12.   Photomicrograph of andesite sample
             Mt8764.   This photomicrograph over-
             represents the volume of phenocrysts
             in this sample (Table 2).   Note the
             sharp crystal faces on the plagioclase
             phenocryst and its clean, unsieved
             nature.   Width of field = 3.0 mm.
             Plane light.

faulting. The predominant rock types are platy to blocky, cliff-forming porphyritic rhyodacite (Table 1) lavas that are commonly flow folded on a large (tens of meters) scale. Samples Mt8791 b-d (Table 1) were collected at 25 m intervals within a thick section of Tvl_3 and illustrate the monotonous character of the unit. Many of these lavas have well-developed basal flow breccias. More massive flows are frequently autobrecciated throughout and commonly are vitrophyric. The profusion of flow structures and the thick monotonous character results in difficulty in determining true structural attitudes and recognizing structure (i.e.: faults) within this unit.

Where Tvl_3 overlies Tvl_2, abundant angular clasts of Tvl_2, rarely as large as 10 m across, are present in the basal flow. The angular nature of these clasts demonstrates that they were incorporated into Tvl_3 lavas in the solid state; unlike magmatic inclusions in Tve_1. The base of Tvl_3 is commonly marked by a dense black vitrophyre (Mt8765; Table 1).

The rhyodacites contain 16% phenocrysts set in an extremely fine-grained pilotaxitic groundmass of glass and plagioclase and Fe-Ti oxide microlites (Figure 13). Variable degrees of oxidation and devitrification have imparted a purple-red color to these rocks. Plagioclase
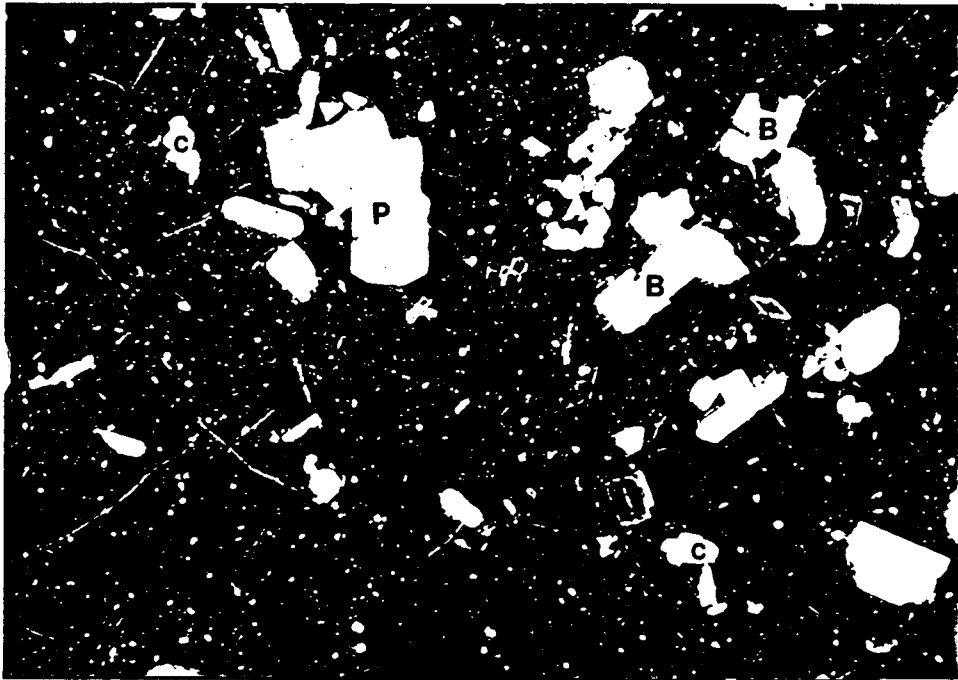
Figure 13.   Photomicrograph of rhyodacite sample
             Mt8765.   Note clean, euhedral nature of
             plagiclase phenocrysts (P) and skeletal
             texture of biotite (B).   C =
             clinopyroxene.   Width of field = 6.0 mm.
             Crossed nichols.

phenocrysts, averaging roughly 1.5 mm in length, dominate the assemblage and are about 10% of the mode. They display normal zoning from around An75 to An40. Commonly, calcic cores are altered to sericite, and a few grains contain glass inclusions as described for older units. Biotite is ubiquitous in all lavas, commonly has a skeletal texture, and is consistently the dominant ferromagnesian phase. Biotite is variably reacted to Fe-Ti oxides. Clinopyroxene, orthopyroxene, and amphibole constitute approximately 1% of the mode and typically occur in glomerocrysts with plagioclase (Table 2). Minor quartz maybe present in some lavas. Apatite and zircon are ubiquitous accessory phases.

Discussion of the Late Group

Following eruption of the middle group a large pulse of high K_2O dacites, rhyodacites, and subordinate andesites were erupted with no field evidence for a temporal hiatus in the area. Elsewhere in east-central Nevada a similar sequence of magmas, initiating with venting of the tuff of North Creek (approximately 35 Ma, 50 km^3), were erupted simultaneously (Grunder, 1989).

Texturally, the late group constitutes an overall trend toward a decrease in the volume and size of phenocrysts present in magmas. The most striking aspects

of the late group are the general absence of textural evidence for a mixed origin, as illustrated by the disequilibrium phenocryst assemblages and textures of the early and middle group magmas, and the large volumes of homogeneous magma erupted over a short period of time.

Summary of Chapter Two

(1) Volcanism in the Egan Range volcanic complex occurred in three distinct stratigraphic, compositional, and petrographic groups: the early, middle, and late groups. Major-element compositions of rocks erupted during each cycle are distinct, although they partially overlap. They define a trend toward increasingly homogeneous compositions. Rocks of the early group are predominantly quartz, two-pyroxene hybrid andesites and dacites with subordinate contaminated mafic inclusions. Those of the middle group are biotite, hornblende, two-pyroxene dacites and rhyodacites. During the late cycle, large volumes of compositionally homogeneous biotite rhyodacite were erupted.

(2) The total volume of volcanic rocks in the Egan Range volcanic complex is approximately 40 km^3. Dacites and rhyodacites, which were erupted primarily in the middle and late groups, comprise >95% of the volume of lavas. Volumes of mafic lava (basaltic andesites and andesites) are greatest in the early group, absent in the middle group, and minor in the late group. The volume of silicic rocks dramatically increases upsection.

(3) Textural evidence for magma mixing is strongest in the earliest eruptive products characterized by disequilibrium phenocryst assemblages, and grows steadily

weaker with time as magmas become more evolved.
Antithetic to this trend is a trend toward decreasing
modal volume, size, and number of species of phenocrysts.

(4) Parallel, contemporaneous eruptive histories for
adjacent volcanic centers in east-central Nevada (i.e.:
Gans et al., 1989; Grunder, 1989) suggest that similar
processes operated over a larger region.

CHAPTER THREE: STRUCTURE OF THE EGAN RANGE VOLCANIC

COMPLEX

A major objective in the study of the Egan Range volcanic complex has been to determine the relationship between magmatism and crustal extension. To this end, several specific points were addressed: (1) the age of the units above and below the unconformity between the Tertiary and Paleozoic sections, (2) the angular discordance across the unconformity, (3) the attitudes and distribution of faults within the volcanic section, and (4) the changes in attitudes of mid-Tertiary units with increasing stratigraphic height. The present attitudes of Oligocene volcanic units and the nature of the pre-volcanic unconformity indicate that tilting and extension in the Egan Range volcanic complex began slightly prior to, and continued after eruption of Oligocene volcanic rocks.

The Pre-Volcanic Unconformity and the Timing of
Extension

The ages of the stratigraphic units which occur above
and below the pre-volcanic unconformity vary at different
localities in the area. Miogeoclinal strata beneath the
pre-volcanic unconformity are limited to Permian and upper
Pennsylvanian rocks and indicate that the Tertiary erosion
surface could not have had more then about 1 km of
stratigraphic relief. This relationship holds true over a
broad region throughout east-central Nevada (Armstrong,
1972; Gans and Miller, 1983).

In the eastern region, the earliest strata above the
unconformity were deposited exclusively on the Permian
Arcturus Formation (Plate 1; Woodward, 1962; Hose and
Blake, 1976). The basal deposits consist of thin,
discontinuous lenses of calcareous pebble conglomerates,
lacustrine limestones, and tuffaceous sediments (map unit
Tves). Clasts within the conglomerates resemble
lithologies of the Permian Arcturus Formation (Woodward,
1962; this study). As discussed in Chapter Two, these
deposits are probably correlative with the Kinsey Canyon
Formation of Young (1960). The age of the Kinsey Canyon
Formation has not been determined independently but is
considered Eocene based on correlation with the Sheep Pass
Formation (Hose and Blake, 1976; Winfrey, 1958).

Stratigraphic position and biostratigraphic studies have established the age of the Sheep Pass Formation as Eocene in the Grant Range, northern Nye County (Kleinhampl and Ziony, 1985). Gans (pers. comm., 1988) has suggested, however, that some exposures of conglomerate in the study area may be Cretaceous in age. Therefore, the unconformity may locally be as old as Cretaceous. Where Tves is not present in the eastern region, the Arcturus Formation is unconformably overlain either by volcanic unit Tve_1, or, in the vicinity of Jones Canyon, by the Kalamazoo tuff.

Angular discordance across the pre-volcanic unconformity in the eastern region is quite variable ($5°$-$30°$). Attitudes obtained on the basal Cretaceous to Tertiary sediments indicate, however, that locally they were deposited roughly conformably on the Paleozoic strata. South of Piscevich Summit calcareous pebble conglomerates at the base of Tves dip $47°$ NW; tuffaceous sediments about 0.25 km to the south dip $40°$ N (Plate 1). Woodward (1962) notes that Permian strata on the west flank of the Egan Range dip $50°$ W, consistent with an attitude of $52°$ W obtained on the Arcturus Formation near Toner Spring in this study (Plate 1). Although these exposures are separated by north-south trending normal faults, the steep dips of the Tertiary sediments relative

to younger Tertiary units suggests they may have been deposited broadly conformably with the Paleozoic strata. Lavas of Tve_1 which are inferred to depositionally overlie the Arcturus Formation near Toner Spring dip $40°$ toward the west suggesting that some structural relief may have developed in the interval between deposition of Tves and Tve_1 (Plate 1).

In the vicinity of Jones Canyon the Arcturus Formation is tilted $19°W$ and is overlain, with approximately $30°$ of angular discordance, by east tilted Tves sediments, whereas 1 km to the north, the Arcturus Formation is tilted $12°N-NW$ and is overlain unconformably by northeast tilted Kalamazoo tuff (Plate 1, Plate 2). Restoration of the Kalamazoo tuff to a horizontal orientation indicates approximately $18°$ of angular discordance across the unconformity here. These relationships, coupled with the observations noted above, suggest that the amount of pre-Eocene supracrustal deformation in the vicinity of the Egan Range volcanic complex was probably limited to gentle warping (up to $30°$) of the miogeoclinal strata prior to emplacement of the Tertiary units.

Elsewhere in the study area, stratigraphically higher volcanic units depositionally overlie the unconformity. In the central southern region, the Arcturus Formation is

overlain with little to no angular discordance by late
group member Tvl_1 (Plate 1, Plate 2c). Here, the contact
between the Paleozoic and Tertiary rocks does not appear
to be severely eroded in map pattern. Along the western
boundary of the area the angular discordance across the
unconformity increases. In this region, there is a
buttress unconformity between west-dipping Paleozoic
strata and east-dipping Tvm_3 and late group volcanic rocks
(Plate 2b). Restoration of the volcanic rocks to a
horizontal orientation indicates that Paleozoic strata had
20° to 60° of pre-volcanic westward tilt. This
relationship is well exposed along Bothwick Road
approximately 1.5 km NE from its intersection with Thirty
Mile Road (Plate 1, Plate 2b). The buttress unconformity
here is sharp and divides units with approximately 45° of
angular discordance.

Much of the angular discordance across the buttress
unconformity in the western region is not a result of
Tertiary deformation. Douglass (1960) has mapped a broad,
northwest-trending synformal structure of Mesozoic age in
the Butte Mountains. Examination of the geologic map of
White Pine County (Hose and Blake, 1976) indicates that
the eastern, west-dipping limb of this structure extends
beneath the volcanic units along the western boundary of
the area. Beds on this limb dip westward 30° to 35° in

the relatively unextended Butte Mountains suggesting that as much as 35° of the discordance between the Paleozoic and Tertiary strata can be accounted for by an older compressional event (Mesozoic; Douglass, 1960). This compressional event may also account for the locally moderate angular unconformity (approximately 30°) between lowermost Tertiary and Paleozoic units in the southeast part of the study area near Jones Canyon.

Angular unconformities developed within the volcanic section are difficult to detect because many exposures contain blocky or massive lavas from which it is difficult to obtain reliable attitudes. Notwithstanding this problem, there appears to be an angular unconformity beneath unit Tvm_3. In the vicinity of Band Spring in the east-central region, Tves strata are tilted 40° to 47° north and strike roughly east-west. These strata are unconformably overlain by a gentle (approximately 10°) west-dipping section of Tvl_2 and Tvl_3 lavas (Plate 1). Furthermore, throughout the study area, dips of Tertiary strata older then Tvm_3 are variable but are dominantly between 47° and 20°. In contrast, units younger then Tvm_2 dip, with few exceptions, less then 20°.

The stratigraphic relations described above suggest that two episodes of early (?) Tertiary deformation affected the Egan Range volcanic complex: (1) An early

event which commenced slightly prior to or during
deposition of Tves and produced a slight angular
unconformity between the Paleozoic and the earliest
Tertiary (Cretaceous ?) strata, and locally up to 47° of
tilt in pre-Tvm_3 units; and (2) a later event which began
during or after eruption of Tvm_3 lavas and produced
shallow dips in Tvm_3 and younger lavas. The effects of
the early episode appear to have been stronger in the
northeast and central-east parts of the area because in
the southern region volcanic strata of the late group are
paraconformable with the Arcturus Formation (Plate 1,
Plate 2c). This suggests that the forces responsible for
the early extensional tectonism in the Egan Range volcanic
complex may have died out to the south.

Faulting

High-angle normal faults are abundant in the Egan Range volcanic complex. Although Gans (1982) has identified many down-to-the east, shallow dipping normal faults that cut Oligocene volcanic units in the Hunter District, 15 km north of the study area, no evidence for shallow dipping faults was seen in this study, further suggesting that extensional deformation decreases southward.

At least two generations of normal faults have been identified. Older fault sets strike N30-60°E, N30-40°W, and roughly east-west. These faults are cut by a younger set of high-angle, approximately north-south striking normal faults which accommodate east-west extension. Faults of all orientations cut the youngest volcanic unit (Tvl_3), and as such, all had mid-Tertiary or younger displacement. However, several lines of evidence discussed below suggest that the older set of faults was active during eruption of the oldest volcanic rocks, and that much of the displacement on these faults occurred prior to eruptions of Tvm_3 magmas.

Recognition of and therefore the density of mapped faults in the study area was in part dependent on the

distinctiveness of the stratigraphy. Thick, monotonous sequences of flow-folded to massive biotite rhyodacite (map unit Tvl_3) in the central region have greatly limited the recognition of structures. In spite of this problem, the southern region appears to have been less affected by early faulting than adjacent areas to the north. In the south, unit Tvl_2 can be traced over long distances and is not extensively displaced by faults of the earlier set (Plate 1). In contrast, in the northeast region at least 6 early faults have been identified (Plate 1). These faults appear to have relatively small displacements, although some may accommodate offsets as great as 600 m. Most of the faults juxtapose volcanic units high in the stratigraphic section although, one fault, whose trace begins approximately 1.2 km southeast of Robinson Ranch and strikes roughly east-west, places Tve_1 against Tvl_3 (Plate 1). The vertical throw on this fault is a minimum of 550 m based on the displacement of the top of unit Tve_1 and assumption of no left-lateral strike-slip component. The trace of this fault continues to the east and is cut and offset in an apparent left-lateral sense by a younger north-south trending fault.

The effects of the older faulting episode are well exposed in the extreme northeast corner of the area (Plate

1). Here, block-rotation along a northeast trending
normal fault, with down-to-the south displacement, has
tilted rock units so that they strike N60°E and dip 20°
NW. These rocks have not been significantly disrupted by
later north-south striking faults. Prior to the onset of
the younger faulting, the entire northeast region of the
Egan Range volcanic complex may have consisted of many
similar fault blocks tilted N20°W .

Several lines of evidence suggest that much of the
displacement on the older faults occurred during eruption
of the early and middle volcanic groups. First, as
discussed above, dips within Tertiary units indicate that
an angular unconformity exists beneath Tvm_3 lavas.
Second, northeast trending fractures (possibly due to a
NW-SE least principal stress) appear to have controlled
vent locations of Tvm_3 lavas. Inliers of Tvm_3 in
Quaternary alluvium in the northern part of the area
define a N40°E trend essentially on line with a mapped
northeast trending fault (Plate 1). Moreover, the
elongation of all Tvm_3 outcrops trends approximately
N40°E, suggesting that vent loci of Tvm_3 lavas may have
been controlled by a system of similar northeast trending
faults (Plate 1). The trends and timing of faulting
suggested in this study are similar to the sequence of
events in the nearby Hunter District where the

relationship between faulting and magmatism is well

documented. For the Hunter District, Gans (1982) has

demonstrated that the earliest sets of Tertiary normal

faults strike roughly N50°E and east-west and that they

guided many of the feeder dikes for associated volcanic

rocks. Although volcanic rocks in the Hunter District are

slightly older, the same regional stress field appears to

have controlled vent loci of Tvm_3 lavas.

The major north-south trending normal faults in the

area are responsible for the present, typical Basin and

Range topography (Plate 2). Although none of the mapped

faults are exposed, their map patterns suggest they are

high-angle normal faults. Displacements are up to 400 to

500 m along some of the larger faults based upon offset of

unit Tvl_2 which forms a distinctive stratigraphic marker

unit. Spacing between the largest traceable faults is

quite regular and averages approximately 1.7 km. Most, if

not all, postdate the Tertiary volcanic rocks because late

group rocks and the Permian Arcturus Formation are

paraconformable in the southern region where some of the

most impressive block faulting has occurred (Plate 1,

Plate 2c). This relationship does not preclude active

faulting during eruption of late group rocks; however, the

monotonous nature of the late group rhyodacites makes

demonstration of upward decreasing tilts in the upper part

of the volcanic section difficult. Elsewhere in east-
central Nevada (and the entire Great Basin) faulting of
similar geometry is commonly referred to as "Basin and
Range" faulting (e.g. Stewart, 1980; Zoback et al., 1981).
Although not well constrained, most workers in White Pine
County consider north-south faulting to have initiated in
the Miocene (approximately 22 Ma) based upon basin-fill
chronology and radiometric age dates of presumably coeval
volcanic rocks (Hose and Blake, 1976).

The present structure of the area is a series of
approximately north-south trending horsts and grabens.
The largest of these grabens is surficially expressed as
Cottonwood Canyon to the north (Plate 2b) and Gleason
Creek Valley to the south (Plate 2c). This region is
characterized by numerous springs which issue along the
graben bounding faults which appear to have served as
conduits. The structural geometry of the area is well
illustrated in cross-section (Plate 2b,c). In the south-
western region of the area at least four high-angle normal
faults have down-to-the west displacement resulting in
higher elevations eastward, culminating at Robinson Peak
(Plate 1, Plate 2c). Robinson Peak is a horst bounded on
the east and west by east- and west-dipping high-angle
normal faults, respectively. The southeastern region of
the area is virtually a mirror image of the western half;

east-dipping normal faults have down-to-the east
displacement creating a topographically elevated horst at
the "three peaks" area west of Wildcat Spring (Plate 1,
Plate 2c). Faults bounding a smaller horst in the
southeast corner of the area have uplifted and exposed the
Tertiary unconformity between map unit Tves and the
Arcturus Formation. Unlike the larger horsts, however,
this horst is topographically low probably due to
preferential erosion of Tves tuffaceous sediments and
Permian Arcturus sandstones relative to more competent
silicic volcanic rocks of the late group. The antiformal
structure drawn within the Paleozoic section on the west
side of Plates 2b and 2c is required because west of
Robinson Summit Paleozoic units dip westward, while to the
east they are paraconformable with east-dipping volcanic
rocks.

Summary and Discussion

(1)   The ages of Paleozoic strata beneath the Tertiary unconformity in the Egan Range volcanic complex range from Permian to Pennsylvanian.   Clasts within early Tertiary pebble conglomerates consist solely of Permian Arcturus Formation lithologies.   These observations indicate that at the time of deposition of the earliest Tertiary strata, the paleosurface beneath the unconformity had less than 1 km of stratigraphic relief.   Therefore, the vicinity of the Egan Range volcanic complex probably experienced relatively little supracrustal deformation prior to deposition of Tertiary units.

(2)   The nature of the unconformity varies locally. Near Piscevich Summit Tves sediments appear to have been deposited with little angular discordance (approximately 5°) upon Paleozoic strata.   In the southeast region they have as much as 30° of angular discordance.   Evidence presented above suggests that some of this discordance may be the consequence of a Mesozoic compressional event which produced broad gentle folds in the Paleozoic strata (Hose and Blake, 1976, Gans and Miller, 1983).

(3)   Dips of Tertiary strata suggest two episodes of deformation; an older event which commenced slightly prior to or during deposition of Tves and extended until eruption of Tvm_3 lavas, and a younger event which probably

postdates the volcanic rocks. The older episode is observed primarily in the northern part of the area.

(4) Two generations of faulting are observed; older sets of N30-60°E, N30-40°W, and roughly east-west trending faults, and a younger set of approximately north-south trending faults. Both sets cut all the mid-Tertiary volcanic rocks. Evidence presented above suggest that the older set initiated during eruption of pre-Tvm_3 lavas and waned during eruption of later units. The age of initiation of movement on the younger set is post-Tvl_3 because these faults cut the older set which cuts Tvl_3 lavas.

(5) Although Gans (pers. comm., 1988) has demonstrated that mid-Tertiary volcanic units have been folded in the White Pine Range to the west, I interpret both east and west dips in Tertiary volcanic units in the Egan Range volcanic complex as due to faulting rather than folding. (Plate 2).

The relationships described above indicate that the earliest volcanic rocks were erupted during a period of on going crustal extension. In nearby areas of east-central Nevada Gans (1982), Gans and Miller (1983), and Gans et al. (in press) have thoroughly documented the close temporal ties between magmatism and extension. The coincidence between these two events probably bears

strongly on the style of volcanic activity seen in east-central Nevada during the mid-Tertiary. While thousands of km^3 of silicic lavas were erupted during this time period, surprisingly few large ash-flow tuffs are present. In contrast, volcanic products of the Indian Peak caldera complex (32 to 27 Ma), which represents the southerly migration of the same (?) thermal pulse which produced the east-central Nevada lavas, are dominated by dacitic and rhyolitic ash-flow tuffs; lavas are greatly subordinate (Christiansen et al., 1988). There appears to be little extension associated with the magmatic event at Indian Peak (Christiansen et al., 1988). The difference in eruptive style between the two areas may be controlled by the amount of extension associated with each event. In east-central Nevada active faulting may have continuously degassed magma chambers reducing the possibility for build-up of volatile pressures necessary to cause tensile fracture and failure of wallrocks and formation of calderas and ash-flow tuffs. In this context, it is noteworthy that there is little to no evidence for the existence of a caldera related to the eruption of the Kalamazoo tuff although its source region can be fairly well defined (Gans et al, 1989; Grunder pers. comm., 1989).

CHAPTER FOUR: PETROGENESIS OF METALUMINOUS VOLCANIC ROCKS OF THE EGAN RANGE VOLCANIC COMPLEX

This chapter concerns the phenocryst mineral chemistry and the major, trace, and isotope geochemistry of high-K, metaluminous volcanic rocks in the Egan Range volcanic complex. These data indicate that crustal melting, magma mixing, and crystal fractionation processes, in varying proportions, are responsible for the compositional diversity of these rocks.

Analytical Techniques

Most major and trace element analyses were done by X-ray fluorescence using a Rigaku 3370 spectrometer in the laboratory of Dr. Peter Hooper at Washington State University, Pullman. Powdered samples were fused into disks with lithium tetraborate flux in a ratio of flux:rock of 2:1. Data are normalized to 100% because totals are systematically high (>100% at high SiO_2). Normalized values agree well with data for some duplicates analyzed in other laboratories (U.S.G.S. Denver and Stanford University). Precision on major elements is estimated at better than 1% (one-sigma S.D.) except for FeO, MnO, P_2O_5, MgO, and Na_2O ($\leq$ 3%). For trace elements, one-sigma S.D. values are estimated as better than 2 to 10%. Analyses of Ni are regarded only as semiquantitative because of low Ni concentrations.

REE, Cs, Th, U, Sc, Hf, Ta, Cr, and Co are reported in ppm and were acquired by instrumental neutron activation analysis (INAA) following the procedure outlined by Laul (1979). Sample powders were prepared by grinding in an alumina ceramic shatterbox for five minutes. Aliquots of sample powders weighing 0.5-1.0 g were irradiated at 1 megawatt for 6 hours with equivalent volumes of U.S.G.S. and in-house standards SRM 1633A, CRB II, and SPG #1 at the O.S.U. Triga reactor facility.

Gamma ray spectra were collected on Adcam 918 multichannel analyzers coupled with Ge(Li) crystal gamma ray detectors. Two counts, one week after irradiation and one month after irradiation, were preformed to acquire data on the various isotopes. Raw data were reduced via Ortec EG&G software supplied with the analyzers. All recognized interferences were corrected for. Estimated precision is better than 5% (one-sigma S.D.) for Sc, Co, Cs, La, Sm, Eu, Tb, Yb, Lu, Hf, Ta, and Th, and 5-15% for Cr, Nd, and V.

Oxygen isotope determinations were preformed at the stable isotope laboratory of Dr. S.M. Wickham at the University of Chicago. Prior to analysis, purified separates of plagioclase, sanidine, and quartz were treated with dilute hydrofluoric acid for 2 to 3 minutes to remove any alteration products. An error of $\pm$ 0.2 permil is estimated for $\delta^{18}O$.

Sr and Nd isotope determinations were preformed in the laboratory of Dr. G.L. Farmer at the University of Colorado, Boulder. Pb isotope determinations were preformed by Dr. James Wright in the the laboratory of John Wooden at the U.S.G.S., Menlo Park. Prior to analysis, whole rock samples were prepared by grinding in a tungsten carbide disk grinder and sieved to obtain a 80-120 mesh size fraction. Samples were treated with dilute hydrofluoric acid for 2 to 3 minutes to remove any

alteration products. Errors are estimated to be $\pm$ 0.00001 for Sr and Nd isotope ratios (two-sigma), and 0.1% for Pb isotope ratios (one-sigma).

Chemical analyses of phenocrysts from Egan Range volcanic complex samples were preformed using JEOL 733 electron microprobes at the University of Washington, and Stanford University. Beam diameters used were 5 microns and 20 microns at the University of Washingtion and Stanford University, respectively. Operating conditions on both instruments were an accelerating potential of 15 kv, a sample current of 15 na, and counting times of 20 seconds. Natural and synthetic minerals close in composition to the unknowns were used as standards. Replicate analyses of standards were preformed at the beginning and end of each analytical session and were in excellent agreement with previously determined values. Data were corrected for matrix interferences via the Bence Albee method (1968) at the University of Washington, and via the ZAF method at Stanford University.

Mineral Chemistry

Feldspar

Plagioclase is ubiquitous in Egan Range volcanic complex lavas; in most flows it is the most abundant crystalline phase. Sanidine occurs in rhyodacites and it has also been observed in early group andesite sample Mt8760. The distribution of core compositions and zoning trends of plagioclase in individual samples and map units (Figures 14a and b) suggest that magma mixing played a major role in the petrogenesis of these lavas.

Rocks of the early group have at least two populations of plagioclase phenocryst cores in all bulk compositions (Table 3a): (1) calcic cores (An81-An70), and (2) a relatively sodic population (An46 to An31). Calcic cores are riddled with irregularly shaped melt inclusions indicating disequilbruim with the enclosing magma. In rhyodacites they are mantled by euhedral, more sodic overgrowths (An56-An48). Sodic cores in rhyodacites are relatively unzoned; in andesites and dacites they are surrounded by cloudy or strongly reversely zoned rims (An65-An80). High calcium contents of these rims relative to liquid indicate that they are not equilibrium compositions. More likely, they represent diffusion controlled nonequilibrium growth compositions. Experimental
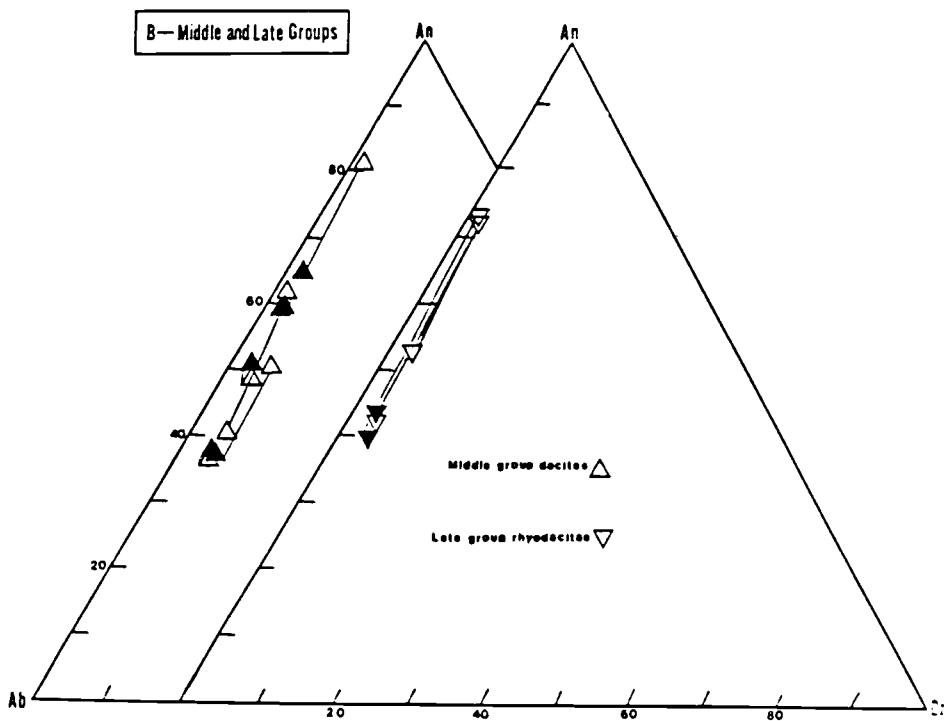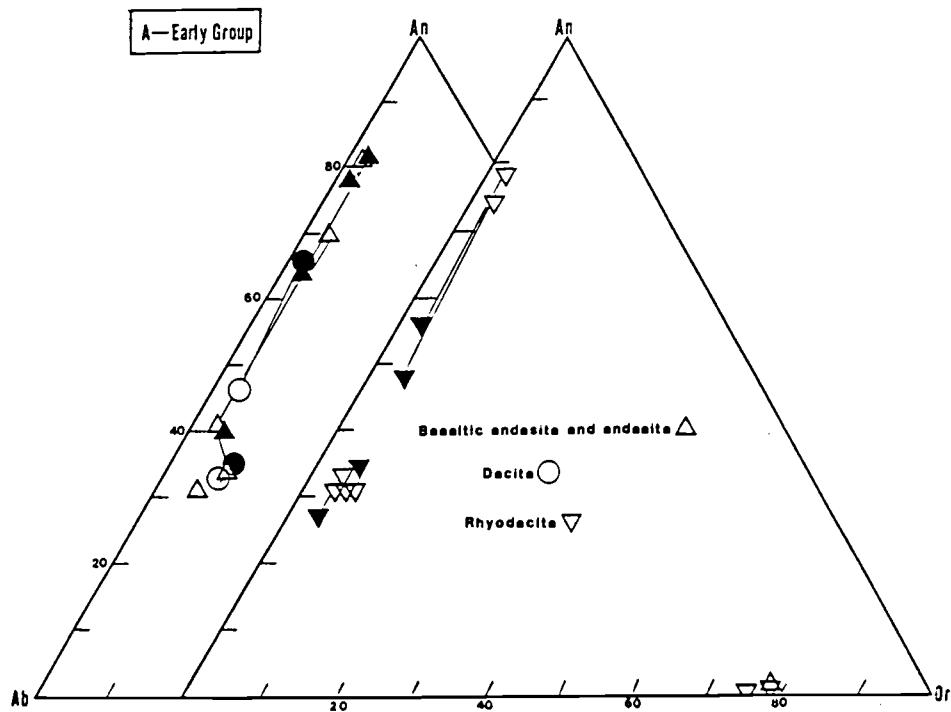
Figures 14 A and B. Ternary projections of feldspar compositions of the Egan Range volcanic complex. Each point represents an analysis. Open symbols are cores and non-zoned compositions; filled are rim compositions. Tie lines connect core and rim of individual crystals.

Table 3e: Representative analyses of plagioclase in early group lavee.

Sample	Mt8787		Mt8787		Mt8749		Mt872		Mt872		Mt8786	
Type	NA*		NA		BA		HD		HD*		HRD*	
Strat. Unit	Tvs		Tvs		Tvel		Tvel		Tvel		Tvel	
	"Core	Rim	Core	Rim	Core	Rim	Core	Rim	"Core	Rim	Core	Rim
SiO2	48.2	48.9	60.0	58.1	52.7	52.0	59.8	59.9	56.1	51.4	48.7	54.1
Al2O3	33.1	32.5	24.8	26.3	28.0	29.8	24.9	24.8	27.2	30.4	31.5	28.9
FeO*	0.40	0.40	0.21	0.20	0.65	0.42	0.17	0.20	0.26	0.40	0.43	0.35
CaO	16.09	15.65	6.73	8.67	13.44	12.87	7.17	7.27	9.66	13.33	15.47	11.29
Na2O	1.97	2.27	6.52	6.54	2.23	3.77	7.17	7.00	5.70	3.65	1.96	4.65
K2O	0.13	0.15	1.26	0.88	1.08	0.41	1.42	1.13	0.76	0.30	0.36	0.48
BaO	0.06	0.12	1.03	0.07	0.17	0.04	0.00	0.00	0.07	0.00	0.03	0.11
SrO	0.11	0.11	0.00	0.00	0.06	0.02	0.00	0.03	0.00	0.00	0.04	0.03
Total	100.07	100.15	100.56	100.73	98.47	99.39	100.65	100.41	99.86	99.48	98.59	100.03
An	81.2	78.4	33.6	40.2	70.3	63.8	33.8	34.2	46.3	65.7	79.6	55.7
Ab	18.0	20.6	58.9	54.9	23.7	33.8	59.4	59.5	49.4	32.5	18.3	41.5
Or	0.8	0.9	7.5	4.9	5.9	2.4	7.7	6.3	4.3	1.8	2.2	2.8

Sample	Mt8786		Mt876		Mt876		Mt8760		Mt8760
Type	HRD		HRD*		HRD		NA*		NA
Strat. Un	Tvel		Tvel		Tvel		Tvel		Tvel
	Core	Rim	Core	Rim	Core	Rim	Core	Rim	Unzoned
SiO2	59.4	61.2	49.9	55.7	60.3	60.0	58.7	47.6	61.2
Al2O3	25.3	24.0	31.8	27.7	24.8	25.1	26.0	33.0	24.4
FeO*	0.18	0.13	0.36	0.33	0.16	0.23	0.26	0.39	0.14
CaO	7.21	5.94	15.02	10.13	6.66	7.27	8.60	16.82	6.55
Na2O	7.50	8.49	2.70	5.46	7.48	7.01	6.48	1.97	7.42
K2O	0.65	0.82	0.27	0.77	0.93	1.04	0.65	0.09	0.98
BaO	0.00	0.00	0.12	0.05	0.04	0.16	0.06	0.01	0.05
SrO	0.00	0.00	0.06	0.11	0.00	0.04	0.15	0.00	0.08
Total	100.31	100.58	100.23	100.28	100.33	100.86	101.00	99.71	100.78
An	33.4	26.7	74.3	48.4	31.3	34.3	40.8	80.3	36.0
Ab	63.0	68.9	24.2	47.2	63.5	59.8	35.6	17.0	63.5
Or	3.6	4.4	1.5	4.4	5.2	5.8	3.6	2.7	5.5

* is plagioclase phenocryst with sieved core

An = mole fraction of CaAl2Si2O8, Ab = mole fraction of NaAlSi3O8, Or = mole fraction of KAlSiO8

"indicates composition used in models involving crystal fractiontion.

NA = hybrid andesite, BA = basaltic andesite, HD = hybrid dacite, HRD = hybrid rhyodacite

Table 3b: Representative analyses of plagioclase in middle and late group lavas

Sample	Mt8712		Mt8712		Mt8712		Mt8743		Mt8743		Mt8743	
Type	*Vd		Vd*		Vd		Dd		Dd		Dd*	
Strat. Unit	Tvm1		Tvm1		Tvm1		Tvm3		Tvm3		Tvm3	
	Core	Rim	Core	Rim	Core	Rim	Core	Rim	Core	Rim	Core	Rim
SiO2	58.7	52.9	48.2	52.3	52.1	52.7	59.2	58.6	58.5	57.8	56.6	55.2
Al2O3	25.5	29.2	32.6	29.9	29.0	28.8	25.5	25.6	25.7	25.8	27.6	28.1
FeO*	0.20	0.22	0.42	0.51	0.30	0.35	0.26	0.12	0.11	0.20	0.30	0.29
CaO	7.93	12.03	16.48	13.35	11.90	11.72	7.47	7.72	7.48	7.78	9.55	10.04
Na2O	5.94	4.36	2.01	3.83	3.98	4.30	6.73	6.50	6.51	6.32	5.11	4.99
K2O	0.74	0.29	0.18	0.37	0.32	0.32	0.77	0.81	0.85	0.64	0.64	0.46
BaO	0.05	0.08	0.03	0.01	0.01	0.00	0.02	0.00	0.06	0.03	0.02	0.02
SrO	0.18	0.18	0.33	0.27	0.37	0.26	0.01	0.15	0.04	0.00	0.21	0.16
Total	99.34	99.28	100.38	100.70	98.07	98.52	99.98	99.50	99.33	98.59	99.94	99.34
An	40.5	59.4	81.0	64.4	61.1	59.0	36.3	37.8	36.8	38.9	48.8	51.2
Ab	55.0	38.9	17.9	33.4	37.0	39.1	59.2	57.5	58.1	57.2	47.3	46.0
Or	4.5	1.7	1.1	2.1	1.9	1.9	4.5	4.7	5.1	3.8	3.9	2.8

Sample	Mt8765		Mt8765		Mt8765		
Type	Vrd		Vrd*		Vrd*		
Strat. Unit	Tvu3		Tvu3		Tvu3		
	Core	Rim	"Core	Rim	Core	Middle	Rim
SiO2	49.1	56.0	56.7	56.9	53.4	49.2	55.7
Al2O3	31.9	25.9	26.7	26.6	28.1	31.7	26.8
FeO*	0.47	0.35	0.29	0.26	0.29	0.31	0.30
CaO	13.66	7.88	8.06	8.25	10.55	13.89	8.77
Na2O	2.56	6.14	5.73	5.63	4.81	2.70	5.86
K2O	0.13	0.63	0.60	0.66	0.50	0.18	0.55
BaO	0.00	0.08	0.00	0.04	0.07	0.00	0.06
SrO	0.22	0.38	0.12	0.27	0.25	0.00	0.25
Total	98.10	97.46	98.20	98.70	98.02	98.01	98.28
An	74.0	39.9	42.1	42.9	53.1	73.1	43.8
Ab	25.1	56.3	54.2	54.6	43.8	25.7	52.9
Or	0.9	3.8	3.7	2.5	3.0	1.2	3.3

* is plagioclase phenocryst with sieved core
An = mole fraction of CaAl2Si2O8, Ab = mole fraction of NaAlSi3O8, Or = mole fraction of KAlSi3O8
"indicates composition used in models involving crystal fractionation.
Vd = vitrophyric dacite, DD = devitrified dacite, Vrd = vitrophyric rhyodacite

Table 3c: Analyses of sanidine in early group lavas

Sample Type Strat. Unit	Mt876 Nrd Tve1		Mt8786 Nrd Tve1	Mt8760 Na Tve1	
	Core	Rim	Core	Core	Rim
SiO_2	64.1	64.4	65.6	65.5	65.9
Al_2O_3	18.7	18.6	18.3	18.3	18.3
FeO*	0.09	0.12	0.08	0.08	0.03
CaO	0.19	0.12	0.11	0.20	0.19
Na_2O	2.23	2.80	2.96	2.28	2.12
K_2O	13.07	14.42	14.45	13.23	13.37
BaO	2.38	2.22	0.23	0.68	0.46
SrO	0.14	0.10	0.05	0.01	0.04
Total	100.98	102.8	101.77	100.34	100.4
An	1.0	0.6	0.5	1.0	1.0
Ab	20.4	22.7	23.6	20.5	19.2
Or	78.6	76.8	75.9	78.4	79.8

An = mole fraction of $CaAl_2Si_2O_8$, Ab = mole fraction of $NaAlSi_3O_8$,

Or = mole fraction of $KAlSiO_8$

studies on the chemical interaction between a melting oligoclase xenocryst and molten basalt indicate that Na_2O rapidly diffuses from the oligoclase xenocryst into basaltic melt while CaO is preferentially incorporated into the feldspar (Watson, 1982). Thus, in intermediate magmas, highly calcic overgrowths (e.g., $\geq$ An75; Ussler and Glazner, 1989) surrounding resorbed sodic plagioclase cores strongly suggest derivation from more silicic magmas, and the rim compositions may not reflect equilibrium compositions (Watson, 1982). The clear, unzoned character of the sodic plagioclase phenocrysts in the rhyodacites suggests that they may be in equilibrium with the liquid and that the silicic mixing endmember may be a similar composition.

In addition to plagioclase, rhyodacites contain euhedral to subhedral, unzoned sanidine phenocrysts with high Or components which reflect the high-K nature of the Egan Range magmas (Table 3c). A resorbed sanidine grain of similar composition was found in one andesite (Mt8760; Table 3c, Figure 14a). Sanidine has not been observed in any other early group andesites or dacites, possibly due to the vulnerability of alkali-feldspar to dissolution in hybrid magmas (Glazner et al., 1988). The sanidine grain in the andesite indicates that this magma represents a mixture of a mafic magma and a silicic magma similar in

composition to the early group rhyodacites. Furthermore,
sanidine phenocrysts in the rhyodacites and sample Mt8760
contain inclusions of euhedral sodic plagioclase crystals
which are similar in composition to sodic plagioclase
cores from all early group units (Table 3a). Thus, the
rhyodacite composition may represent a mixing endmember
for the entire early group. In contrast, the high An
component of the calcic cores suggests that the mafic
endmember was relatively primitive.

Cores and rims of plagioclase phenocrysts from two
units of the middle group (Tvm$_1$: Mt8712; Tvm$_3$: Mt8743)
also display variable core textures and the compositional
range is similar to the range observed in early group
magmas (Table 14b). However, unlike the early group, rim
compositions are relatively homogeneous within individual
samples. For example, rims of plagioclase in sample
Mt8712 are zoned normally in a grain with a clear calcic
core (An81 to An64) but reversely in a grain with a sieved
sodic core (An40 to An60; Figure 14b, Table 3b). A
euhedral, clear crystal of plagioclase is unzoned and has
the same composition as the rims that surround the sieved
grains (Table 3b). The convergence of rim compositions to
an intermediate composition is consistent with growth
following mixing of mafic and silicic magmas.
Analogously, the similar chemical composition of the

euhedral fresh grain indicates that it grew after mixing.

Plagioclase compositional zoning trends in late group sample Mt8765 (unit Tvl_3) are similar to middle group samples. Phenocrysts cores have a large compositional range (An74-An42), again suggesting mixing of mafic and silicic magmas (Table 3b). Rims have a narrow compositional range, however, indicating they were precipitated following the mixing event. Core textures are not correlated with compositional zoning profiles; both unzoned and strongly zoned grains may have sieved cores (Table 3b).

The bimodal plagioclase core populations, strong reverse and normal zoning of overgrowths, and resorption of phenocryst cores are common features in presumed hybrid magmas (Dungan, 1987). Rim compositions of plagioclase in early group samples are distinctly different and probably represent nonequilibrium growth compositions. In contrast, plagioclase rims in middle and late group samples have a narrow compositional range and are similar to unzoned grains. These rims and unzoned phenocrysts are interpreted as post-mixing phases. Plagioclase zoning trends indicate that early group magmas were erupted shortly after a magma mixing event and were unable to crystallize equilibrium compositions. Middle and late group magmas may have had a longer residence time in

crustal magma chambers following mixing and therefore were able to precipitate equilibrium composition rims and small phenocrysts.

Pyroxenes

Representative electron microprobe analysis of pyroxene phenocrysts in Tables 4a and b are normalized to 100% because of consistently low analyzed totals (97% to 98.5%) in unknowns analyzed at the Stanford University laboratory. Analysis of standards were, however, close to 100% and in excellent agreement with previously determined values. The low totals are therefore thought to reflect poor sample polish and do not indicate systematic bias of specific elements. Analyses were recalculated according to Lindsley (1983) and are plotted on Figures 15a and b. Clinopyroxene in early group samples have 7.5-10% of the non-quadrilateral components tschermakite + acmite + jadeite.

Clinopyroxene is the most abundant pyroxene in early group basaltic andesite, and is subequal or subordinate to orthopyroxene in dacites through rhyodacites. Clinopyroxene in all early group magmas is augite with low $FeO*/FeO*+MgO$ (and high Cr_2O_3) cores. Compositional
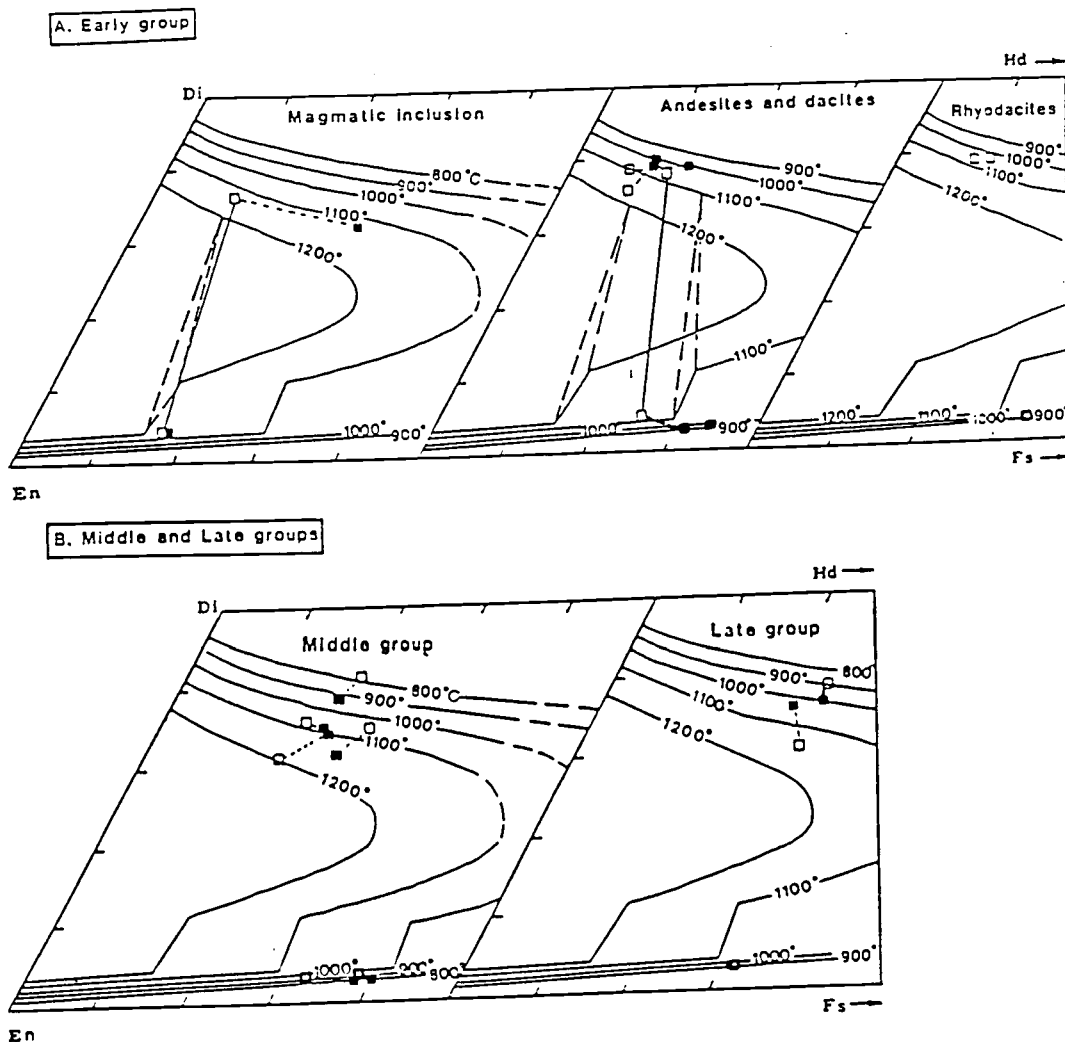
Figures 15 A and B. Pyroxene compositions for Egan Range
    volcanic complex rocks. Each point represents
    an analysis. Compositions recalculated
    according to Lindsley (1983) and plotted
    relative to the isotherms determined by the
    same. Open symbols are core and non-zoned
    compositions; filled are rim compositions.
    Solid lines connect coexisting cpx-opx
    equilibrium pairs. Dashed lines connect core
    and rim of individual crystals.

Table 4a: Representative analyses of pyroxene in early group lavas

Clinopyroxene

Sample	Mt8787		Mt8787		Mt8749		Mt872		Mt876	
Type	Ha		Ha		Ba		Kd		Nrd	
Strat. Unit	Tves		Tves		Tve1		Tve1		Tve1	
	*Core	Rim	Core	Rim	Core	Rim	Core	Rim	*Core	Rim
SiO2	53.7	50.8	52.3	51.8	53.4	47.8	53.0	52.7	51.9	51.8
Al2O3	2.0	3.7	2.2	2.6	1.6	1.9	1.8	2.2	2.7	2.6
FeO*	4.05	9.17	6.45	6.57	5.34	18.39	6.03	6.58	7.53	6.43
MgO	18.03	14.80	16.83	16.65	18.74	13.78	18.78	17.23	16.39	16.83
MnO	0.15	0.20	0.18	0.17	0.14	0.36	0.17	0.18	0.18	0.17
TiO2	0.24	0.70	0.41	0.49	0.18	0.99	0.25	0.40	0.44	0.42
CaO	20.92	20.37	21.28	21.23	19.68	16.15	19.02	20.28	20.48	21.06
Na2O	0.25	0.27	0.19	0.22	0.27	0.38	0.27	0.25	0.24	0.21
Cr2O3	0.74	0.03	0.23	0.26	0.63	0.04	0.67	0.18	0.12	0.48
Si IV	1.953	1.891	1.925	1.912	1.948	1.858	1.937	1.935	1.918	1.910
Al IV	0.047	0.109	0.075	0.089	0.052	0.090	0.063	0.065	0.082	0.090
Al VI	0.036	0.052	0.019	0.026	0.016	..	0.016	0.029	0.035	0.023
Fe	0.123	0.285	0.199	0.202	0.163	0.596	0.184	0.202	0.233	0.198
Mg	0.976	0.823	0.924	0.915	1.019	0.796	1.023	0.943	0.902	0.925
Ca	0.814	0.812	0.840	0.838	0.769	0.670	0.744	0.797	0.810	0.832
Na	0.017	0.020	0.013	0.015	0.019	0.028	0.018	0.017	0.017	0.015
Mn	0.004	0.006	0.006	0.005	0.004	0.012	0.005	0.006	0.005	0.005
Ti	0.006	0.020	0.011	0.013	0.005	0.029	0.007	0.011	0.012	0.012
Cr	0.021	0.001	0.007	0.007	0.018	0.001	0.019	0.006	0.003	0.014
% Quad	92.60	90.00	92.12	90.70	92.00	91.20	91.41	92.22	90.77	90.37
Wo	39.1	39.2	38.3	41.0	37.2	32.2	35.8	39.4	39.4	39.3
En	53.9	46.7	49.6	49.3	55.4	39.1	56.1	51.0	49.8	51.9
Fs	7.0	14.1	12.1	9.7	7.4	28.7	8.1	9.6	10.8	8.8

Orthopyroxene

Sample	Mt8787		Mt8749		Mt872	Mt8786
Type	Ha		Ba		Kd	Nrd
Strat. Unit	Tves		Tve1		Tve1	Tve1
	Core	Rim	Core	Rim	Core	Core
SiO2	51.7	52.5	54.3	54.5	51.1	52.2
Al2O3	3.3	1.6	2.2	2.1	2.5	1.5
FeO*	17.51	20.32	11.86	11.22	22.13	21.64
MgO	24.46	23.42	28.97	29.64	22.03	22.42
MnO	0.36	0.51	0.23	0.19	0.35	0.55
TiO2	0.37	0.25	0.21	0.18	0.36	0.28
CaO	2.32	1.40	1.99	1.87	1.46	1.35
Na2O	0.03	0.02	0.03	0.04	0.02	0.02
Cr2O3	0.03	0.03	0.24	0.29	0.08	0.02
Si IV	1.895	1.943	1.933	1.934	1.912	1.945
Al IV	0.105	0.057	0.067	0.066	0.088	0.054
Al VI	0.036	0.012	0.024	0.021	0.020	0.013
Fe	0.537	0.629	0.353	0.333	0.692	0.674
Mg	1.337	1.293	1.538	1.569	1.228	1.244
Ca	0.091	0.055	0.076	0.071	0.059	0.054
Na	0.002	0.001	0.002	0.003	0.002	0.002
Mn	0.011	0.016	0.007	0.006	0.011	0.017
Ti	0.010	0.007	0.006	0.005	0.010	0.008
Cr	0.001	0.001	0.007	0.008	0.002	0.001
% Quad	92.87	96.06	95.17	95.21	94.04	96.24
Wo	5.1	3.0	3.9	3.6	3.0	2.7
En	70.0	66.2	78.2	79.5	62.1	63.1
Fs	24.9	30.8	18.0	16.9	34.9	34.2

Analyses normalized to 100% using total Fe as FeO
Wo, En, and Fs calculated according to Lindsley (1983).
Structural formula calculated using 6 oxygens; Fe as Fe2+.
*indicates composition used in models involving crystal fractionation.

Table 4b: Representative analyses of pyroxene in middle and late group lavas

Clinopyroxene

Sample	Mt8712		Mt8712		Mt8743		Mt8743		Mt8765		Mt8765	
Type	Vd		Vd		Od		Od		Vrd		Vrd	
Strat. Unit	Tvm1		Tvm1		Tvm3		Tvm3		Tvl3		Tvl3	
	Core	Rim	Core	Rim	Core	Rim	Core	Rim	*Core	Rim	Core	Rim
SiO2	52.5	50.2	53.4	51.5	52.8	53.3	52.0	51.5	51.8	51.3	49.6	53.0
Al2O3	3.2	4.6	2.9	3.8	1.2	2.4	2.0	2.4	1.3	1.1	2.2	1.5
FeO*	9.00	10.58	8.54	10.27	13.73	11.54	12.08	11.42	14.50	15.08	17.79	12.91
CaO	20.35	19.55	18.18	19.65	18.50	18.16	20.01	19.87	19.26	20.19	17.20	18.98
MgO	14.25	13.40	16.64	13.76	12.60	13.41	12.89	13.67	11.58	11.27	11.12	12.41
MnO	nd	nd	nd	nd	0.66	0.45	0.34	0.42	0.61	0.68	0.62	0.56
TiO2	0.25	0.77	0.27	0.65	0.22	0.42	0.27	0.42	0.19	0.23	0.06	0.30
Na2O	0.35	0.40	0.07	0.37	0.28	0.32	0.37	0.25	0.37	0.23	1.34	0.30
Cr2O3	nd	nd	nd	nd	0.03	..	..	..	..	..	..	..
Si IV	1.945	1.892	1.955	1.916	1.995	1.982	1.961	1.936	1.974	1.816	1.821	1.994
Al IV	0.055	0.108	0.045	0.084	0.005	0.018	0.039	0.064	0.026	0.045	0.102	0.006
Al VI	0.086	0.092	0.080	0.084	0.047	0.089	0.050	0.041	0.032	..	..	0.059
Fe	0.279	0.331	0.262	0.320	0.433	0.359	0.381	0.359	0.462	0.447	0.576	0.404
Mg	0.786	0.745	0.908	0.763	0.709	0.743	0.725	0.765	0.657	0.595	0.642	0.696
Ca	0.807	0.781	0.713	0.784	0.748	0.724	0.808	0.800	0.801	0.766	0.713	0.765
Na	0.026	0.029	0.005	0.026	0.020	0.023	0.027	0.018	0.027	0.016	0.100	0.022
Mn	nd	nd	nd	nd	0.017	0.014	0.011	0.014	0.020	0.012	0.020	0.018
Ti	0.007	0.022	0.007	0.018	0.006	0.012	0.010	0.012	0.011	0.006	0.002	0.008
Cr	nd	nd	nd	nd	0.001	..	..	..	..	..	..	..
% Quad	88.70	87.66	85.24	88.88	93.21	89.90	92.35	92.43	93.00	93.63	70.01	90.79
Wo	36.0	34.5	31.6	35.0	35.0	31.8	41.8	38.7	38.7	36.7	30.8	35.6
En	47.2	45.4	53.0	45.8	40.3	46.0	38.2	42.3	36.0	37.9	43.6	41.1
Fe	16.8	20.1	15.4	19.2	24.6	22.2	20.1	18.9	25.3	25.4	25.6	23.3

Orthopyroxene

Sample	Mt8712		Mt8743		Mt8765
Type	Vd		Od		Vrd
Strat. Unit	Tvm1		Tvm3		Tvl3
	Core	Rim	Core	Rim	Core
SiO2	53.7	52.7	53.7	53.4	52.7
Al2O3	0.9	1.5	1.5	1.1	1.5
FeO*	23.70	24.78	21.64	23.37	20.42
CaO	1.54	1.31	1.35	1.19	1.40
MgO	19.97	19.48	20.93	20.07	23.26
MnO	nd	nd	0.73	0.72	0.42
TiO2	0.12	0.12	0.18	0.18	0.29
Na2O	..	0.10	..	0.01	..
Cr2O3	nd	nd	..	..	..
Si IV	2.008	1.984	1.993	1.998	1.950
Al IV	..	0.016	0.007	0.002	0.499
Al VI	0.041	0.048	0.058	0.045	0.016
Fe	0.741	0.779	0.672	0.732	0.632
Mg	0.119	1.092	1.317	1.120	1.283
Ca	0.062	0.053	0.054	0.048	0.056
Na	..	0.007	..	0.001	..
Mn	nd	nd	0.022	0.023	0.013
Ti	0.003	0.003	0.002	0.005	0.008
Cr	nd	nd	..	..	..
% Quad	95.52	93.76	93.47	94.70	93.35
Wo	3.1	2.7	2.6	2.5	2.8
En	58.2	56.8	64.5	59.0	65.7
Fa	38.5	40.5	32.9	38.5	31.5

Analyses normalized to 100% using total Fe as FeO
nd = element not analysed for
Wo, En, and Fs calculated according to Lindsley (1983).
Structural formula calculated using 6 oxygens; Fe as Fe2+.
*indicates composition used in models involving crystal fractionation.

zoning with respect to FeO*/FeO*+MgO is normal and is usually 8-9 mole% $MgSiO_3$, except for an equant augite phenocryst in a magmatic inclusion (sample Mt8749) which decreases by 25 mole% $MgSiO_3$. This decrease is accompanied by a decrease in Cr, and increases in Ti, Mn, Al, and Na. CaO contents of rims are similar or higher than in cores (Table 4a). The association of high CaO rims and high MgO (and Cr_2O_3) cores suggests that primitive magmas may have mixed with cooler, silicic magmas.

Clinopyroxene in the middle and late group samples are augite (Table 4b) and are distinct in composition from augite in early group magmas; FeO*/FeO*+MgO values are higher and MgO (and Cr_2O_3) contents are lower (Table 4b). In addition, augites in the middle and late group rocks have greater, up to 30%, and more variable proportions of nonquadrilateral components (Table 4b).

Distribution of core compositions and zoning patterns of phenocrysts are diverse and they provide a great deal of information about the crystallization history of these lavas. Sample Mt8712 (map unit Tvm_1) contains augite with bimodal core compositions of $Wo_{36}En_{47}Fs_{17}$ and $Wo_{32}En_{53}Fs_{15}$; rims that surround these cores converge on an intermediate composition ($Wo_{35}En_{45}Fs_{20}$; Table 4b, Figure 15b). Analogous to plagioclase zoning trends, these zoning profiles

suggest that this sample represents a mixed magma and that the phenocryst rims grew subsequent to the mixing event. In contrast, augite in sample Mt8743 (map unit Tvm_3) have slightly Mg-rich rims. These Mg-rich rims may result from an increase in magmatic fO_2, which in turn, may reflect a pre-eruptive influx of water, as suggested for pyroxenes in pre-1961 hornblende andesites from Volcan Colima, Mexico (Luhr and Carmichael, 1980). The proportion of Fe_2O_3 to FeO is increased in the magma, which results in an increased Mg/Fe^{2+} ratio (Luhr and Carmichael, 1980).

Cores of two clinopyroxenes in late group sample Mt8765 have widely separated compositions of $Wo_{31}En_{44}Fs_{25}$ and $Wo_{39}En_{36}Fs_{25}$ (Figure 15b). Both phenocrysts are zoned to rim compositions intermediate between the two cores (Figure 15b). These relations are thought to reflect pre-eruptive mixing of hot, basic magma and cooler silicic magma because zoning involves only changes in the WO component while the FeO*/FeO*+MgO ratio remains relatively constant. Thus, zoning trends are not due to closed system crystallization nor due to changes in the oxidation state of the magma.

In contrast to clinopyroxene, orthopyroxene in the basaltic andesite magmatic inclusion (sample Mt8749) is unzoned and has a greater EN component relative to more evolved magmas. The core of this phenocryst appears to be

in equilibrium with coexisting clinopyroxene (Figure 15b).
The apparent crystallization temperature of the cores of
these coexisting pyroxenes is approximately 1170°c. This
temperature is consistent with the relatively primitive
major element composition of this sample.

Compositions of orthopyroxene in an early andesite
and dacite range from En70 to En62 (Figure 15a).
Orthopyroxene in the andesite (Mt8787) is more magnesium
than in the dacite (Mt872), appears to be in equilibrium
with coexisting clinopyroxene (Figure 15a), and yields an
approximate crystallization temperature of 1100°c. The
single orthopyroxene grain analyzed in the early group
dacite sample (Mt872) is not in equilibrium with
coexisting clinopyroxene.

Orthopyroxene core compositions in middle group
dacite and late group rhyodacite are more magnesian than
orthopyroxene cores in early group rhyodacites (Table
15b). They do not appear to be in equilibrium with
coexisting clinopyroxene.

Amphibole and Biotite

Structural formulae of amphiboles (Table 5) were
calculated based on 23 oxygens, and Fe_2O_3 was calculated
as the average Fe_2O_3 value by the method of Spear and
Kimball (1984). Because amphibole compositions have

Table 5:   Representative analyses of amphibole from the Egan Range volcanic complex lavas

Sample Type Strat. Unit	Mt872 Hd Tve1		Mt8786 Hrd Tve1		Mt8786 Hrd Tve1		Mt876 Hrd Tve1		Mt8712 Vd Tvm1		Mt8712 Vd Tvm1	
	Core	Rim	Core	Rim	Core	Rim	Core	Rim	"Core	Rim	Core	Rim
SiO2	41.3	41.7	42.0	42.2	42.1	43.3	42.4	42.6	41.7	43.2	42.4	42.9
TiO2	3.38	3.13	2.56	2.71	3.13	2.20	3.22	2.73	2.94	2.13	3.10	2.83
Al2O3	12.0	11.7	11.5	11.0	11.5	10.1	11.4	11.5	11.8	9.6	11.4	11.0
FeO	11.42	9.73	14.56	12.54	14.61	16.72	12.42	10.11	9.55	17.26	5.81	9.14
Fe2O3	1.96	3.94	0.94	4.28	0.25	1.12	1.48	4.09	5.03	3.30	6.74	4.58
MgO	13.39	12.90	11.84	10.87	12.13	10.97	12.67	12.63	12.05	8.45	13.11	12.92
CaO	11.41	11.56	11.44	11.17	11.20	10.92	11.19	11.09	11.43	10.75	11.05	11.09
Na2O	1.98	2.22	1.69	1.73	1.88	1.72	1.81	1.82	0.81	1.78	1.95	1.95
MnO	0.16	0.17	0.21	0.25	0.21	0.28	0.16	0.22	0.33	0.37	0.14	0.24
K2O	2.29	1.92	1.40	1.75	1.03	1.41	1.01	1.58	1.32	1.08	1.24	1.25
Cl	0.02	0.03	0.03	0.06	0.03	0.07	0.02	0.04	0.04	0.10	0.04	0.02
F	0.44	0.27	0.26	0.37	0.33	0.41	0.30	0.27	0.00	0.00	0.00	0.11
Total	99.77	99.31	98.36	99.06	98.39	99.20	98.13	98.70	97.01	97.96	96.92	98.02
O=F,Cl	0.20	0.13	0.12	0.17	0.15	0.19	0.13	0.13	0.01	0.02	0.01	0.50
Total	99.57	99.18	98.24	98.89	98.24	99.20	98.00	98.57	97.00	97.94	96.01	97.52
Si IV	6.050	6.078	6.272	6.237	6.271	6.459	6.260	6.222	6.330	6.384	6.142	6.252
Al IV	1.950	1.922	1.728	1.763	1.729	1.541	1.740	1.778	1.670	1.616	1.858	1.748
Al VI	0.129	0.083	0.292	0.153	0.281	0.235	0.253	0.194	0.439	0.297	0.085	0.141
Fe+2	1.464	1.298	1.820	1.677	1.828	2.126	1.585	1.352	1.296	2.141	0.847	1.241
Fe+3	0.226	0.474	0.105	0.516	0.028	0.129	0.170	0.491	0.226	0.368	0.883	0.560
Mg	2.924	2.828	2.638	2.392	2.691	2.440	2.787	2.747	2.725	2.077	2.832	2.808
Mn	0.020	0.021	0.027	0.031	0.027	0.036	0.021	0.026	0.043	0.032	0.017	0.029
Ti	0.373	0.343	0.287	0.300	0.351	0.247	0.358	0.300	0.335	0.215	0.338	0.310
Sum Oct	5.136	5.046	5.169	5.069	5.205	5.213	5.175	5.110	5.064	5.130	5.002	5.090
Ca	1.793	1.803	1.831	1.767	1.786	1.746	1.771	1.733	1.858	1.753	1.716	1.732
Na (M4)	0.072	0.151	0.000	0.165	0.009	0.041	0.054	0.157	0.079	0.117	0.281	0.179
Na (A)	0.492	0.475	0.491	0.329	0.533	0.456	0.464	0.357	0.159	0.407	0.267	0.373
K (A)	0.429	0.357	0.266	0.330	0.196	0.267	0.191	0.294	0.255	0.232	0.229	0.232
Sum (A)	0.921	0.831	0.757	0.659	0.728	0.724	0.654	0.651	0.414	0.639	0.496	0.605

FE2O3 calculated as the average FE2O3 value by the method of Spear and Kimball (1984)
Structural formula calculated using 23 oxygens
"indicates composition used in crystal fractionation models.

$(Ca+Na)_B > 1.34$ and $Na_B < 0.67$, all are calcic amphiboles
(Leake, 1978). Roughly half the analyses have $(Na+K)_a \geq$
0.50 and $Fe^3 \leq Al^{VI}$, and extend from ferroan pargasitic
hornblende to ferroan pargasite (Leake, 1978). Other
analyses have $Fe^3 > Al^{VI}$ and extend from magnesian
hastingsitic hornblende to magnesian hastingsite (Leake,
1978). Amphibole cores have a restricted range of Mg-
number ($Mg/Mg+Fe^{2+}$ = 0.59-0.77) and rims exhibit a weak
increase or decrease in Mg-number relative to cores.
Amphiboles in dacites are, in general, more Mg-rich
compared to rhyodacites (Table 5).

Analyses of biotite (Table 6) have a fairly restricted
range; biotite in rhyodacite does not appear to differ
appreciably from that in dacite.

Table 6: Representative analyses of biotite from the Egan Range volcanic complex

Sample Type Strat. Unit	Mt8786 Hrd Tve1	Mt876 Hrd Tve1	*Mt8712 Vd Tvm1	Mt8712 Vd Tvm1
SiO2	36.1	35.8	37.3	36.3
Al2O3	13.6	14.0	13.5	13.0
TiO2	3.60	4.78	4.38	5.17
FeO*	22.54	21.60	21.71	22.49
MgO	10.32	10.45	10.52	8.97
CaO	0.01	0.00	0.00	0.00
Na2O	0.40	0.43	0.45	0.43
MnO	0.25	0.17	0.10	0.14
K2O	10.48	10.83	8.88	8.33
Cl	0.06	0.02	0.10	0.12
F	0.62	0.56	0.00	0.20
Total	98.01	98.65	97.00	95.22
O=F,Cl	0.28	0.24	0.02	0.11
Total	97.73	98.41	96.98	95.11
Si IV	5.462	5.379	5.645	5.583
Al IV	2.435	2.478	2.355	2.358
Al VI	--	--	0.059	--
Ti	0.410	0.540	0.499	0.597
Fe+2	2.855	2.713	2.749	2.890
Mn	0.033	0.022	0.013	0.092
Mg	2.328	2.340	2.374	2.055
Sum Oct	5.626	5.615	5.635	5.635
Ca	0.002	--	--	--
Na	0.116	0.124	0.133	0.127
K	2.023	2.076	1.716	1.633
Sum A	2.142	2.200	1.849	1.760

All Fe calculated as FeO. Structural formula calculated using 22 oxygens.
*indicates composition used in crystal fractionation models.

Whole-Rock Chemistry

Magmas erupted in the Egan Range volcanic complex range from high-K basaltic andesite to rhyolite (Tables 7a-c). Classification is on the basis of wt.% SiO_2: basaltic andesite (52-57); andesite (57-63); rhyodacite (68-72); and rhyolite (> 72). Fresh rocks are metaluminous (molar $Al_2O_3/[CaO+K_2O+Na_2O]$ = 0.69 to 1.02), hypersthene normative, and are typical of Paleogene metaluminous volcanic rocks erupted during crustal extension in the northern Basin and Range province (e.g. Gans et al., 1989) and the Rio Grande rift (e.g. the Latir volcanic field; Johnson and Lipman, 1988; Thompson et al., 1986). All rocks lie within the calc-alkaline field on the AFM plot of Irvine and Baragar (Figure 16) and the suite as a whole has an alkali-lime index of 61.5 (Figure 4; Peacock, 1931). Overall, the high-K calcalkaline character of the Egan Range volcanic complex magmas is identical to the composition of volcanic rocks erupted in continental arcs overlying thick crust (e.g., Hildreth and Moorbath, 1988).

Table 7a: Compositions of early group volcanic rocks

Sample #	Mt8749	Mt879	Mt8787	Mt8789	Mt8760	Mt8763	Mt8711	Mt872	Mt8786	Mt876	Mt8735
Type:	MI	MI	DL	DL	DL	DL	VL	DL	VL	DL	P
Strat. Unit	Tvl1	Tvl1	Tves	Tves	Tvl1	Tvl1	Tvl1	Tvl1	Tvl1	Tvl1	Tvesa
XRF Analyses											
SiO2	54.0	56.6	59.6	59.9	61.4	63.2	63.6	65.8	68.1	70.9	70.1
Al2O3	15.3	15.4	15.0	16.0	15.8	15.1	15.7	15.3	15.5	14.4	16.0
FeO*	9.0	7.6	6.5	6.3	6.1	5.4	5.6	5.0	3.6	3.2	2.6
MgO	6.4	5.4	4.9	3.9	3.2	3.3	2.1	2.0	1.0	0.7	1.7
CaO	8.8	8.4	7.1	6.4	5.9	5.7	5.2	4.2	3.2	2.7	3.3
Na2O	2.0	2.1	2.3	2.5	2.7	2.6	2.8	2.8	3.0	3.0	2.4
K2O	2.7	2.9	3.2	3.6	3.7	3.5	3.8	3.9	4.8	4.5	3.3
TiO2	1.20	1.10	0.88	0.93	0.85	0.79	0.83	0.76	0.56	0.48	0.42
P2O5	0.42	0.31	0.28	0.30	0.36	0.25	0.26	0.22	0.19	0.16	0.09
MnO	0.15	0.13	0.12	0.11	0.10	0.09	0.10	0.08	0.06	0.06	0.10
XRF Analyses											
Ni	15	17	24	13	15	16	12	13	7	9	15
V	140	148	143	97	101	109	92	92	62	54	8
Ba	1328	1204	1237	1299	1242	1167	1079	1045	1211	1133	1781
Rb	81	94	112	130	123	123	137	146	186	170	108
Sr	556	574	507	551	490	475	442	390	396	337	454
Zr	201	210	202	225	223	212	226	233	232	198	225
Y	32	30	28	28	30	31	30	30	28	23	23
Nb	21	22	19	23	22	22	23	21	24	23	19
Ga	16	21	18	17	18	20	19	15	19	21	19
Cu	17	13	10	21	8	11	24	16	8	8	17
Zn	94	86	77	82	75	72	81	77	66	77	46
INAA Analyses											
La	41.8	41.2	44.8	53.3	56.0	52.9	52.7	52.2	75.0	70.4	106.0
Ce	80	81	89	104	113	105	102	107	149	135	227
Nd	34	38	35	41	44	42	37	36	46	45	66
Sm	7.6	6.9	7.1	7.7	8.0	7.8	7.4	7.5	9.0	7.9	9.4
Eu	1.9	1.8	1.6	1.7	1.6	1.6	1.6	1.5	1.5	1.3	1.8
Tb	1.0	0.9	0.8	0.8	0.9	1.0	1.0	0.8	0.8	0.7	0.6
Yb	3.0	2.7	2.5	2.7	2.8	2.9	2.6	2.9	2.6	2.1	2.1
Lu	0.43	0.37	0.35	0.35	0.36	0.38	0.35	0.37	0.29	0.26	.22
Sc	25.7	21.5	20.3	15.5	14.6	14.9	13.1	12.0	6.7	5.8	5.3
Cr	282	283	192	64	88	160	75	73	11	8	6
Co	29.0	24.0	23.4	18.0	15.0	15.0	14.5	11.8	6.5	6.0	4.0
Cs	1.7	2.5	3.6	3.2	1.3	3.1	2.3	3.5	3.9	1.4	2.0
Hf	6.5	5.6	6.0	6.1	6.1	6.2	6.5	6.5	6.5	6.3	6.1
Ta	1.0	1.1	1.0	1.2	1.4	1.4	1.2	1.3	1.3	1.4	1.0
Th	9	11	14	17	21	19	18	20	32	32	25
U	2	2	3	3	4	4	2	4	6	5	3

Rock types: MI = magmatic inclusion, DL = devitrified lava, VL = vitrophyric lava, P = pumice
Data normalized to 100% anhydrous

Table 7b: Compositions of middle group volcanic rocks

Sample#	Mt871a	Mt8712	Mt8717	Mt8734	Mt8720	Mt8737	Mt8743	Mt8778
Type:	VC	VL	VL	VL	DL	DL	DL	DL
Strat. Unit	Tvm1	Tvm1	Tvm1	Tvm1	Tvm2	Tvm3	Tvm3	Tvm3
XRF Analyses								
SiO2	65.7	66.3	65.7	66.2	68.5	67.0	67.2	67.7
Al2O3	16.1	15.9	16.1	16.0	15.5	15.9	15.8	15.7
FeO*	4.3	4.2	4.4	4.1	3.5	4.0	3.9	4.0
MgO	1.4	1.3	1.3	1.2	0.8	1.2	1.2	0.9
CaO	4.0	3.8	3.9	3.7	2.7	3.2	3.2	3.2
Na2O	2.9	3.1	3.2	3.1	3.3	3.2	3.2	3.4
K2O	4.7	4.5	4.3	4.7	4.8	4.6	4.6	5.1
TiO2	0.65	0.65	0.69	0.65	0.54	0.63	0.62	0.61
P2O5	0.21	0.21	0.23	0.23	0.20	0.20	0.21	0.21
MnO	0.07	0.07	0.07	0.07	0.06	0.05	0.06	0.04
XRF Analyses								
Ni	7	11	9	10	9	9	10	8
V	74	70	73	72	45	55	57	46
Ba	1207	1217	1246	1452	1217	1277	1265	1262
Rb	163	167	162	166	162	175	173	181
Sr	428	414	425	409	321	376	373	354
Zr	220	231	225	233	230	232	230	231
Y	27	29	27	28	30	28	27	28
Nb	22	24	23	23	25	23	23	22
Ga	21	19	21	21	20	22	19	21
Cu	14	17	10	17	12	13	15	20
Zn	71	73	67	78	67	67	63	67
INAA Analyses								
La	64.6	-	64.8	66.3	72.4	-	66.1	67.9
Ce	113	-	126	136	145	-	138	129
Nd	47	-	41	46	43	-	50	47
Sm	8.2	-	8.3	8.2	8.2	-	8.4	8.1
Eu	1.5	-	1.5	1.6	1.4	-	1.5	1.4
Tb	0.8	-	0.8	0.9	0.8	-	0.8	0.8
Yb	2.7	-	2.7	2.7	2.8	-	2.8	2.5
Lu	0.31	-	0.32	0.33	0.30	-	0.31	0.32
Sc	8.1	-	9.1	8.7	5.6	-	7.5	7.1
Cr	12	-	9	11	8	-	11	9
Co	8.5	-	8.5	8.5	6.0	-	7.5	7.0
Cs	3.4	-	3.2	3.5	3.2	-	3.9	2.8
Hf	6.3	-	6.2	6.9	6.3	-	6.8	6.2
Ta	1.3	-	1.3	1.5	1.7	-	1.4	1.4
Th	28	-	27	30	37	-	31	29
U	6	-	5	6	6	-	6	6

Rock Types: VC = vitroclastic lava, VL = vitrophyric lava, DL = devitrified lava
Data normalized to 100% anhydrous.

108

Table 7c: Compositions of late group volcanic rocks

Sample # Type: Strat. Unit	Mt8781 L Tvl1	Tf872 L Tvl2	Mt8764 L Tvl2	Mt8759 D Tvl2	Mt8765 VL Tvl3	Mt8775 DL Tvl3	Mt8791b DL Tvl3	Mt8791c DL Tvl3	Mt8791d DL Tvl3
XRF Analyses									
SiO2	66.0	58.4	58.0	57.3	69.6	68.3	69.7	69.2	69.0
Al2O3	16.5	17.1	17.0	16.5	15.5	15.8	15.5	15.5	15.6
FeO*	4.1	7.6	7.6	7.8	2.8	3.3	2.8	3.2	3.2
MgO	0.9	2.6	3.0	3.8	0.5	0.5	0.5	0.4	0.5
CaO	3.2	6.2	6.4	7.2	2.3	2.5	2.1	2.2	2.3
Na2O	3.4	2.9	2.9	2.6	3.1	3.5	3.3	3.4	3.4
K2O	5.1	3.6	3.4	3.1	5.6	5.3	5.4	5.4	5.3
TiO2	0.70	1.18	1.17	1.18	0.45	0.51	0.46	0.48	0.49
P2O5	0.21	0.45	0.43	0.38	0.11	0.15	0.12	0.15	0.14
MnO	0.04	0.11	0.12	0.11	0.06	0.07	0.03	0.06	0.07
XRF Analyses									
Ni	10	12	5	13	14	10	9	10	10
V	46	170	177	170	19	27	17	24	30
Ba	1520	1253	1245	1219	1257	1346	1273	1309	1320
Rb	214	138	124	110	224	216	225	225	224
Sr	459	550	553	530	292	347	289	305	316
Zr	251	256	260	273	287	290	291	286	285
Y	33	32	35	36	36	33	34	35	35
Nb	23	22	21	22	28	27	26	26	25
Ga	22	21	18	21	17	19	18	17	18
Cu	8	8	11	24	9	5	5	14	9
Zn	67	88	85	92	57	60	59	81	72
INAA Analyses									
La	58.5	55.0	55.2	57.7	75.9	69.1	-	-	71.3
Ce	116	108	108	107	149	142	-	-	143
Nd	44	42	50	49	49	42	-	-	54
Sm	8.1	8.3	8.4	8.7	9.3	8.4	-	-	8.9
Eu	1.7	2.0	2.0	2.0	1.5	1.6	-	-	1.5
Tb	0.8	1.0	1.0	1.1	1.0	0.9	-	-	1.0
Yb	2.9	3.1	3.4	3.6	3.8	3.3	-	-	3.5
Lu	0.40	0.44	0.46	0.50	0.46	0.43	-	-	0.47
Sc	9.0	16.1	17.0	19.9	5.3	6.2	-	-	6.1
Cr	-	6	17	41	3	2	-	-	4
Co	5.1	19.0	20.8	24.1	3.1	-	-	-	3.9
Cs	13.9	6.6	2.9	1.8	4.4	4.2	-	-	5.1
Hf	7.0	7.0	6.7	7.2	8.2	8.4	-	-	8.4
Ta	1.3	1.1	1.0	1.0	1.5	1.5	-	-	1.5
Th	23	14	13	13	34	30	-	-	30
U	5	3	2	2	7	6	-	-	6

Rock types: L = lava, D = dike, VL = vitrophyric lava, DL = devitrified lava
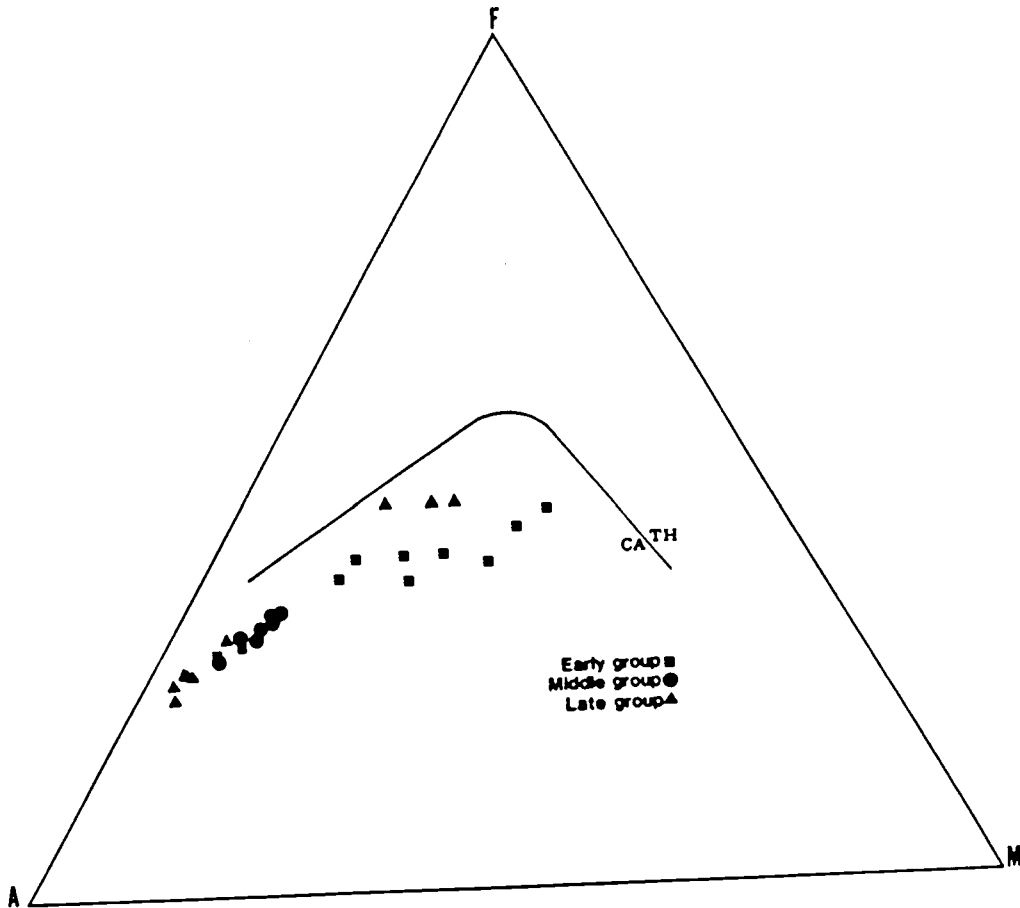Data normalized to 100% anhydrous

Figure 16. AFM diagram with calc alkaline-tholeiitic divide from Irvine and Barager (1971).

Early Group

In the early group correlations between elements, whether major or trace, are linear, which suggests that intermediate composition magmas originated through two-component mixing of basaltic and silicic endmembers (Figures 17 and 18). Gaps in silica content appear to be present between 56.5% and 59.6% SiO2 and 65.8% and 68.1% SiO_2, but these may be an artifact of incomplete sampling. MgO, FeO*, TiO_2, CaO, MnO, and P_2O_5 decrease, and Na_2O and K_2O increase with increasing SiO_2. Al_2O_3 remains constant. Although K_2O and Na_2O contents are fairly high and rocks are often strongly oxidized, variation diagrams show little scatter (Figure 17), which indicates that magmatic compositions have not been strongly effected by alteration. Basaltic andesite magmatic inclusions are the only rocks with SiO_2 contents less then 57% and are among the most mafic Oligocene volcanic rocks present in east-central Nevada. Their small volume is consistent with observations that mafic volcanic rocks are relatively rare in Paleogene synextensional volcanic terranes in the western United States (Johnson and Lipman, 1988; Thompson et al., 1986, Gans et al., 1989; Wernicke et al., 1987). Where detailed stratigraphic relations are known, these
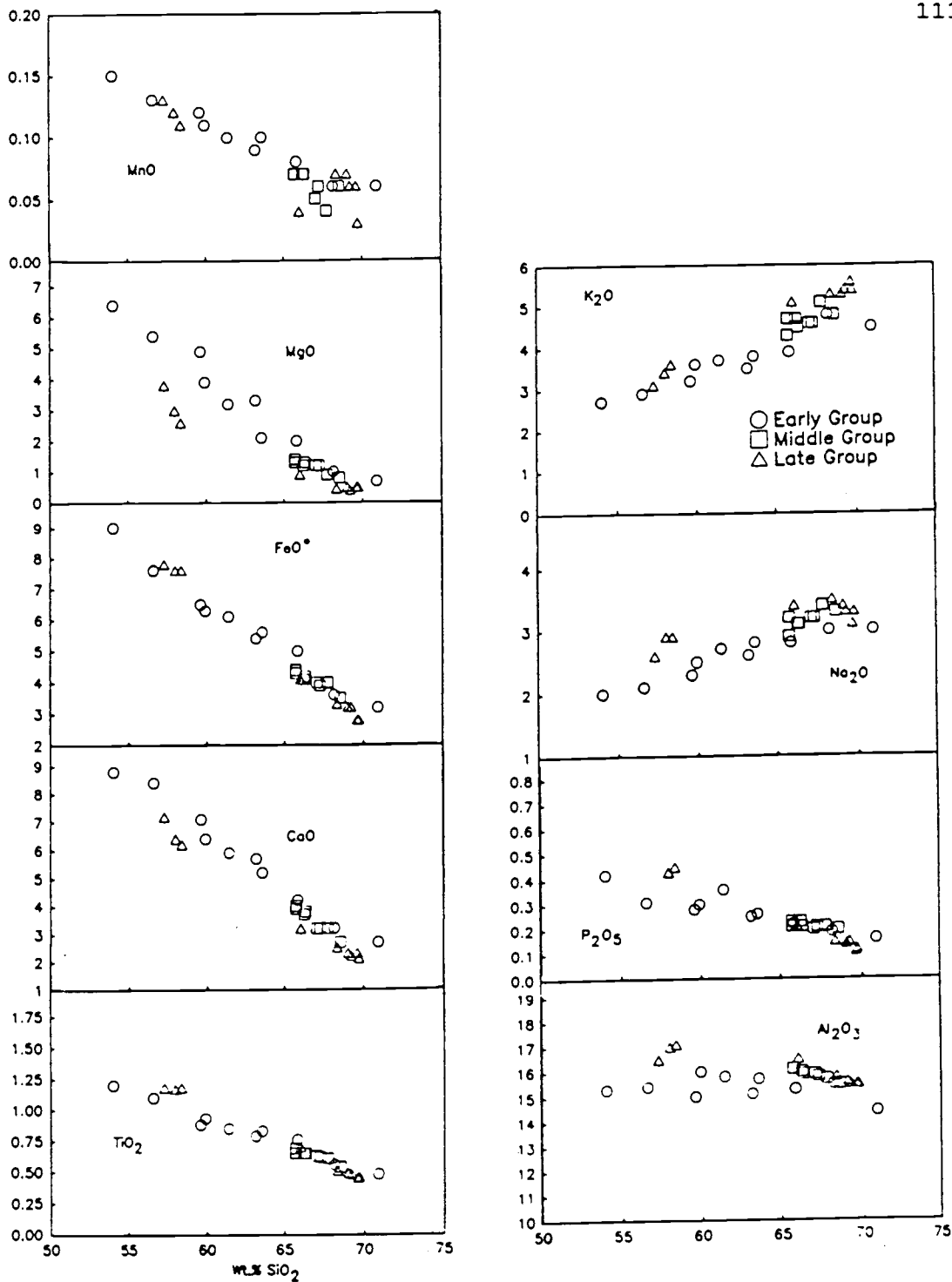
Figure 17. Variation of major elements versus wt.% SiO_2 for volcanic rocks from the Egan Range volcanic complex. Data are normalized to 100% anhydrous.
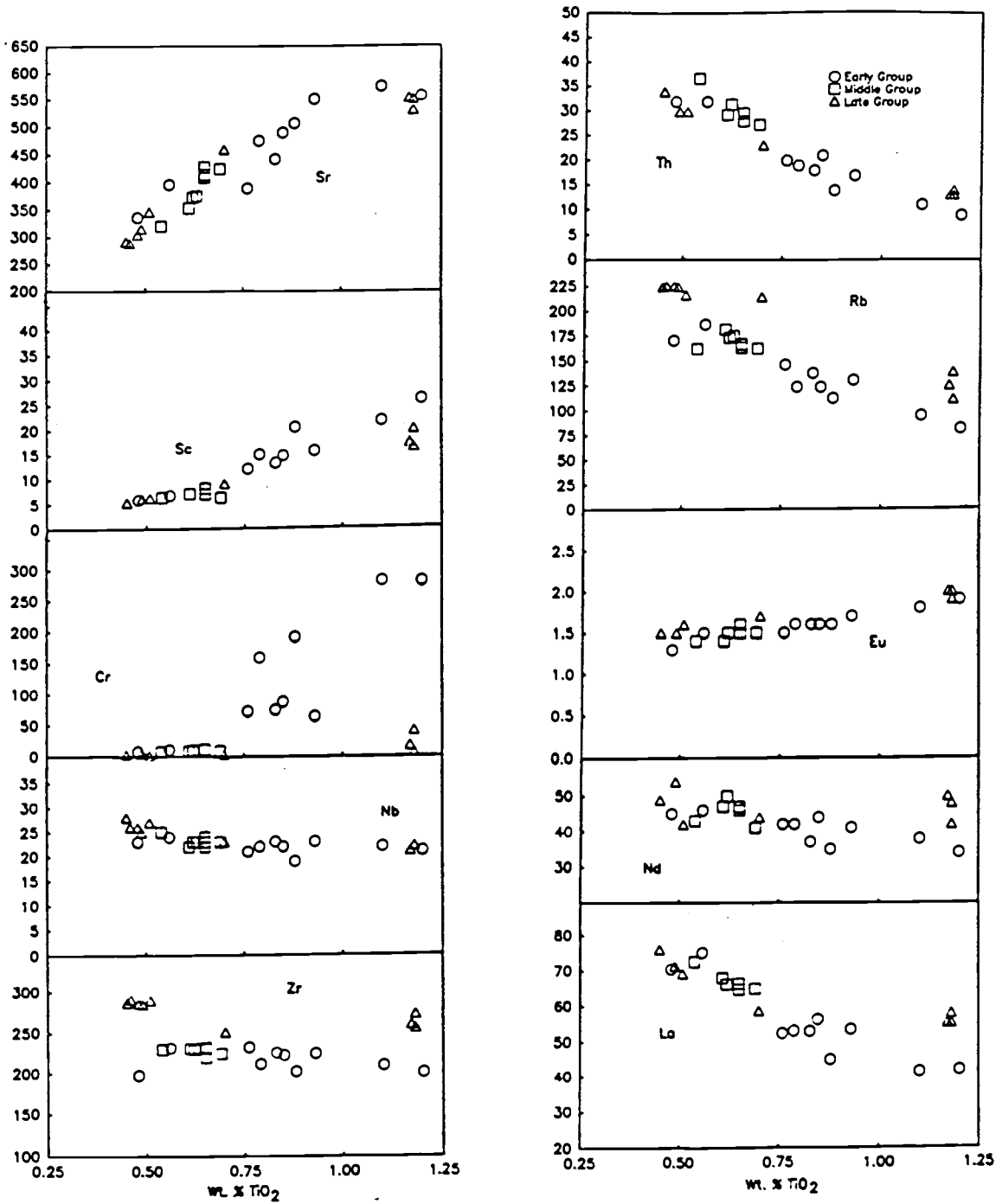
Figure 18. Variation of trace elements versus wt.% TiO$_2$ for volcanic rocks from the Egan Range volcanic complex.

magmas are typically among the oldest volcanic rocks in a given section (Gans et al., 1989; Johnson and Lipman, 1988).

Trace-element variation diagrams (Figure 18) are plotted versus TiO_2 because TiO_2 is strongly correlated with SiO_2, and its interlaboratory analytical precision is much better than that of SiO_2. Incompatible elements (e.g. Rb, Ba, U, Th) are highly enriched in basaltic andesites through dacites, although elements compatible to major phenocryst phases (Cr, Sc, Sr) are also highly elevated. This feature has been previously ascribed to open system processes in which mafic and silicic magma mix to form hybrid intermediate composition magmas (McMillian, 1984; Bacon, 1986; McMillian and Dungan, 1988;). For the early group as a whole the compatible elements Cr, V, Sc, Co, and Sr decrease while incompatible elements Rb, Th, and U increase with decreasing TiO_2. Y, Ba, and the high field strength elements (HFSE) Zr, Hf, Nb, and Ta, display little to no variation with increasing differentiation.

Rare earth element (REE) variations within the early group are illustrated in Figure 19. All magmas are strongly light rare earth element (LREE) enriched with LREE values from 134 to 240 and heavy rare earth element (HREE) values about 13 to 9 times chondrites. LREE enrichment becomes more pronounced with increasing
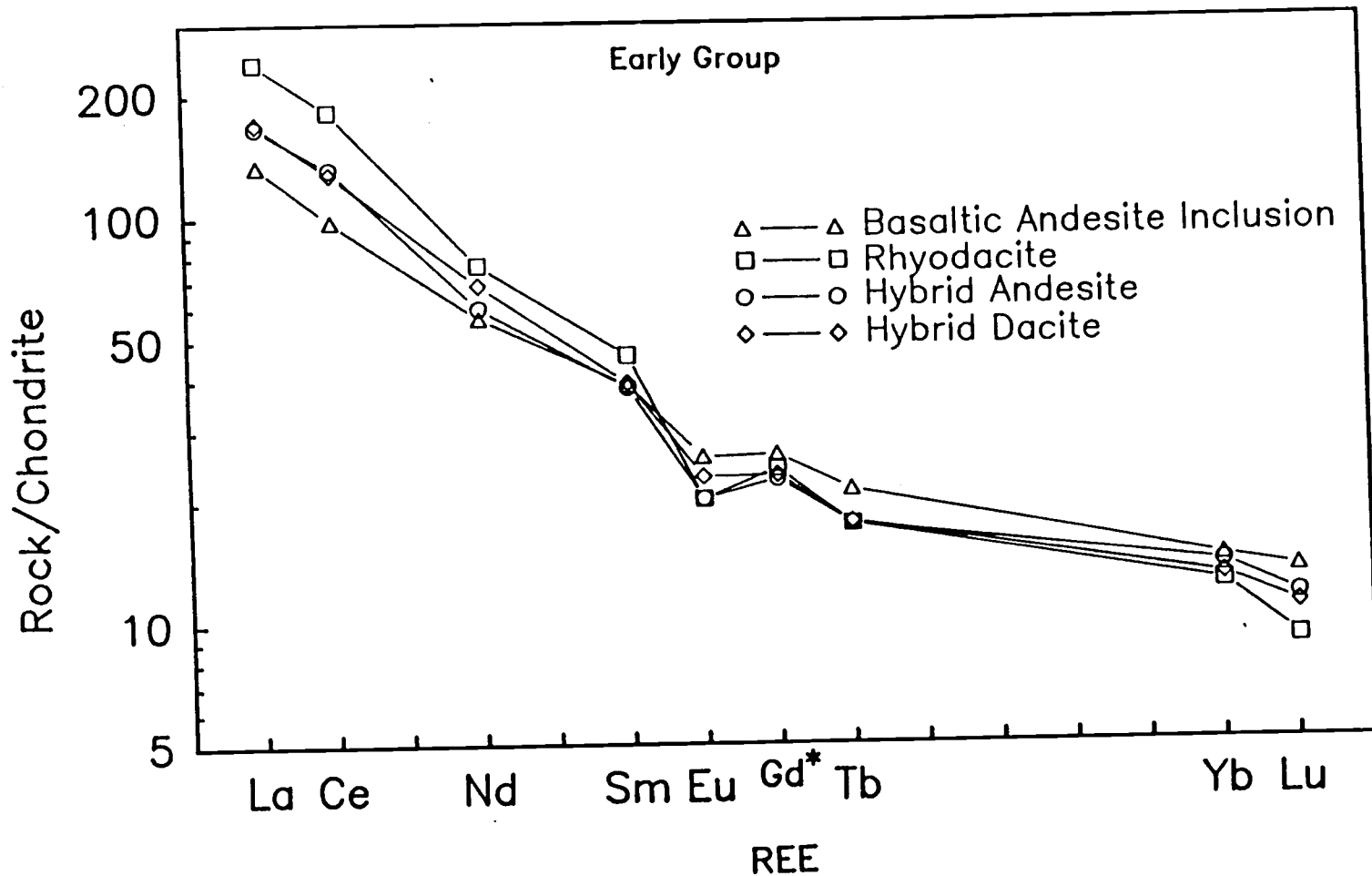
Figure 19. Chondrite-normalized abundances of rare-earth elements for select early group samples. Rare-earth element contents of chondrite are C-1 non-volatile abundances from Anders and Ebihara (1982). Gd* is interpolated between Sm and Tb.

differentiation. Negative Eu anomalies are moderate
(Eu/Eu* = .78-.55) and increase with increasing
differentiation. In addition, with increasing
differentiation, HREE become progressively depleted
resulting in a fanning set of patterns with the fulcrum
between Sm and Eu (Figure 19). Decreasing TiO_2 content in
the early group corresponds to increasing La/Lu_n (9.9_{mafic}
to $26.7_{silicic}$).

Middle Group

The middle group dacites and rhyodacites form a
coherent package of compositions that fill the gap in SiO_2
content between 65.8-68.1 of the early group (Table 7b;
Figure 17). These rocks are slightly lower in MgO, FeO*,
and TiO_2 than early group rocks of comparable SiO_2
content, and higher in K_2O and Al2O3. The rhyodacite of
Tvm_2 is virtually identical to an early group rhyodacite
(Mt8786) except for slightly lower CaO.

An important distinction between the early and middle
group dacites and rhyodacites is the significantly lower
Cr, Sc, and Co concentrations in the middle group rocks
(Figure 18). These depletions suggest that clinopyroxene
may have fractionated. Y, Ba, and the HFSE
concentrations display little to no variation with

increasing differentiation and are similar to early group rocks.

REE patterns of the middle group dacites and rhyodacites are similar in shape to REE patterns of the early group rocks although they occupy an intermediate position (Figure 20). Consistent with major-element variations, La/Lu$_n$ (21.6$_{dacite}$ to 25$_{rhyodacite}$) and Eu/Eu* (0.60$_{dacite}$ to 0.57$_{rhyodacite}$) fill the gap defined by early group magmas. These features suggest that mixing of magmas similar in major and trace element composition to early group magmas played an important role in the petrogenesis of the middle group.

Late Group

Lavas of the late group comprise a bimodal suite of fine grained biotite dacites and rhyodacites with 66 to 69 wt.% SiO$_2$ and subordinate fine-grained pyroxene ($\pm$ olivine) andesites with 57 to 58% SiO$_2$ (Table 7c). These lavas plot at a lower alkali-lime index (approximately 58) than the slightly calcic early and middle group rocks.

The late group andesites (Tvl$_2$) are distinguished by higher TiO$_2$, FeO*, Na$_2$O, Al$_2$O$_3$, P$_2$O$_5$, V, Zr, and Y, and lower MgO, Mg#, CaO, and Cr relative to andesites of similar SiO$_2$ content in the early group (Tves; Mt8787, Mt8789). LREE are strongly fractionated (La/Sm$_n$ =
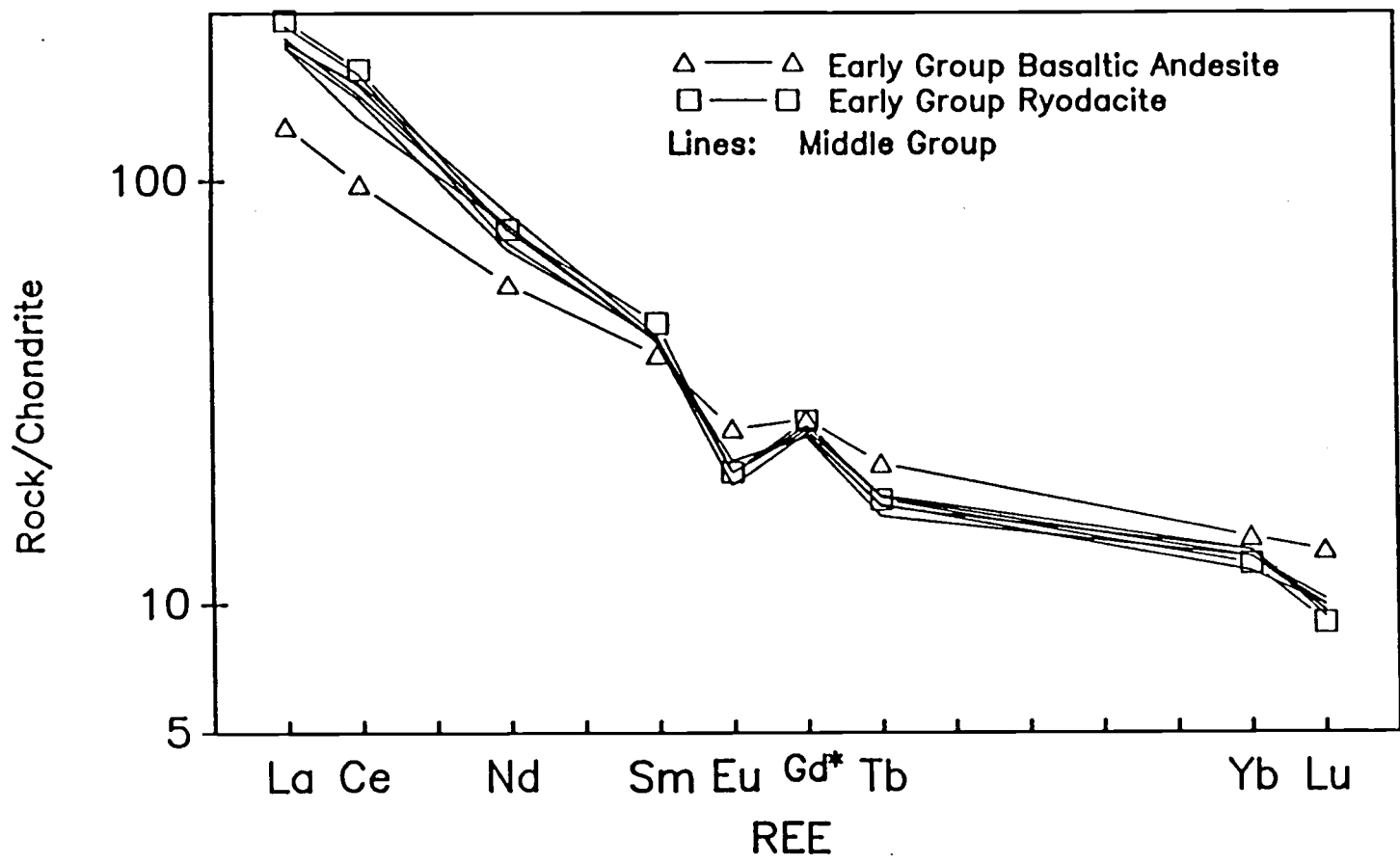
Figure 20. Chondrite-normalized abundances of rare-earth elements for select middle group samples shown relative to an early group basaltic andesite (Mt8749) and rhyodacite (Mt8786). Rare-earth contents of chondrite are C-1 non-volatile abundances from Anders and Ebihara (1982). Gd* is interpolated between Sm and Tb.
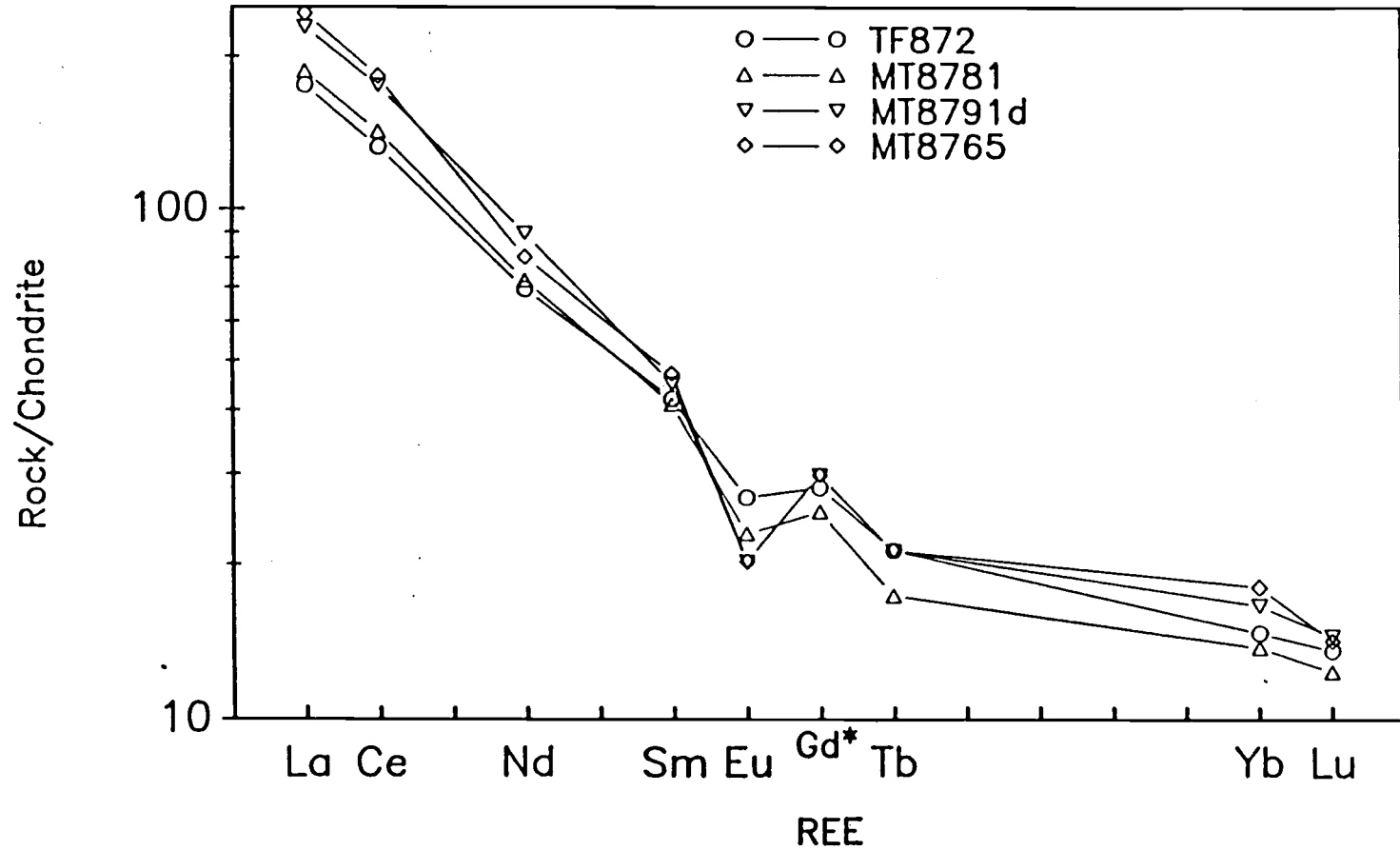
Late Group

Figure 21. Chondrite-normalized abundances of rare-earth elements for select late group samples. Rare-earth contents of chondrite are C-1 non-volatile abundances from Anders and Ebihara (1982). Gd* is interpolated between Sm and Tb.

4.2), HREE are slightly fractionated (Tb/Lu_n = 1.5) and Eu anomalies are moderate ($Eu/Eu*$ = 0.77; Figure 21). LREE contents are similar to early group andesites, although MREE and HREE of the late group andesites are slightly elevated.

Tvl_3 rhyodacites are relatively homogeneous in major- and trace-element composition (Table 7c). At similar SiO_2 contents Tvl_3 dacites and rhyodacites are more potassic, as well as enriched in incompatible element contents, particularly Rb, Zr, and Hf, and depleted in MgO, CaO, Sr and slightly in TiO_2 when compared to early group rhyodacites. Rhyodacites have LREE and MREE contents that are virtually identical to early and middle group rhyodacites (compare Mt8786 versus Mt8765).

Isotopes

Sr, Nd, Pb, and O isotope compositions for a limited number of Egan Range volcanic complex samples are in Table 8. The whole rock initial $^{87}Sr/^{86}Sr$ ratios of early group rocks range from 0.71149 (andesite) to 0.71235 (rhyodacite) and are correlated positively with 1/Sr and SiO_2 (Figures 22 and 23). At equivalent SiO_2 content, initial Sr isotope ratios for the middle and late groups are higher than those for the early group and may indicate that the crustal contaminant of the former was generated

Table 8: Isotopic compositions of Egan Range volcanic complex rocks

Sample	Rock Type	$\delta^{18}O$‰	$^{87}Sr/^{86}Sr_i$	εNd_i	$^{206}Pb/^{204}Pb$	$^{207}Pb/^{204}Pb$	$^{208}Pb/^{204}Pb$
Early group							
Mt8749	MIba	--	--	--	19.134	15.738	39.872
Mt8787	Da	qtz 10.2, 10.1, 9.9 plag 8.7, 8.8, 8.8	0.71149	-14.83	19.325	15.728	39.751
Mt8763	Da	--	0.71203	-15.92	--	--	--
Mt8786	Vrd	sanidine 8.6, 8.4	0.71235	-17.89	--	--	--
Middle group							
Mt8743	Dd	plag 8.3, 8.1, 8.3 qtz 9.9	0.71292	-19.47	--	--	--
Late group							
Mt8765	Vrd	plag 7.8	0.71449	-20.13	19.08	15.783	40.274
Mt8764	Aa	--	0.71274	-15.92	--	--	--

Estimated error on $\delta^{18}O$ is 0.1 permil. Estimated error on Pb isotopes is 0.1%.

Errors on Sr and Nd isotopes are +1 in last digit reported.

Rock types: MIba = basaltic andesite magmatic inclusion; Da = devitrified andesite; Vrd = vitrophyric rhyodacite; Dd = devitrified dacite; Aa = aphyric andesite.
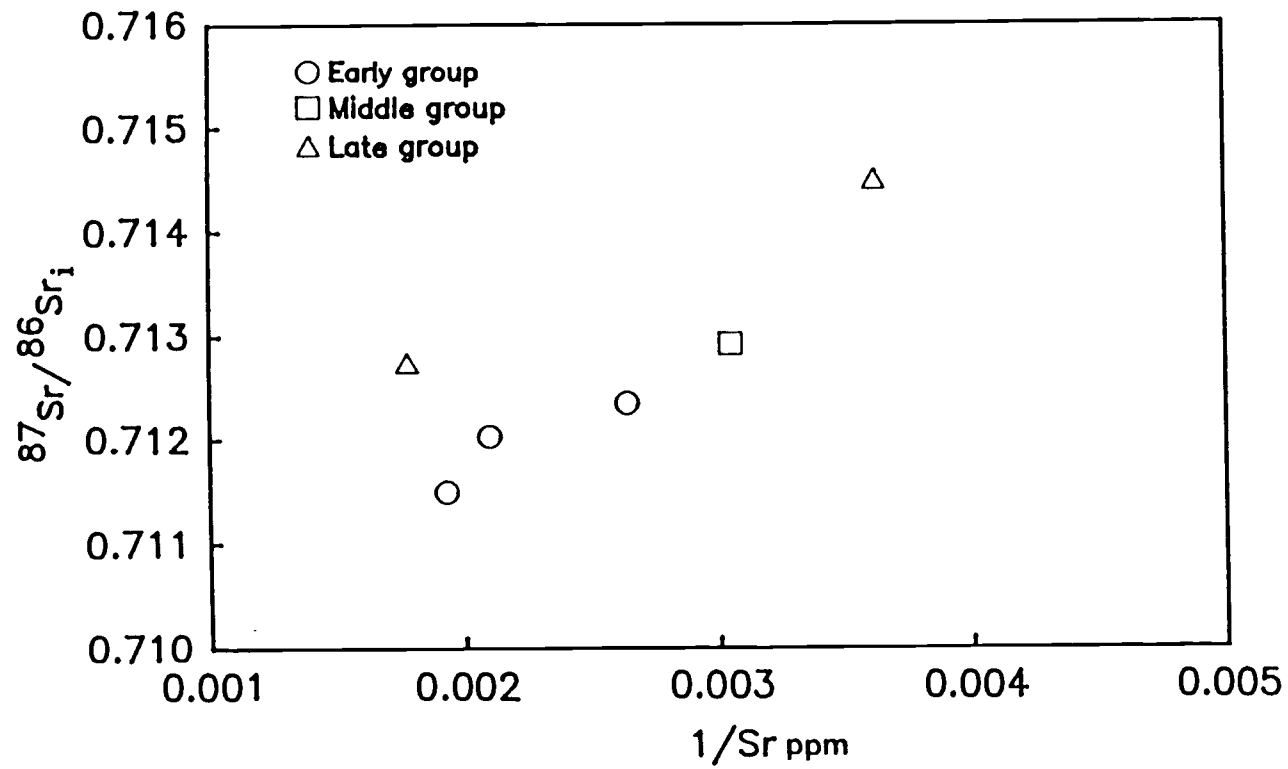
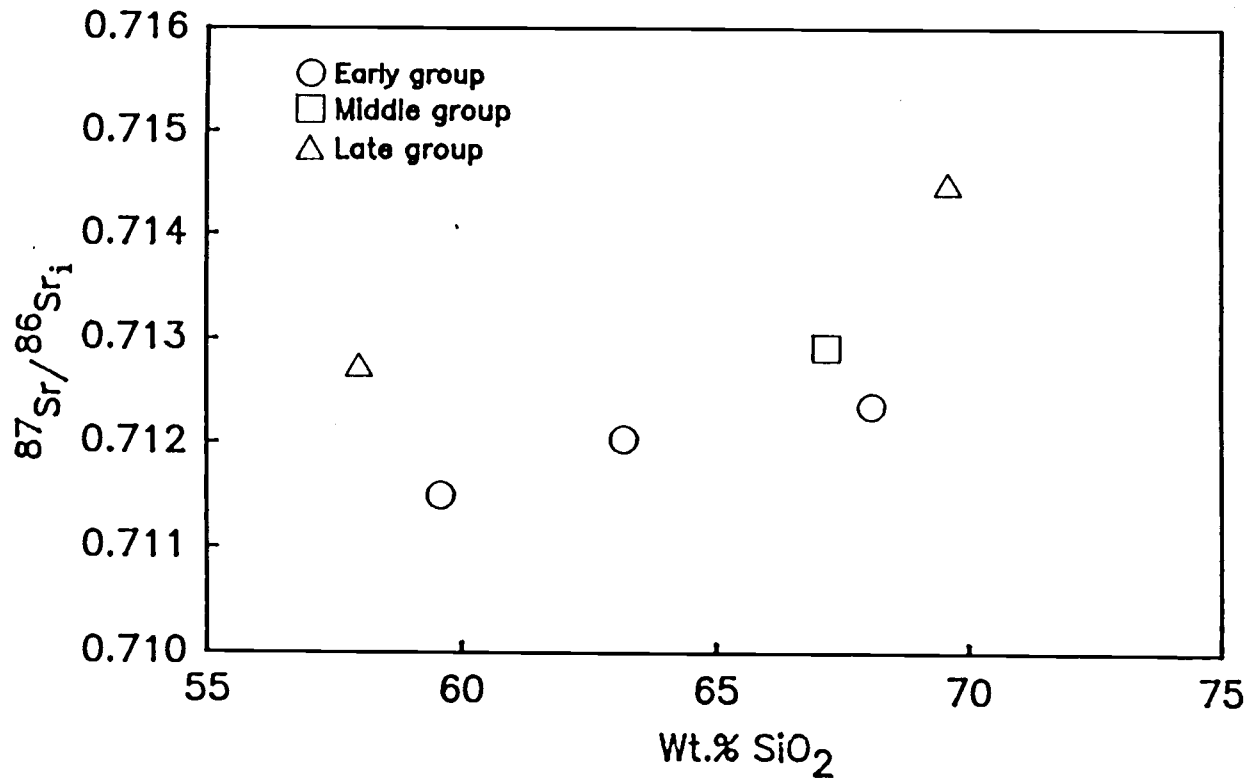Figure 22. Variation of initial $^{87}Sr/^{86}Sr$ versus 1/Sr for Egan Range volcanic complex magmas.

Figure 23. Variation of initial $^{87}Sr/^{86}Sr$ versus SiO_2 for Egan Range volcanic complex magmas.

at deeper (older) crustal levels (Grunder and Feeley, 1989). Initial $^{143}Nd/^{144}Nd$ ratios (ϵNd = -14.46 to -19.71) become less radiogenic with increasing SiO_2 (Figure 24), and middle and late group magmas have ϵNd less radiogenic than early group magmas at equivalent SiO_2 content.

The range in initial Pb isotope ratios is more restricted than that of Sr and Nd ratios and they do not vary systematically with differentiation (Table 8). All ratios are highly radiogenic ($^{206}Pb/^{204}Pb$ = 19.08, $^{207}Pb/^{204}Pb$ = 15.78-15.763, $^{208}Pb/^{204}Pb$ = 39.751-40.274).

$\delta^{18}O$ values of magmas from the Egan Range volcanic complex range from 7.8 to 8.8‰ (Table 8) and are similar to those of most silicic volcanic rocks (Taylor, 1968). In this study, plagioclase $\delta^{18}O$ values are considered to represent magmatic values, because the fractionation between plagioclase and melt in intermediate composition volcanic rocks is negligible (Grunder, 1987). Quartz, on the other hand, has a strong tendency to concentrate ^{18}O relative to magma at a given temperature (Epstein and Taylor, 1967). This tendency is reflected in $\delta^{18}O$ values 1.5 to 1.6‰ higher in quartz complared to $\delta^{18}O$ in coexisting plagioclase (Figure 25). Small, yet analytically significant differences in $\delta^{18}O$ exist among different stratigraphic groups. In general, $\delta^{18}O$ of
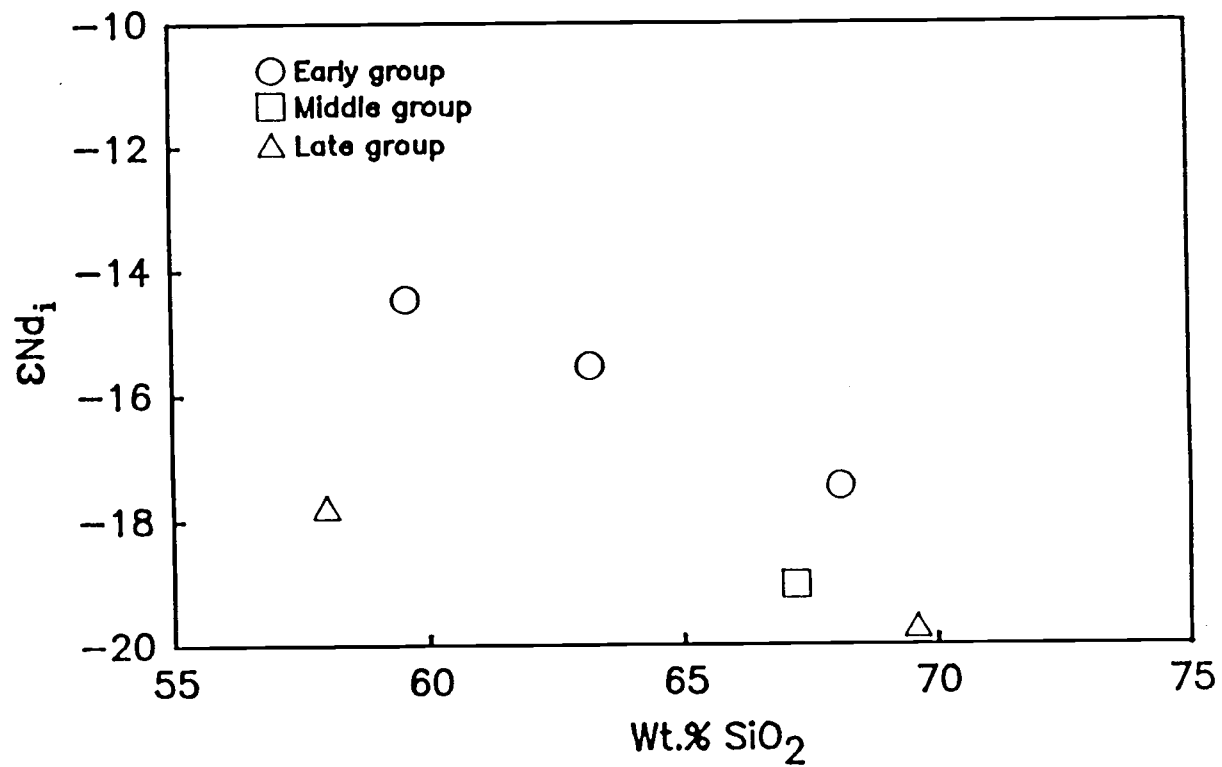
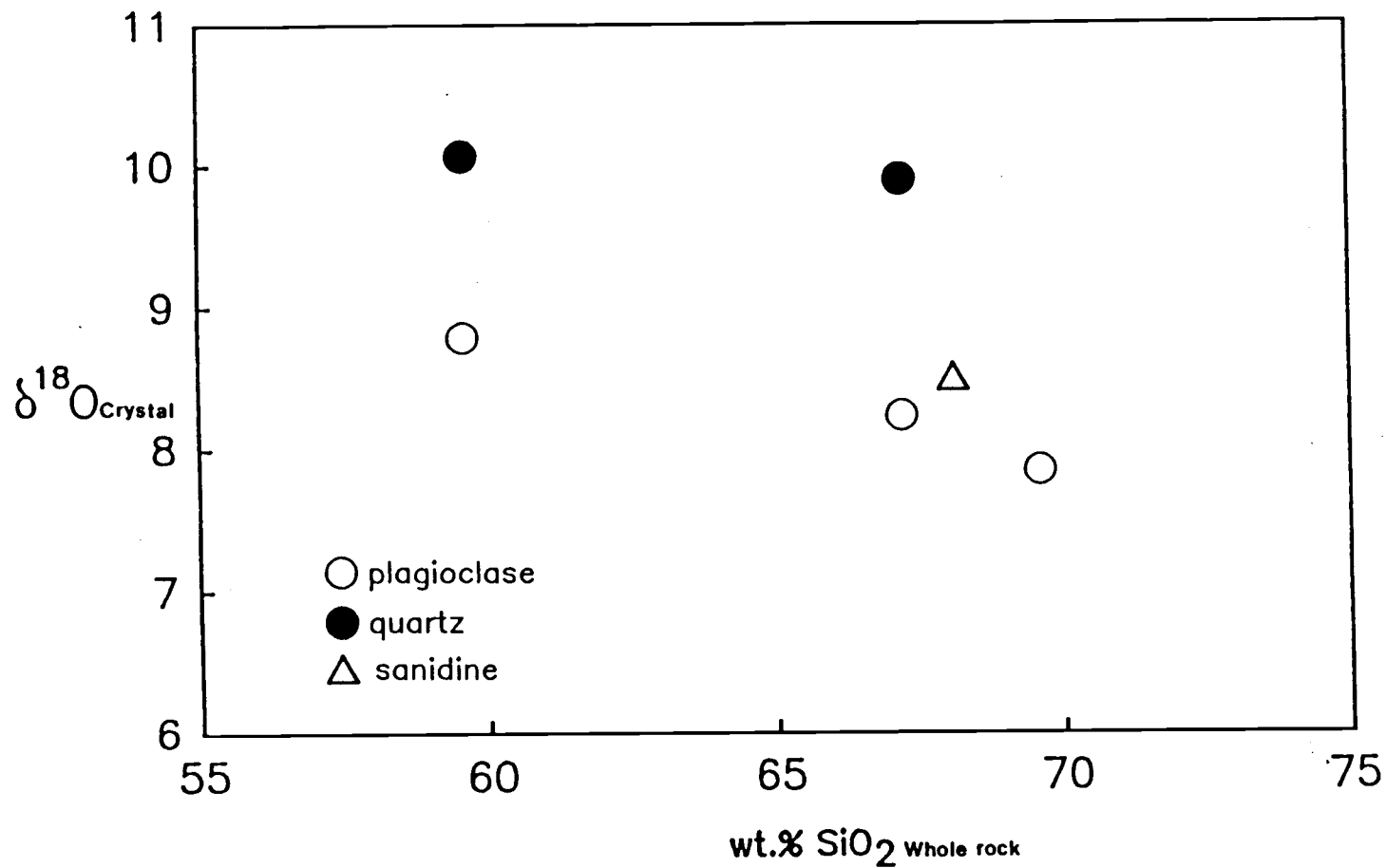Figure 24. Variation of initial ε Nd versus SiO_2 for Egan Range volcanic complex magmas.

Figure 25. $\delta^{18}O$ of mineral separates versus wt.% SiO_2 of host rock from Egan Range volcanic complex lavas. Each point represents the average of multiple analyses of a single sample. Estimated analytical error is $\pm$ 0.2 permil.

magmas are negatively correlated with stratigraphic position and bulk composition; early group andesite sample Mt8787 has the highest $\delta^{18}O$ value (8.8‰) and late group rhyodacite sample Mt8765 has the lowest $\delta^{18}O$ value (7.8‰; Figure 25 and 26).
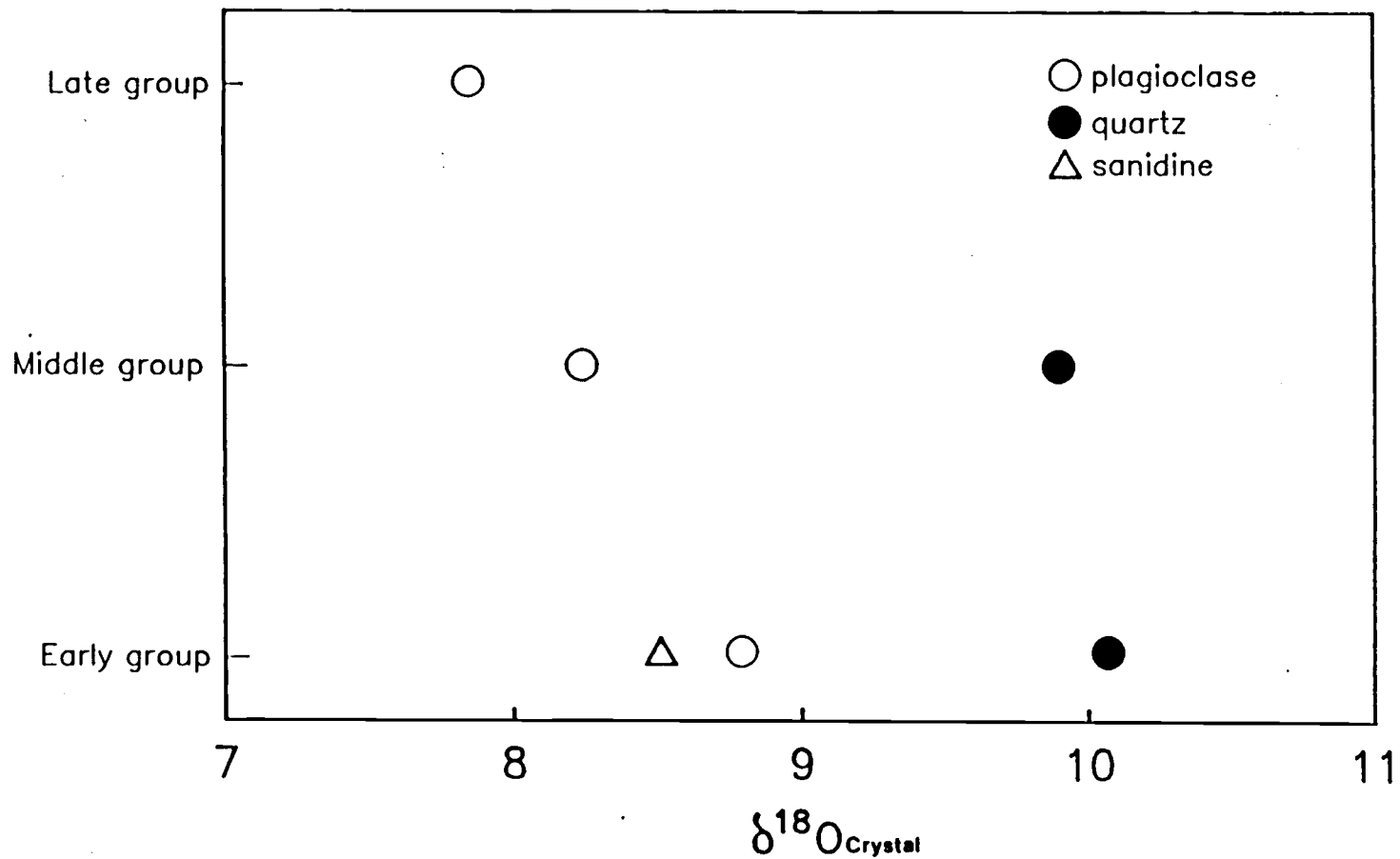
Figure 26. Evolution of $\delta^{18}O$ of the Egan Range volcanic complex as recorded by mineral separates from early, middle, and late group lavas. Each point represents the average of multiple analyses of a single sample.

Petrogenesis of Magmas of the Egan Range Volcanic Complex

In the past two decades, the mixing of magmas has become increasingly recognized as an important petrologic process (Eichelberger, 1975; Anderson, 1976; Langmuir, 1978; Bacon, 1986; McMillian and Dungan, 1986; Koyaguchi, 1986; Dungan, 1987). Literally, magma mixing implies blending of compositionally distinct magmas into a single, homogeneous magma (Anderson, 1976). Yet review of many recent studies indicates that a continuum of products result from interaction between two or more contrasting magmas. At one extreme, the presence of fine-grained, mafic magmatic inclusions with textural evidence for rapid undercooling within more silicic hosts provides compelling evidence for simultaneous coexistence of compositionally distinct magmas and incomplete mixing (Bacon and Metz, 1984; Bacon, 1986; Koyaguchi, 1986). At the other extreme, many magmas referred as "hybrids" display little to no textural or mineralogic evidence for magma mixing (Dungan, 1987). In the latter case, mixing usually involves the blending of low viscosity mafic liquids; support for the mixing model is mainly in the form of whole rock chemical trends (Dungan, 1987). Intermediate between these two endmembers are magmas with abundant petrographic evidence for blending of compositionally

distinct magmas. Rocks that form by this process can be identified by anomalous zoning patterns in phenocrysts, profound mineralogic disequilibrium, and the coincidence of high concentrations of both incompatible and compatible elements that cannot be accounted for by crystal fractionation models (McMillan and Dungan, 1987; Dungan, 1987; Koyaguchi, 1986; Feeley et al., 1988).

This section presents chemical evidence to support a model in which different modes of mixing have played a major role in the petrogenesis of magmas of the Egan Range volcanic complex. Early group volcanic rocks contain fine-grained basaltic andesite magmatic inclusions which are hosted by andesites, dacites, and rhyodacites that have abundant petrographic evidence for a mixed origin. In contrast, hybrid dacites and rhyodacites of the middle group have sparingly little textural evidence for a mixed origin; recognition of these rocks as hybrids might go unnoticed without the close stratigraphic association of mixing endmembers and whole-rock chemical trends.

Methods

Possible evolution paths for the volcanic rocks were examined for each stratigraphic group. In mixing models (Appendix II), trace-element compositions of the model hybrid magmas were calculated using the program MAGMA86.

Proportions of mixing endmembers and fractionating
phenocryst phases in the middle and late groups were
determined by best fit major-element models using the
Basic program IGPET1. In light of the strong textural and
compositional evidence for magma mixing and decoupling of
major and trace elements in early group magmas, trace-
element constraints on evolution were evaluated
independently of major-element constraints. Bulk
distribution coefficients for middle and late group models
were calculated using published mineral-melt distribution
coefficients (Table 9) and using the proportions of
fractionating phenocryst phases predicted from least
squares calculations of major elements. Due to the strong
compositional and temperature dependence of distribution
coefficients, major and trace elements models in the late
group are examined over two intervals; andesite to dacite
and dacite to rhyodacite. Compositions of phenocryst
phases used in evolution models were determined by
electron microprobe (Tables 3-6).

Early Group

The disequilibrium phenocryst assemblages and the
presence of fine-grained basaltic andesite magmatic
inclusions in early group lavas is consistent with an
origin due to mixing of basaltic and silicic magmas. In

Table 9
*Partition coefficients used in fractional crystallization models.

Element	Data source[**]	olivine	Augite		Plagioclase		Amphibole	Magnetite		Biotite	Apatite
			Int.	silicic	Int.	silicic		Int.	silicic		
Rb	(1,7)	0.00	0.01	0.03	0.02	0.20	0.01	0.00	0.00	4.00	0.11
Sr	(1,7	0.01	0.08	0.52	3.00	4.50	0.26	0.00	0.00	0.27	0.39
Ba	(1,7)	0.00	0.03	0.13	0.48	0.30	0.14	0.00	0.00	10.0	0.05
La	(1,2,3,4)	0.02	0.23	0.76	0.29	0.42	1.30	0.29	0.90	0.30	25.00
Ce	(1,2,3,4,7)	0.01	0.36	0.36	0.18	0.20	1.50	0.35	1.10	0.32	30.00
Nd	(1,2,3,4,7)	0.01	0.70	0.94	0.14	0.20	2.50	0.45	1.65	0.29	31.10
Sm	(1,2,3,4,7)	0.01	1.30	1.52	0.12	0.20	3.00	0.55	2.00	0.26	40.00
Eu	(1,2,3,4,7)	0.01	1.20	1.11	1.13	5.00	2.70	0.53	0.47	0.24	27.30
Tb	(1,2,3,4)	0.00	2.00	4.60	0.05	0.15	3.75	0.50	2.50	0.33	25.00
Yb	(1,2,3,4,7)	0.01	1.40	1.14	0.04	0.20	3.75	0.26	1.10	0.44	21.00
Lu	(1,2,3,4,7)	0.02	1.40	1.28	0.04	0.20	3.75	0.60	0.50	0.33	17.80
Zr(Hf)	(1,5)	0.00	0.34	0.50	0.01	0.20	2.80	0.63	2.40	0.65	0.00
Th	(1)	0.00	0.02	0.20	0.01	0.05	0.25	0.06	0.14	0.31	2.50
U	(1)	0.00	0.01	0.20	0.01	0.10	0.05	0.12	0.35	0.15	2.50
Sc	(1)	0.30	9.20	44.00	0.04	0.05	63.0	3.00	15.2	8.60	0.10
Cr	(6)	0.40	30.0	60.00	0.00	0.10	40.0	4.00	10.0	17.0	0.05
Co	(6)	0.30	4.50	40.00	0.00	0.10	20.0	6.00	6.0	25.0	0.05

*Partition coefficient = (concentration mineral/concentration melt)

**1. Grunder (1988). 2. Nagasawa and Schnetzler (1971). 3. Nagasawa (1970). 4. Luhr et al. (1984). 5.Pearce and Norry (1979).

6. Gill (1978). 7. Arth (1976).

Int. = basaltic andesite to dacite. Silicic = dacite to rhyolite.

mixing calculations (Appendix II) a basaltic andesite magmatic inclusion (Mt879 or Mt8749) serves as the mafic endmember, and an early group rhyodacite (Mt8786) is used as the silicic endmember. A model was considered satisfactory if trace element concentrations considered in the model were within the range of analytical error of the observed content. In most cases, these chemical mixing models require removal of minor amounts of clinopyroxene (< 3.5%) and apatite (< 1%) prior to or during mixing to obtain the best fits for Cr, Sc, and the REE's. Some discrepancies between the observed and modeled compositions of a few trace elements probably result from uncertainties in distribution coefficients; others may reflect differences between the model endmembers used and the actual endmember compositions.

The trace-element calculations (Appendix II) indicate that early group andesites and dacites can be produced by mixing of approximately 55 to 65% basaltic andesite with 45 to 35% rhyodacite. In natural samples, with increasing silica content, LREE's become progressively enriched while HREE's become progressively depleted (Figure 27a) resulting in a fanning set of patterns rotated about an axis between Sm and Eu. Simple two component mixing of basaltic andesite and rhyodacite
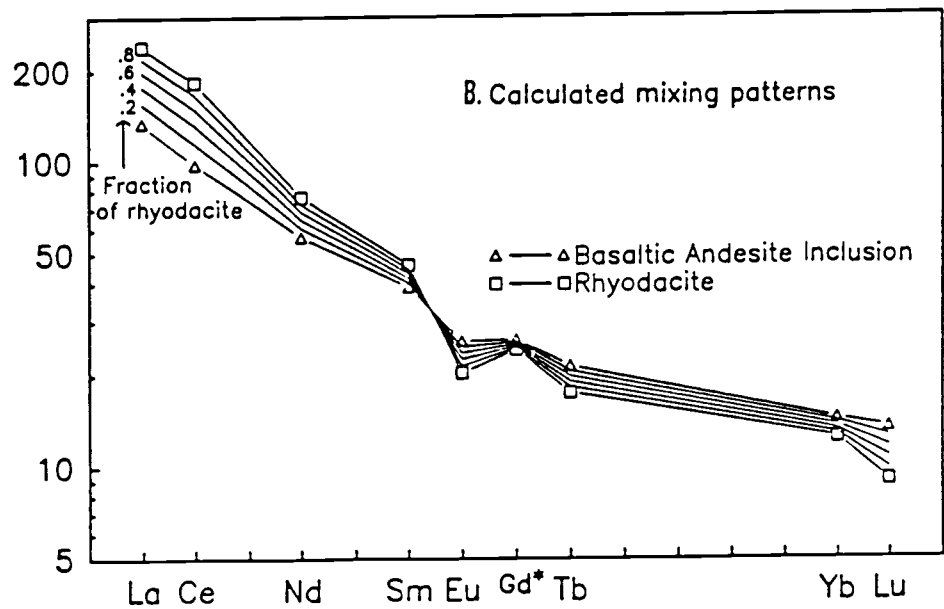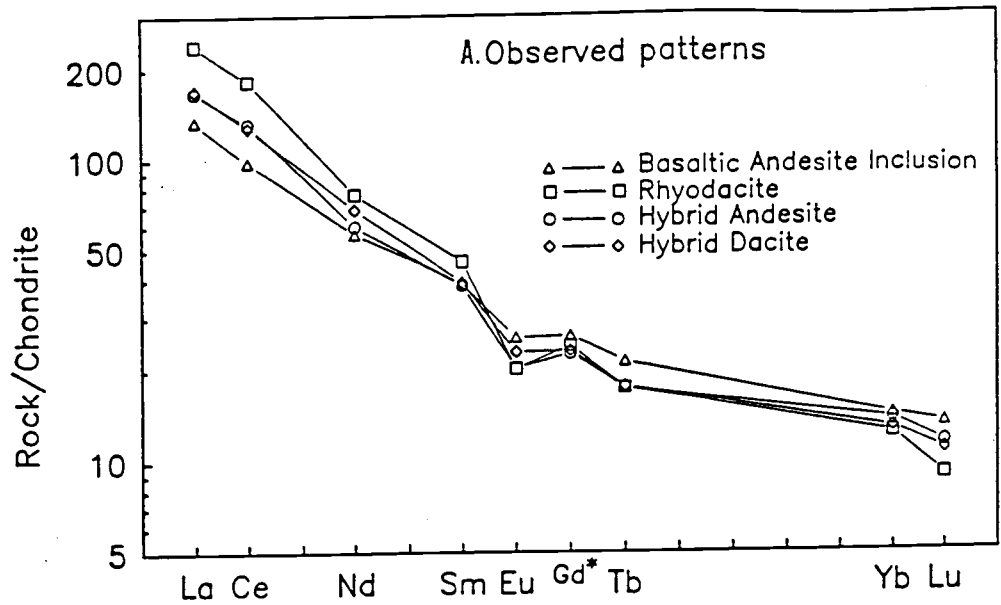
Figure 27. A. Chondrite-normalized abundances of rare-earth
elements for select early group samples.
B. Chondrite-normalized rare-earth element patterns
calculated by mixing an early group basaltic andesite
(Mt3749) and rhyodacite (Mt8786) in varying
proportions. *In both figures, Gd* is interpolated
between Sm and Tb.

compositions in the above proportions yields REE patterns similar to observed patterns (Figure 27b).

Evolution models invoking closed system fractional crystallization were not considered satisfactory because initial Sr isotopic ratios of the early group increase from 0.71149 (andesite) to 0.71235 (rhyodacite) (Table 8); isotopic ratios should be unaffected by crystal fractionation. Assimilation-fractional crystallization (AFC; DePaolo, 1981) modeled by fractionation of a plagioclase dominated assemblage cannot have produced the REE patterns because the LREE's and HREE's are not simultaneously enriched and the negative Eu anomaly is not sufficiently great.

The purity of the mixing relationship is examined in Figure 28a where the ratio Sc/Nd, elements with markedly contrasting geochemical behavior, are plotted against a similar ratio, La/Cr, after the method of Langmuir et al. (1978). The data fall along a hyperbolic curve defined by hypothetical mixing of the magmatic inclusion (Mt8749) and a rhyodacite (Mt8786) used in the other mixing models. The hyperbolic nature of the curve illustrates the mixing process (Langmuir et al., 1978). Figures 28b and 28c are companion plots (Langmuir et al., 1978) in which one of the ratios is plotted against a ratio of the denominators
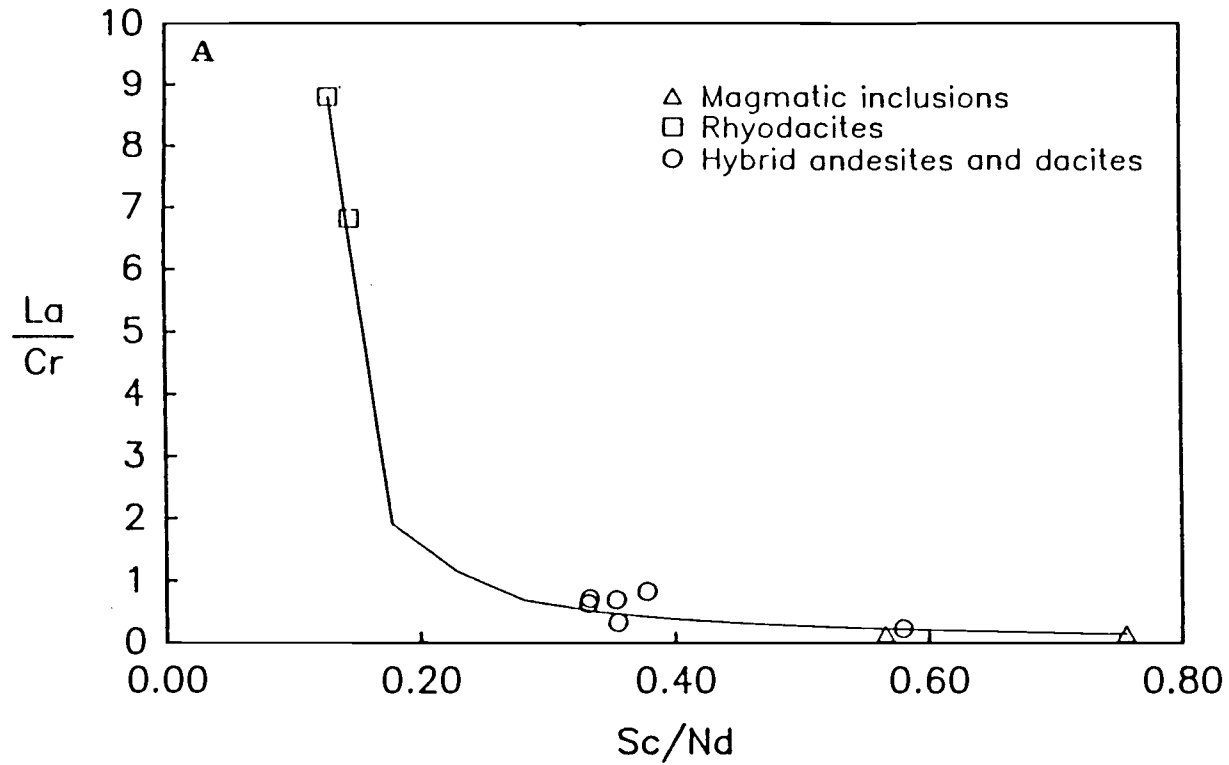
Figure 28. A. La/Cr versus Sc/Nd mixing diagram for early
          group lavas. Mixing hyperbola is calculated by the
          method of Langmuir et al. (1978) using early basaltic
          andesite sample Mt3749 and rhyodacite sample Mt8786
          as endmember compositions. Kinks in the mixing
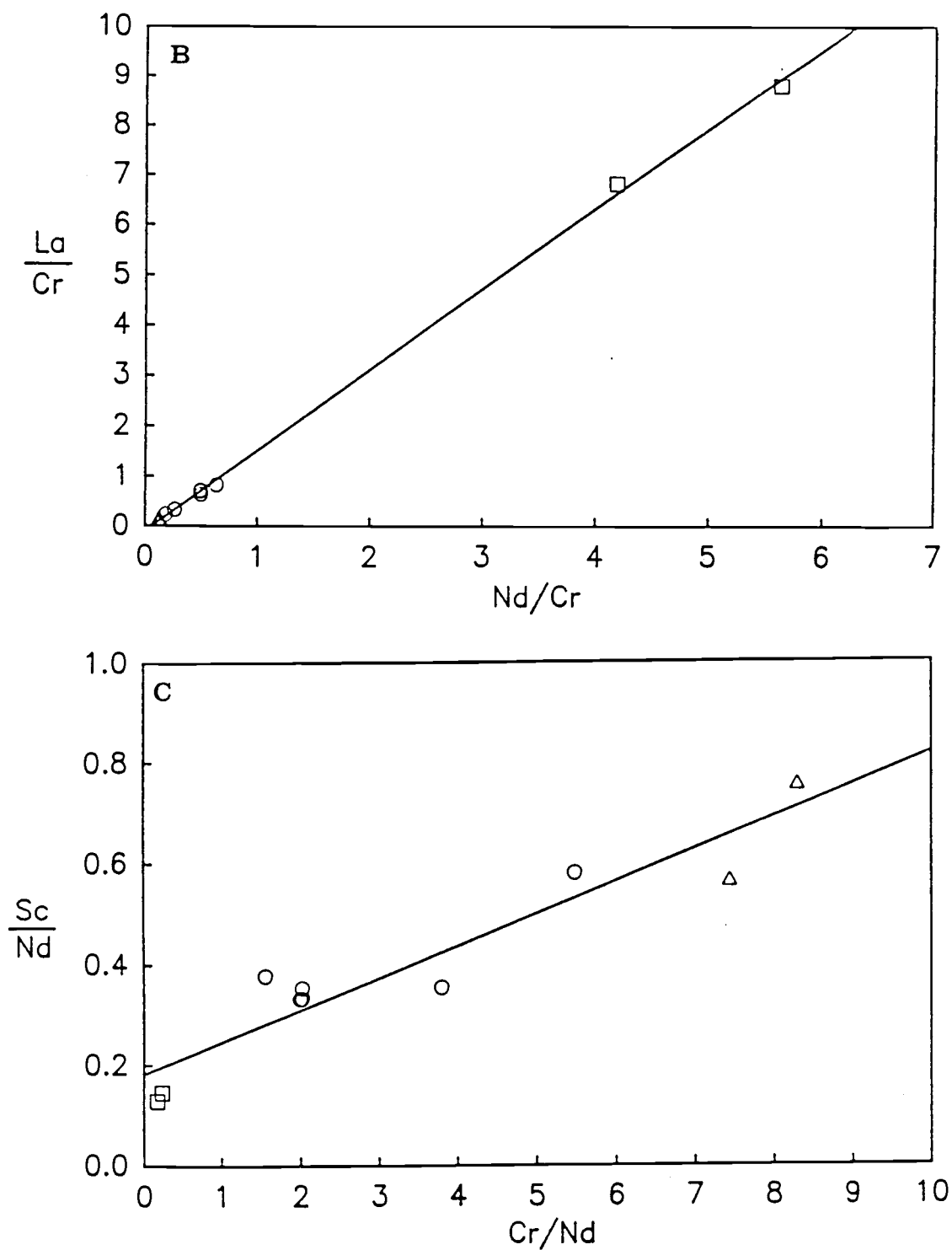   hyperbola result from mixing in 10% increments.

Figure 28. B and C. Companion plots where ratios of the
denominators in A are plotted against one of the
original ratios in A. Lines are first order
regression lines. Symbols are as in A.

in Figure 28a. These plots illustrate the consistency of
the mixing curve in Figure 28a because the data points
define linear trends (Langmuir et al., 1978).

The large variation in Cr and Sc concentrations at
roughly equivalent TiO_2 contents of some samples (ie.,
samples Mt8787 and Mt8789; Table 7a) indicates that pure
mixing of basaltic andesite and rhyodacite is too
simplistic a model. As indicated by the mixing
calculations (Appendix II), minor amounts of clinopyroxene
fractionation can explain these data. For example, in
Figure 29 hybrid andesites and dacites are produced either
by pure mixing of mafic and silicic magmas or by mixing
rhyodacite with mafic magmas that have fractionated less
than 3.5% clinopyroxene. This modest amount of
fractionation does not significantly affect the form of
the incompatible element trends.

Experimentally determined partition coefficients for
REE between clinopyroxene and silicate melt, and amphibole
and silicate melt have convex upward patterns with higher
values for the HREE (Figure 30; Green and Pearson, 1985a;
Green and Pearson, 1985b). This suggests that
fractionation of a large proportion of these phases paired
with some assimilation of crustal rocks may account for
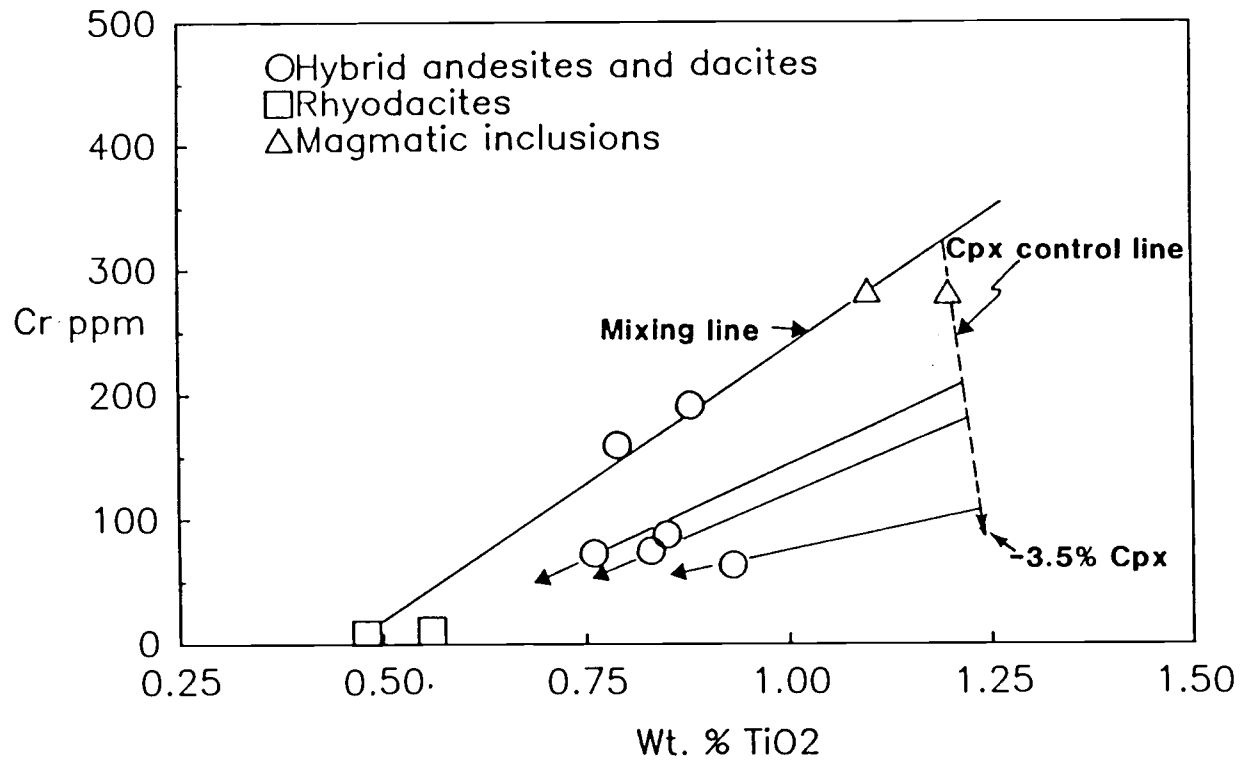the fanning out REE patterns. Removal of clinopyroxene in

Figure 29. Cr versus TiO$_2$ variation diagram for early group lavas. Dashed line is fractionation control line for clinopyroxene (cpx). Solid lines are binary mixing lines.
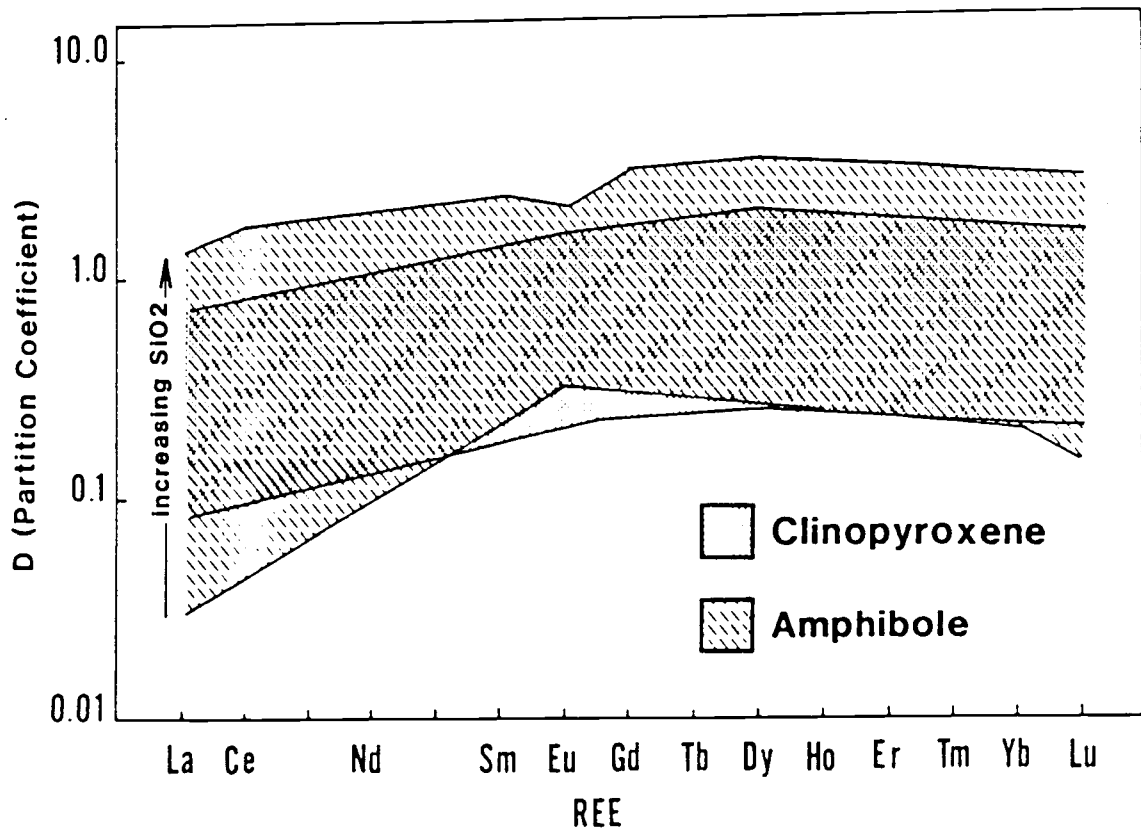
Figure 30. Summary of REE partition coefficients for clinopyroxene and amphibole phenocrysts and coexisting basaltic to andesitic groundmass compositions. (After Green and Pearson, 1985a,b)

large proportions would, however, have a stronger negative effect on the Cr content of early group andesites and dacites than observed. For example, in order to reproduce La/Lu ratios observed in early group andesites and dacites by an AFC process involving removal of clinopyroxene, the assimilant would need an unrealistically high La/Lu ratio of 2855, and 85% of the original magma would need to crystallize (Figure 31). This high degree of crystallization would deplete the Cr contents in the magma to less then 1 ppm. Furthermore, because Cr is as compatible in amphibole as in clinopyroxene, removal of amphibole would also rapidly deplete the magma in Cr with increasing differentiation. This is not consistent with observed trends (Figure 17).

The presence of zircon in all early group lavas raises the possibility that fractionation of accessory phases produced the REE patterns (Gromet and Silver, 1983). Zircon has a characteristic preference for the heavy relavtive to light REE (Nagasawa, 1970). However, mineral-melt distribution coefficients for Hf (and Zr) in zircon are much larger than for Lu (Irving and Frey, 1984). Therefore, the increase in the Hf/Lu ratio from 15.1_{mafic} to $24.2_{silicic}$ cannot result from fractionation of zircon.
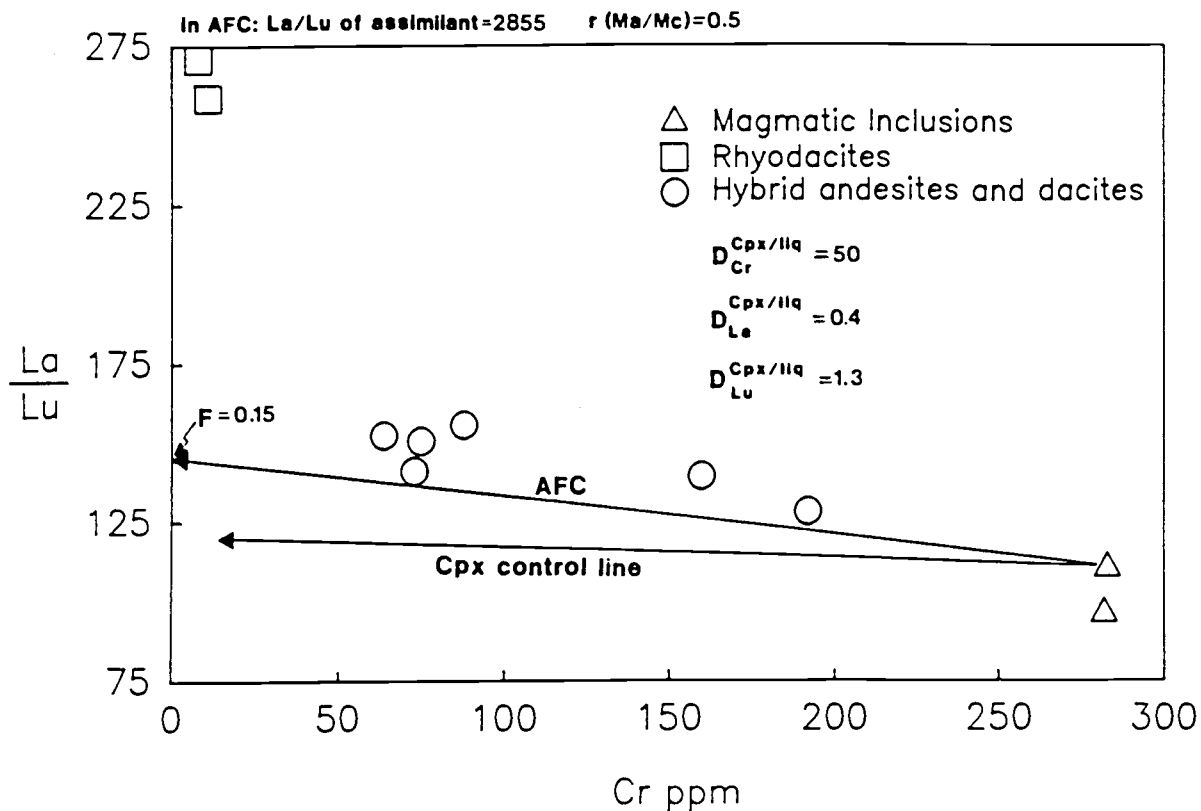
Figure 31. La/Lu versus Cr variation diagram for early group
lavas. The effects of crystal fractionation and
combined assimilation-fractional crystallization (AFC)
are illustrated schematically. In the AFC model,
La/Lu of the hypothetical assimilant equals 2855;
r (mass assimilated/mass fractionated) equals 0.5.

The major element compositions of some early andesites and dacites cannot be reproduced by mixing of mafic and silicic endmembers in the proportions derived from the trace-element models (Appendix II). The trace-element models discussed above indicate that early group andesites and dacites evolved largely by binary mixing of basaltic and silicic magmas. Therefore, at least one endmember may have had trace-elements decoupled from major-elements. Such decoupling of major- and trace-elements has been described by O'Hara and Matthews (1981) for a model magma chamber undergoing continuous fractionation, periodic replenishment with primitive magma, and periodic mixing with silicic crustal melts. Major- and trace-element concentrations are decoupled during the AFC process because the major-element compositions of assimilated and fractionated materials are not very different (Taylor, 1980).

Because of the absence of primitive basaltic magmas in east-central Nevada, it is not possible to quantitatively model the evolution of the basaltic andesites. However, the effects of AFC are evident in the composition of the basaltic andesite magmatic inclusions. These samples are similar in REE, high-field strength elements, and Cr concentrations, although their major-element compositions are variable. Major-element least-

squares mixing calculations (Appendix II) suggest that the more evolved basaltic andesite inclusion (Mt879) can be modeled as a mixture of 83% magmatic inclusion sample Mt8749 and 17% rhyodacite sample Mt8786. Sample Mt879 contains xenocrystic biotite and quartz which is consistent with a larger degree of silicic contamination in this sample relative to sample Mt8749 (Appendix I). The premixing trace-element composition of sample Mt879 is significantly different for many trace-elements and an AFC process could explain these differences. Additional evidence for the AFC process are low Ni and Mg concentrations in the magmatic inclusions which indicate fractionation of olivine from a primitive magma concurrent with assimilation.

In conclusion, the compositional trends exhibited by early group magmas can be attributed to a two stage evolutionary history. The first stage involved fractionation of olivine paired with assimilation of country rock, possibly in lower crustal magma chambers. This process rapidly depleted Ni and Mg contents while highly enriching magmas in incompatible-elements. In the second stage, basaltic andesites fractionated small amounts of clinopyroxene and mixed with silicic melts just prior to eruption. Because the silicic endmember does not lie on a reasonable liquid line of descent from basaltic

andesites, they are assumed to be largely crustal melts. The silicic endmember must be more evolved than the most silicic rhyodacite observed because the latter contains mafic magmatic inclusions and disequilibrium phenocryst assemblages, which indicate mixing with mafic magmas.

Middle Group

REE patterns of the middle group dacites are similar in shape to REE patterns of early group dacites and rhyodacites, although they occupy an intermediate position (Figure 20). This relationship suggests that middle group dacites are probably mixed magmas and that the endmembers are middle group rhyodacites and early group andesites or dacites.

The results of chemical modeling indicate that Tvml magmas can be produced by mixing of approximately 50% early group andesite Mt8763 with 50% middle group rhyodacite Mt8720 coupled with fractionation of approximately 4% clinopyroxene (Appendix II). The strong correlation between observed and model compositions does not strictly require that Mt8763 and Mt8720 represent the actual endmember compositions; the actual compositions may lie at any point along the mixing line. The andesite composition was chosen as the mafic endmember because: (1) this sample appears to have been produced by mixing of

early group basaltic andesite and rhyodacite with little subsequent modification by crystal fractionation (see Appendix II); (2) this sample represents an average early group composition; and (3) a more mafic endmember (e.g. magmatic inclusions) would probably be unable to homogenize with the increasing proportion of silicic endmember without rapid chilling (Sparks and Marshall, 1985; Bacon, 1986). The middle group rhyodacite composition was chosen as the silicic endmember because of its stratigraphic association with the middle group dacites. The major-element composition of this sample is virtually indentical to early group rhyodacite Mt8786 except that it has a slightly lower CaO content.

Models involving fractional crystallization of observed phenocrysts in modal proportions or assimilation paired with large amounts of fractional crystallization from less evolved early group magmas fail to reproduce Tvm_1 compositions. For example, the large decrease in the La/Th ratio (Figure 32) with increasing SiO_2 content cannot be explained by a fractionation dominated process because La and Th are both strongly incompatible in a plagioclase dominated assemblage. The most efficient way to decrease La/Th is to mix with low La/Th magmas such as middle group rhyodacite sample Mt8720 (Figure 32). Furthermore, the decrease in the La/Th ratio with
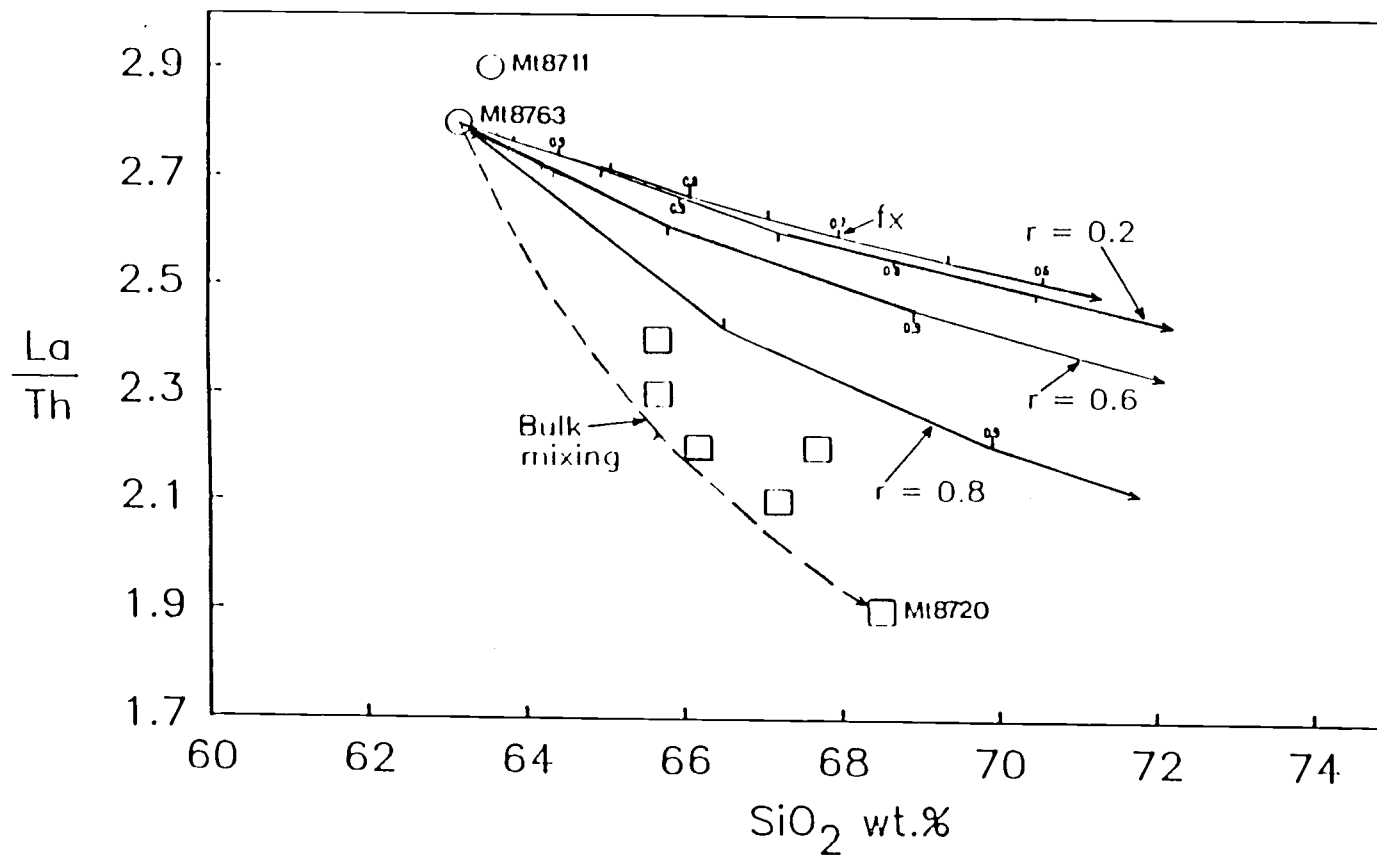
Figure 32. La/Th versus SiO$_2$ variation diagram for middle group lavas. Circles are early group andesite samples (Mt8763, Mt8711). Squares are middle group samples. The effects of closed system crystal fractionation (fx; plag + pyx + mag), bulk mixing, and AFC are illustrated using middle group rhyodacite (Mt8720) as the contaminant. Tick marks on fx and afc curves are at F intervals of 0.05. Kinks in fx and afc curves in this and subsequent figures reflect the F increment modeled.

increasing SiO_2 content is not a result of zircon
fractionation because Kd for Th in zircon are much larger
than for La. Thus, fractionation of zircon should elevate
the La/Th ratio. A few samples fall off the mixing line
in Figure 32 suggesting that modest amounts of
fractionation of major phenocryst phases may have
occurred. However, I interpret these samples as mainly
reflecting mixing of endmembers with La/Th ratios
different from the endmembers chosen in this model (ie.,
sample Mt8711, Figure 32).

Dacites of map unit Tvm3 can be successfully modeled
as a mixture of 56% middle group rhyodacite Mt8720 and 44%
middle group dacite Mt871A (Appendix II). In this case,
these magmas are similar to magmas of unit Tvm_1 although
they contain a larger proportion of the silicic component.

The incompatible element enriched composition of
middle group rhyodacite sample Mt8720 suggests that it
formed largely by anatexis of crustal rocks, although it
is somewhat fractionated relative to early group
rhyodacite sample Mt8786.   A model involving
fractionation of 1.3% plagioclase + 1.7% clinopyroxene +
0.3% Fe-Ti oxides from early group sample Mt8786
reproduces middle group sample Mt8720 with very small
values of R^2 (Appendix II). The best fit is obtained when
calcic plagioclase and Mg-rich clinopyroxene compositions

are used as fractionating phases. Because even the early group rhyodacites have petrographic and mineral composition evidence for magma mixing (such as sieved, mafic plagioclase xenocrysts) fractionation of the plagioclase, clinopyroxene, and Fe-Ti oxides may have occurred in the mafic endmember prior to mixing. This can account for the chemical evidence for clinopyroxene fractionation to derive middle group rhyodacites in the absence of clinopyroxene as a phenocryst phase.

Late Group

Andesite of the late group (map unit Tvl_2) has elevated FeO*, TiO_2, and Al2O3, and depleted MgO, CaO, Cr, and Sc relative to early group andesites. These geochemical characteristics suggest that fractionation of olivine and clinopyroxene was important in controlling major-element trends of the late group andesites. High alumina concentrations in basaltic magmas can be attributed to fractionation of olivine plus clinopyroxene at elevated pressures (e.g. Crawford et al., 1987; DeBari and Coleman, 1989). Least-squares mass balance calculations indicate that late group andesites can be related to early group basaltic andesites by removal of 23-31% of the the assemblage cpx + plagioclase + olivine from the basaltic andesites (Appendix II). Clinopyroxene,

plagioclase, and olivine are all phenocryst phases in late group andesite.

For the compositional interval of andesite to dacite (Tvl_2 to Tvl_1), trace-element modeling suggests that fractional crystallization paired with assimilation of silicic crust can approximate the dacite composition (ie., Figures 33 and 34). The parental composition for the interval from andesite to dacite is sample Tf872 which represents the most evolved late group andesite composition (Table 7c). The silicic contaminant used is sample Mt8765 which represents the most evolved late group rhyodacite (Table 7c). This sample is more potassic, as well as enriched in incompatible elements, particularly Rb, Zr, and Hf when compared to early and middle group rhyodacites. Two component bulk-mixing lines between andesite and rhyodacite are illustrated for reference along with differentiation paths for the best fit model involving closed system fractional crystallization. AFC trajectories are for liquid compositions crystallizing the same assemblage as in the closed system model in addition to assimilation of a mass of rhyodacite equal to 20% of the mass of crystals fractionated (r = 0.20, DePaolo, 1981). The value of r is consistent with the heat budget estimated for assimilation under upper crustal conditions (Grove et al., 1982). Fractional crystallization and AFC

Figure 33. Th versus Rb variation diagram for late group lavas.
The effects of closed system crystal fractionation (fx;
plag + amph + cpx + mag), bulk mixing, and AFC are
illustrated using late group rhyodacite (Mt8765) as the
contaminant. Tick marks are at F intervals of 0.1. Fx
and AFC curves are terminated at F (mass magma/mass
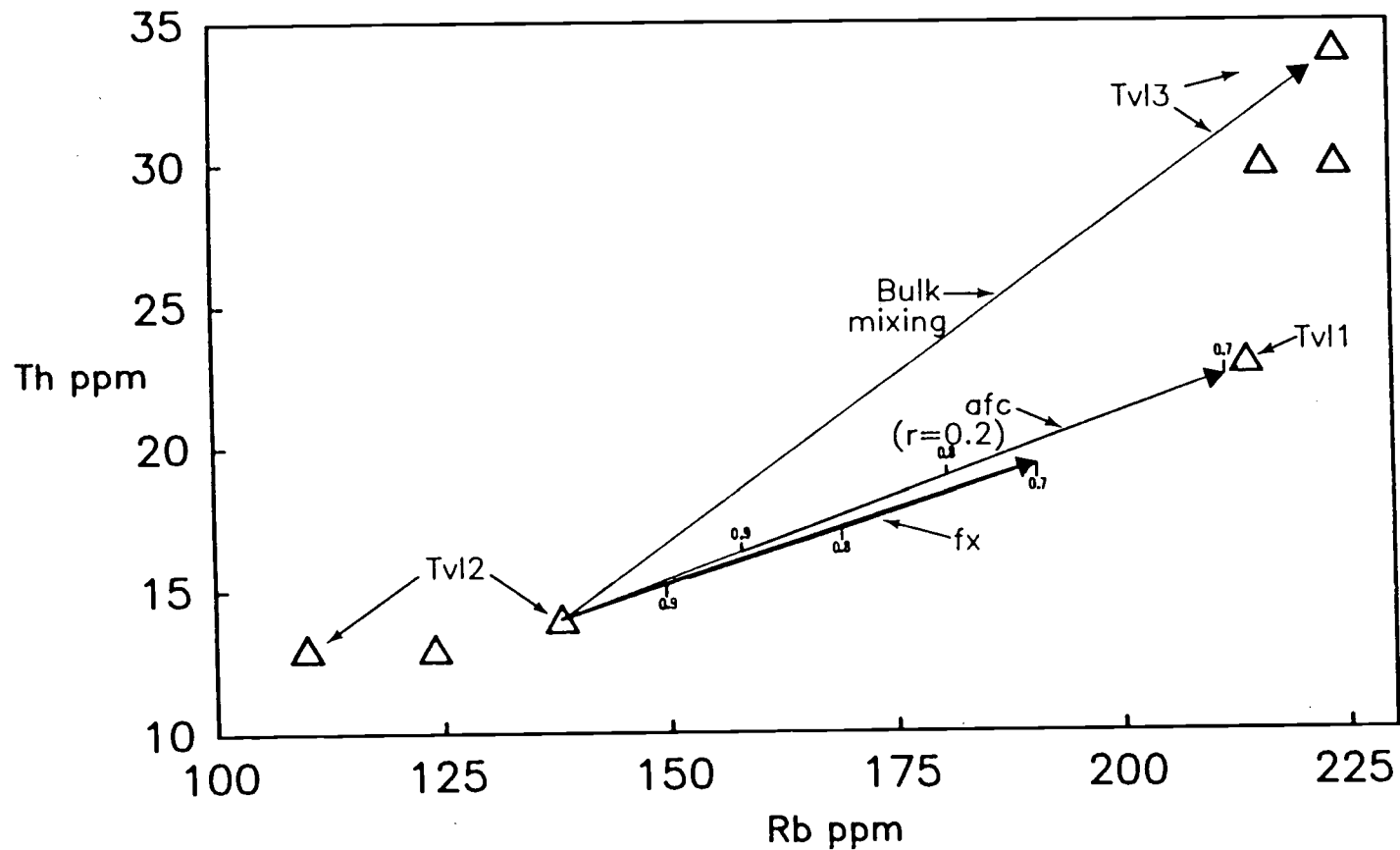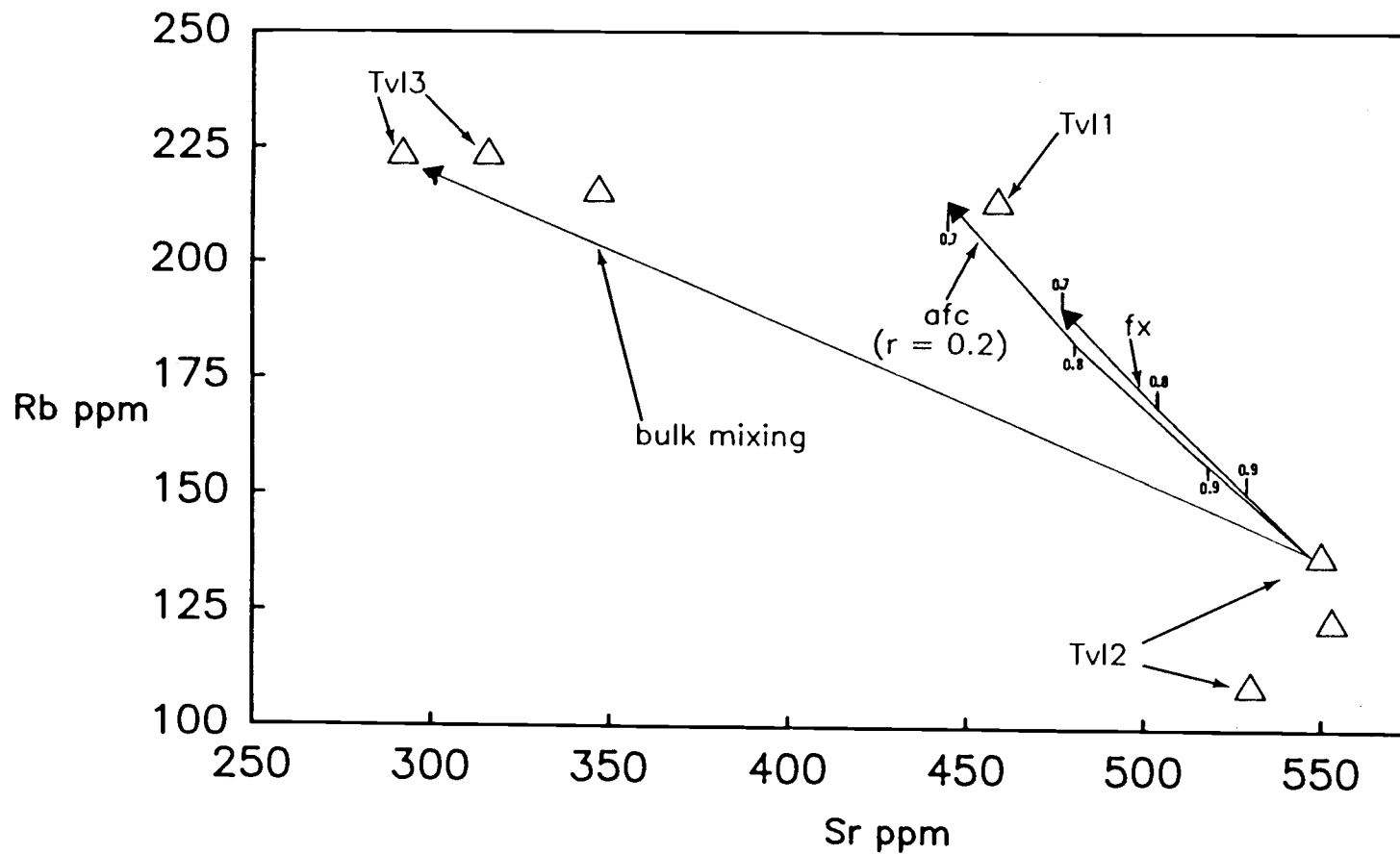original magma) = 0.7.

Figure 34. Rb versus Sr variation diagram for late group lavas. The effects of closed system crystal fractionation (fx; plag + amph + cpx + mag), bulk mixing, and AFC are illustrated using late group rhyodacite (Mt8765) as the contaminant. Tick marks are at F intervals of 0.1. FX and AFC curves are terminated at F = 0.7.

projections are terminated at F (= mass of magma/mass of

original magma) = 0.70 in order to illustrate differences

between the models at a constant value of F. Assimilation

of a late group rhyodacite component does not differ

significantly from major-element fractionation models

because, in this case, the contaminant is similar in

composition to the evolving magma. The effect of

assimilation is to increase the value of F, although the

proportions and compositions of mineral phases being

removed from the evolving magma will not drastically

change (Taylor, 1980; Nielsen, 1988). Therefore, to a

first approximation, major-element compositions of the

late group can be satisfactorily modeled by crystal

fractionation.

Least-squares mass-balance calculations indicate that

major-element variations between andesite and dacite may

be accounted for by approximately 30% (F=0.70)

fractionation of the assemblage plagioclase > amphibole >

clinopyroxene = Fe-Ti oxides (Appendix II). Within the

range of distribution coefficients, most trace elements

can also be satisfactorily modeled by crystal-liquid

fractionation of this assemblage (Appendix II). The

predicted fractionation model predicts low Rb and Th (and

U) relative to the observed composition of sample Mt8781

(Figures 33 and 34). Assimilation of rhyodacite brings

the modeled and observed compositions into coincidence and indicates that the system was open with respect to Rb and Th contamination. Many elements, including the REE, however, do not require additional enrichment by AFC. Therefore, it is likely that the rhyodacite is not a representative sample of the material assimilated, or that involvement of trace phenocryst phases (e.g.: zircon) modified trace element systematics. Neither closed system fractional crystallization nor two-component bulk-mixing can account for the trace-element composition of the late group dacites. The former because it cannot account for elevated Rb, Th, and U in the dacites (Figures 33 and 34). The latter because it predicts lower concentrations of Rb and Sr then observed in the dacites (Figures 33 and 34). In addition, magma mixing cannot account for depleted HREE concentrations, and constant LREE and Zr concentrations in dacites relative to andesites.

The proportion of amphibole in the fractionating assemblage suggested by the mass-balance calculations is higher than observed in the mode of the late group dacites (Table 2). Amphibole is present in the dacites in varying proportions although it is subordinate to clinopyroxene. Several lines of evidence suggest, however, that amphibole may have fractionated in proportions greater then observed in the mode. First, when amphibole is included in large

proportions in major element least squares calculations, fits are as good, or better, than when amphibole is not included. Second, both amphibole and clinopyroxene have convex upward distribution coefficient patterns for the REE, and in dacitic compositions REE may be highly compatible in amphibole, while only slightly compatible in clinopyroxene (Nagasawa and Schnetzler, 1971; Arth and Barker, 1976). Thus, significant amphibole fractionation should buffer or deplete REE concentrations (especially the HREE) in the liquid. Third, in addition to the REE, significant amphibole fractionation should buffer or slightly deplete concentrations of Zr (Kd Zr^{amp}=1.4-4.0), Y (Kd Y^{amp}=2.5-6.0), and Nb (Kd Nb^{amp}=1.3-4.0) relative to andesites (Pearce and Norry, 1979). This is precisely the compositional trend observed in the interval andesite to dacite (Table 7c, Figure 18). Moreover, Zr and Nb are incompatible in clinopyroxene and therefore should increase with differentiation if clinopyroxene is removed preferentially to amphibole (Pearce and Norry, 1979).

Removal of zircon with high Kd values for the REE, and HFSE could mimic the above trends. However, zircon is a rare phase in late group rocks. Furthermore, the amount of zircon required to buffer the LREE would severely deplete the magma in LREE relative to observed compositions (Gromet and Silver, 1983). In addition,

removal of zircon should deplete the liquid in U and Th which is inconsistent with observed trends. Th and U are, however, incompatible in amphibole. Based on the above arguments, I conclude that fractionation of amphibole played a major role in trace element compositional trends of late group dacites.

Thompson et al. (1986) describe similar compositional trends in Miocene metaluminous volcanic rocks erupted during the inception of extension in the Rio Grande rift. They argue that constant Zr and depleted HREE concentrations in dacites precluded their derivation from associated andesites by crystal fractionation. Instead, they suggested that the dacites may have been derived from a less alkalic parent then the andesites. The arguments in the preceding paragraph suggest, however, that these compositional trends may be a consequence of amphibole fractionation. Furthermore, the conclusion of Thompson et al. (1986) was reached in spite of least squares mass-balance calculations which indicate that major element variations within the dacites are best explained by removal of amphibole preferential to pyroxenes and Fe-Ti oxides. Although the process by which amphibole is selectively removed from the liquid is unknown, this study and the study by Thompson et al. (1986) suggest that fractionation of amphibole may play a major role in

controlling trace-element compositional trends in metaluminous magmas of intermediate composition erupted during crustal extension in the Oligocene and early Miocene. In both regions the dacites occur late in the eruptive sequence.

The paucity of compositions between the andesites and dacites, apparently related by crystal fractionation, may be explained by analogy to the work of Grove and Donnelly-Nolan (1986). They suggest that early mafic liquids crystallizing olivine, plagioclase, and augite follow a steep liquidus trajectory in temperature-composition space. Along this surface a large drop in temperature results in a small change in melt composition (Figure 35). Upon reaching the reaction point between olivine + augite + liquid, the cotectic surface shallows and subsequently a large compositional change is traversed over a small temperature interval and results in a pacuity of these compostitions. This reaction point occurs at the initial crystallization of an amphibole dominated assemblage at Medicine Lake (Grove and Donnelly-Nolan, 1986).

This model can account for the following. First, the gap in silica content (58.4 to 66.0 wt.% SiO_2) observed between the late group andesites and dacites coincides with the gap in SiO_2 contents inferred for liquids
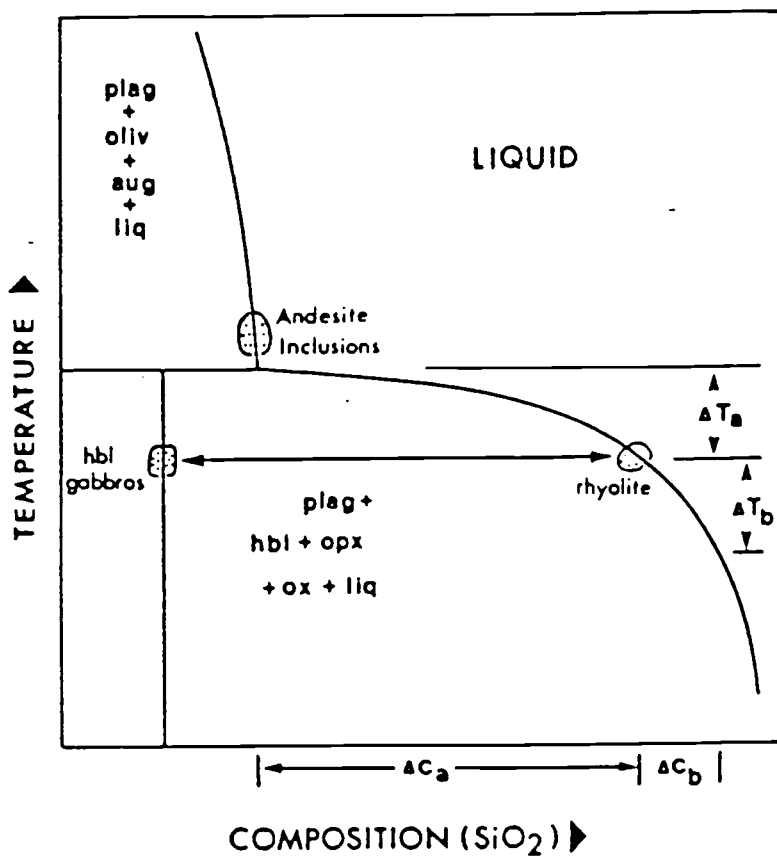
Figure 35. Temperture-composition diagram for crystallization at Medicine Lake Volcano. Weight percent SiO_2 increases to the right. As the magma crystallizes through the temperature interval ΔT_a, a large compositional range (ΔC_a) is traversed favoring the development of a compositional gap. (From Grove and Donnelly-Nolan, 1986).

produced by the above process (60-72%; Grove and Donnelly-
Nolan, 1986). Second, major and trace element geochemical
modeling indicates that late group dacites evolved largely
by crystal fractionation of an amphibole-bearing
assemblage from late group andesites. Over the interval
early basaltic andesite to late group andesite, however,
the fractionating assemblage is characterized by augite,
plagioclase, and olivine (Appendix II). Thus, the
compositional gap initiates at the inferred reaction point
between olivine, augite and liquid, and the initial
crystallization point of the amphibole-bearing assemblage.
The dissimilarities between the inferred proportion of
amphibole removed to produce the dacites, and the
proportion of amphibole observed in the mode, may be
attributed to removal of a large percentage of amphibole
crystals over a narrow temperature interval creating
substantial amounts of gabbroic cumulates not exposed at
the surface.

The results of major- and trace-element modeling are
equivocal for the interval from dacite to rhyodacite.
Least-squares mass-balance calculations for major elements
involving fractionation of a biotite-bearing assemblage,
or simple bulk-mixing of evolved rhyodacite with dacite
both closely approximate the rhyodacite compositions
(Appendix II). Trace-element concentrations calculated

from models involving bulk-mixing of dacite (Mt8781) and evolved rhyodacite (Mt8765) in proportions derived from major- element models are in excellent agreement with observed compositions (Appendix II).

Models involving fractional crystallization can reproduce the constant Rb and K_2O concentrations over the interval dacite to rhyodacite if biotite has replaced amphibole as the main fractionating hydrous phase. This is reasonable in light of modal abundances of major phenocrysts in the rhyodacites (Table 2; Chapter 2). However, only with assimilation of a silicic contaminant do model trace element compositions approach compositions of the rhyodacites. Fractionation of major phenocryst phases cannot account for the elevated LREE, Th, U, and Zr concentrations in rhyodacites (Appendix II). This discrepancy is eliminated if a small amount of assimilation or mixing with evolved rhyodacite sample Mt8765 is included. This aspect is schematically illustrated in Figure 36 in which differentiation paths are drawn for fractional crystallization paired with assimilation and bulk-mixing of dacite and rhyodacite. The AFC models calculated for La and Zr reproduce observed rhyodacite compositions at r=0.20 and F=0.80. The value of F in the AFC model is slightly smaller than F calculated in the major-element fractionation model
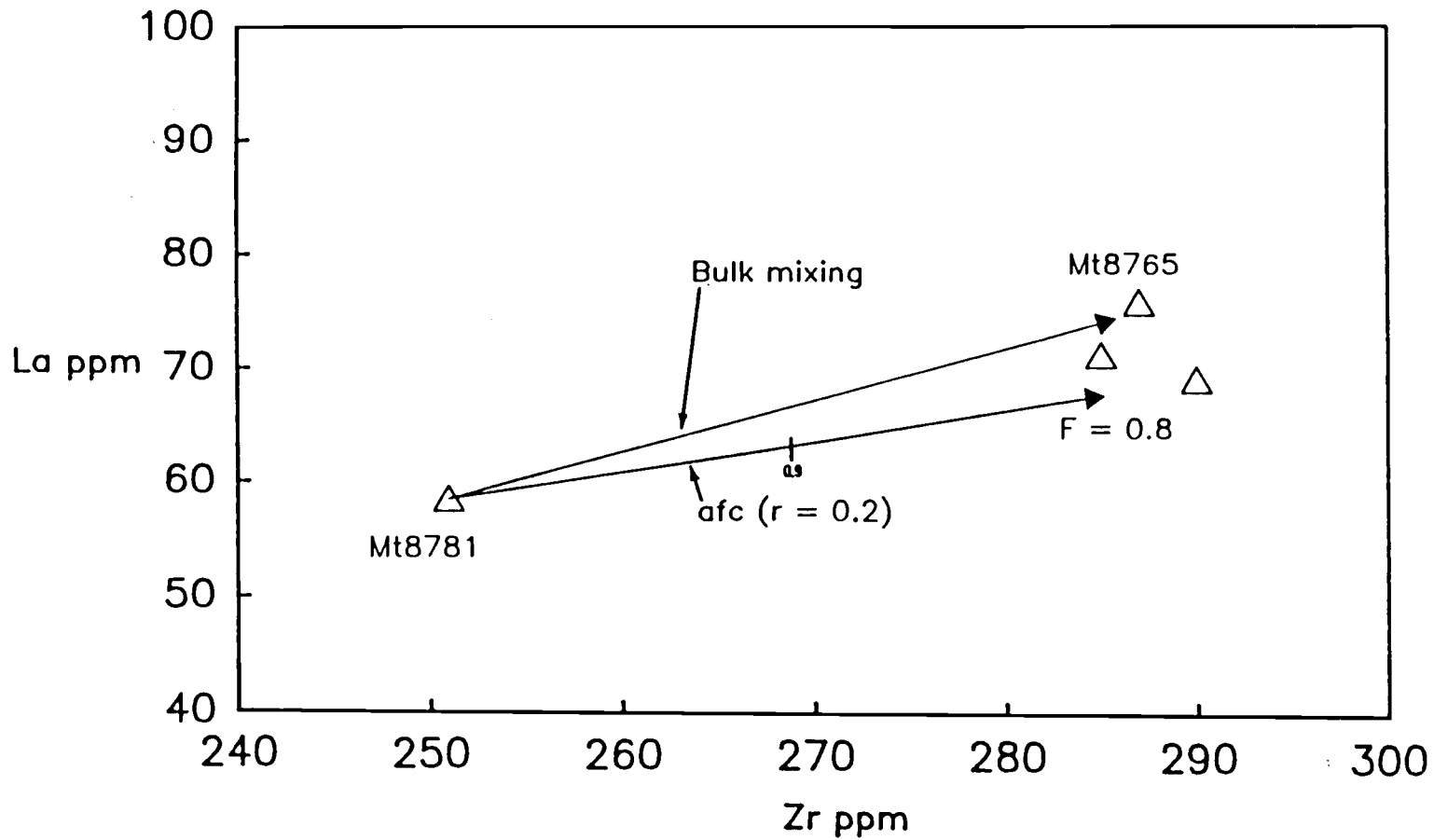
Figure 36. La versus Zr variation diagram for late group dacite (Mt8781) and rhyodacites (Mt8765, Mt8791d, Mt8775). The effects of bulk mixing and AFC (plag + bio + cpx + mag) are illustrated using sample Mt8765 as the contaminant. The AFC curve is terminated at F = 0.8.

(Appendix II). This small difference is insignificant in light of uncertainties in distribution coefficients used in calculations and the choice in the silicic contaminant.

In summary, compositional trends displayed by the late group can be accounted for by models involving mainly crystal fractionation. The largest discrepancies in the trace-element models are in Rb, Th, and U abundances in the interval andesite to dacite, and in Zr, and REE in the interval dacite to rhyodacite. A modest amount of assimilation can account for these discrepancies if the assimilant has elevated concentrations of these elements.

On the other hand, the late group rhyodacites may represent mostly remobilized crustal melts that have been slightly modified by mixing with small amounts of dacite. While it is presently difficult to rule out either interpretation, the former is favored for the following reasons. First, both major- and trace-element variations for the late group as a whole indicate that crystal fractionation was an important process. Second, Tvl_3 rhyodacites are texturally similar to Tvl_2 andesites and Tvl_1 dacites whose generation appears to be dominated by crystal fractionation and assimilation of crustal rocks. In all magma types there is a scarcity of xenocrystic material. Furthermore, the crystal-poor nature of these rocks may indicate separation of phenocrysts from liquid,

in contrast to stratigraphically lower crystal-rich magmas whose generation appears to have been little influenced by crystal fractionation.

Although the ratio of $^{87}Sr/^{86}Sr$ in the analyzed Tvl_3 sample is high (0.71568) and demands contamination by a crustal component, it is at the low end of the range of $^{87}Sr/^{86}Sr$ ratios inferred for mid-crustal rocks of the northeastern Great Basin (Sr_i = 0.71 - 0.74; Lee and Christiansen, 1983). These relations suggest that Tvl_3 rhyodacites are end products of the evolution of mantle-derived basalts that underwent extensive fractional crystallization accompanied by assimilation of mid-crustal rocks.

Musselwhite et al. (1989) came to a similar conclusion for the evolution of the Woods Mountain volcanic center in eastern California. These authors interpreted isotopic and trace element compositions of a large volume of rhyolitic magma to result from AFC of mantle derived basaltic magma. They argue that ϵ Nd values of the rhyolite (-7.5) are too high to have been derived directly from the continental basement whose inferred Nd composition (approximately -17.0) is much lower. The results of the study by Musselwhite et al. (1989) and this study indicate that large volumes of silicic magma in continental regions involve complex processes such as

fractional crystallization accompanied by different amounts of assimilation of crustal rocks rather than solely by anatexis of crustal rocks.

Summary and Discussion

The petrographic and geochemical features of the
early and middle group basaltic andesites through
rhyodacites indicate that these rocks evolved largely by
binary mixing of mafic and silicic magmas. All bulk
compositions have two populations of plagioclase
phenocryst cores. Cores of An80 suggest that the mafic
mixing endmember was basaltic in composition. Lack of
strong zonation in sodic plagioclase phenocrysts in early
group rhyodacites suggests that the silicic endmember may
have been a rhyodacite. However, even the most silicic
rhyodacites have petrographic evidence for magma mixing
and therefore the actual silicic endmember must be more
silicic than these rocks. Extrapolation of mixing lines
to higher silica contents yields zero-intercepts for MgO,
FeO, and CaO contents near 74 wt.% SiO_2 (Figure 17) which
suggests the silicic endmember must have had silica
contents between 71-74 wt.% SiO_2. The basaltic andesite
magmatic inclusions are not primary magmas; low Ni
contents, isotopic ratios atypical of basalts, and quartz
and sodic plagioclase xenocrysts attest to a history of
crustal contamination and olivine dominated fractionation.

Physical Considerations

The magmatic inclusions are important because they represent samples of mafic magma that coexisted in the same system as their more silicic hosts during the early stages of magmatism in the Egan Range volcanic complex. This suggests a scenario in which basaltic magmas were repeatedly injected into the crust to explain the sequence of magma types observed in the early and middle groups (Figure 37). Initially, mafic injections probably stalled at an unknown crustal level and silicic crustal melts may have been generated at the basalt-country rock interface (c.f. Huppert and Sparks, 1988). An initial low basaltic replenishment rate may have limited mechanical mixing and disaggregation of the mafic-silicic magma interface and may explain the lack of basaltic magmatic inclusions and mafic xenocrysts in Tves rhyolites.

Further injections of basaltic magma into the magma chamber produced increasingly larger volumes of silicic magma as the country rock temperature was further elevated (Figure 37). Experimental and theoretical models (Huppert and Sparks, 1988) indicate that crustal melting and generation of silicic magmas will rapidly ensue basalt emplacement when the wall rocks are near their solidus temperature (Huppert and Sparks, 1988). In addition, basaltic magmas either mixed with the silicic magmas or

a) Early group

b)Middle group
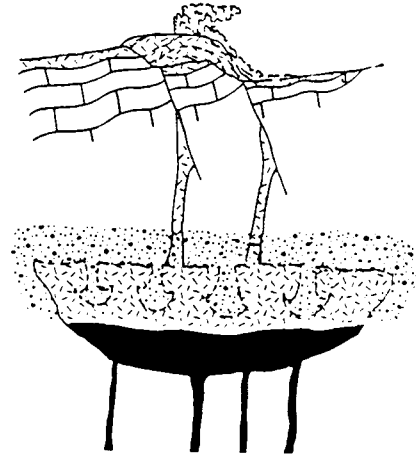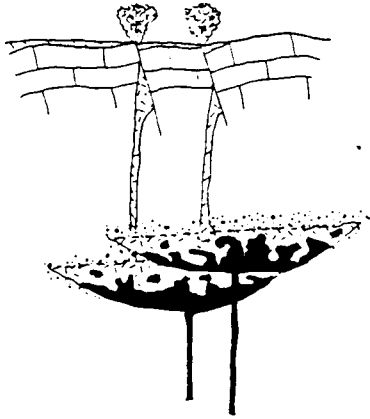
c)Late group
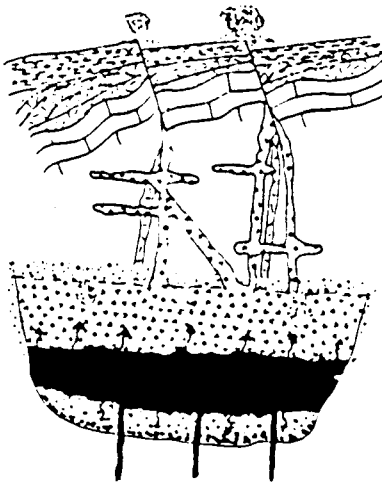
Legend

■ Basic intrusion

▦ Crustal melt

▨ Hybrid intermediate magma

▨ Fractionated silicic magma

▨ Gabbroic cumulates

Figure 37. Cartoon summarizing the evolutionary model for the Egan Range volcanic complex. (a) Early stage where the volume of basaltic magma exceeds the volume of silicic crustal melt. Basalt is able to mix directly with crustal melts to produce intermediate hybrid magmas. (b) The crustal temperature is elevated so that large volumes of silicic crustal melt are produced. Mixing takes place among intermediate magmas formed in (a) and crustal melts. Basalt is trapped beneath these magmas (c) The rate of basaltic replenishment to the system slows or ceases and the large volume of resident basalt crystallizes to produce andesites to rhyodacites, and gabbroic cumulates.

were quenched within them to form magmatic inclusions.

Suggested processes of inclusion formation and their dispersal in host magma fall into three general categories: (1) entrainment of basaltic magma in silicic magma during turbulent convection in a conduit enroute to the surface (Blake and Ivy, 1984; Koyaguichi, 1985), (2) mixing near the interface of a compositionally zoned magma chamber by reduction in density, such as by vesiculation, of the lower, mafic magma (Eichelberger, 1981), and (3) high velocity injection of turbulent plumes of mafic magma into the base of silicic magma chambers (Sparks et al., 1980; Campbell and Turner, 1984).

A critical constraint on the inclusion forming mechanism in the Egan Range volcanic complex is that it must be consistent with the observation that the magmas hosting the inclusions are two component mixtures of silicic crustal melt and inclusion forming magma. This indicates that intitially the volume of basaltic magma in the system was greater than the volume of silicic magma because a large volume of silicic magma favors quenching of the mafic magma rather then mixing of the two magmas (Sparks and Marshall, 1986). In detail, heat transfer process are orders of magnitude faster than chemical diffusion process. Therefore, the ability of magmas to mix depends upon their physical properties after they are

thermally equilibrated (Sparks and Marshall, 1986). A critical physical property controlling whether mafic and silicic magmas will mix is the viscosity of the magmas following thermal equilibration. Theoretical modeling by Sparks and Marshall (1986) indicates that viscosities of contrasting magma types will be favorable for mixing only when there is a larger proportion of mafic magma; typically 50% or greater. In this context, it is probably not fortuitous that mixing calculations indicate that the early group andesites and dacites are mixtures of 65 to 55% basaltic andesite and 35 to 45% rhyodacite. Once the volume ratio of silicic hybrid magma to incoming basaltic magma becomes too large to permit complete hybridization to occur, formation of magmatic inclusions becomes the dominant style of interaction between mafic and silicic magmas. Alternatively, inclusion formation may have occurred during forced convection of mafic and hybrid magmas in a conduit enroute to the surface (Koyaguchi, 1985), provided mixing of the endmember compositions to produce the hosts took place at an earlier time.

The disappearance of the magmatic inclusions in the middle group magmas indicates that the dacite-rhyodacite portion of the magma chamber became isolated from direct interaction with each new input of basaltic magma (Figure 37). This probably reflects the larger proportion of

silicic mixing endmember contained within the middle group dacites and rhyodacites. Experiments by Huppert and Sparks (1986) pertaining to the problem of mixing mafic and silicic magmas indicate that when a hot, dense fluid is emplaced beneath a larger volume of lighter, cool fluid, a sharp double-diffusive interface develops across which heat transfer, but not mass transfer, occurs. Thus, a possible explanation for the lack of magmatic inclusions in the middle group magmas is that a large volume of early group hybrid magma developed into a large crustal reservoir through which new inputs of basaltic magma could no longer penetrate. New inputs of basalt, however, could trigger rapid crustal melting at the silicic roof of the chamber (Huppert and Sparks, 1988). Once the roof of the chamber became partially molten, then by analogy with the experiments of Huppert and Sparks (1988), mixing and homogenization with the resident early hybrid magma proceeded by descending plumes of crustal melt into the underlying hot convecting interior of the reservoir (Figure 37).

The early group records the initial injections of basaltic magma into the crust, production of silicic crustal melts, and wholescale mixing of these magmas. The middle group records further melting of the crust and, thus, an increase in the volume of silicic magma in the

system. As discussed above, this volume was large enough to prevent wholescale mixing of basalt and silicic crustal melt, although newly generated crustal melts mixed with resident hybrid intermediate magmas. The strong chemical evidence for crystal fractionation, as opposed to magma mixing, controlling the evolution of the late group magmas indicates that the rate of supply of basaltic magma to the system slowed down or ceased altogether. As a result, thermal gradients and, therefore, convective velocities began to decline and crystallization and fractionation of the large volume of basaltic magma previously injected into the crust ensued. This model suggests that the thermal state of the magma system controls whether magmas evolve by crystal fractionation or magma mixing; it does not require a special tectonic regime.

Mantle Versus Crustal Sources

A major objective in the study of the Egan Range volcanic complex has been to estimate the relative volumes of mantle versus crustal sources contained within the mid-Tertiary volcanic rocks. This information is important for two reasons. First, previous models for mid-Tertiary magmatism in eastern Nevada have argued against major involvement of mantle-derived magmas in the generation of these rocks primarily on the basis of reconnaissance

isotope studies and the apparent absence of mafic igneous rocks (Farmer and DePaolo, 1983; Lee and Christiansen, 1983; Wernicke et al., 1986; Sonder et al., 1986). This view is in conflict with the currently accepted idea that large volume intermediate to silicic, continental magmatic systems are fundamentally basaltic in the sense that mantle-derived basalts either represent the starting point in a suite of magmas related largely by crystal fractionation (e.g., Musselwhite et al., 1989), or that basalts supply the necessary heat to generate intermediate to silicic crustal melts (e.g. Hildreth, 1981; Huppert and Sparks, 1988). Second, the geometry and kinematic interpretation of the Snake Range decollement is currently a controversial subject (c.f., Miller et al., 1983; Bartley and Wernicke, 1984; Gans and Miller, 1985; Wernicke and Bartley, 1985). Miller et al. (1983) and Gans (1987) infer that 5 to 10 km of new mantle-derived magma must be added to the crust during extension in east-central Nevada to account for (1) a relatively constant crustal thickness before and after 100 to 200% upper crustal extension, and (2) a constant present-day crustal thickness (approximately 35 km) in both highly extended and little extended domains. This also requires that lower crustal material flowed laterally from the little extended to the highly extended domains. In contrast, the

model of Bartley and Wernicke (1984) considers only extension in the Snake Range and requires no large additions of mantle-derived magma to the crust during mid-Tertiary extension.

The proportion of mantle versus crustal sources required by the volcanic rocks in the Egan Range volcanic complex cannot be determined precisely because of the lack of compositional or isotopic data on primary basaltic magmas and the wide range in possible isotopic compositions of the crustal source (Lee and Christiansen, 1983). However, a broad estimate of the relative proportions of mantle versus crustally derived materials can be estimated from the geochemical models developed above.

In order to make such estimates, it is necessary to reconstruct a possible primary basaltic magma composition to use as a starting point from which to derive the observed silicic compositions. Realistically, this is a formidable task because inverse modeling of a periodically recharged magma chamber will not produce a unique solution (Nielsen, 1988). However, the relative proportions of the different sources required by the more evolved compositions depends less on the exact composition of the primary basalt than they do on the differentiation processes that generated them. These processes can be

deduced from the textures and compositional trends of the evolved rocks and, thus, the choice of the inferred primary basalt composition is somewhat arbitrary provided that it is reasonable within petrologic constraints.

Composition of the Primary Basalt

The main petrologic constraint used in this model is the Ni content of the primary magma. Sato (1977) observed that during partial melting of peridiotitic mantle, the variation of the Ni content in olivine is small. Using a select range in Ni-Mg exchange partition coefficients between olivine and magma, Sato (1977) calculated equilibration with respect to Ni-MgO space for magmas in equilibrium with mantle olivine and compared them to compositional trends of ocean-floor basalts. The intersections of the ocean-floor basalt trends with the equilibration lines suggest that primary magmas in equilibrium with mantle olivine have Ni contents of 300 to 500 ppm (Sato, 1977). Therefore, in this study, a Ni content of 400 ppm is used to identify a primary magma composition. The major- and trace-element composition of this hypothetical basalt is in Table 10.

The calculation of the primary basaltic composition was made as follows. In the first step the composition of a mafic parent was calculated assuming that an early group

Table 10:   Chemical composition of model primary basalt

SiO2	48.5
Al2O3	11.3
FeO	7.6
Fe2O3	2.0
MgO	16.0
CaO	8.6
Na2O	1.2
K2O	1.2
TiO2	0.94
P2O5	0.29
MnO	0.14
Rb	29
Sr	481
Ba	980
La	11
Ce	23
Nd	19
Sm	4
Eu	1.3
Tb	0.6
Yb	1.9
Lu	0.3
Zr	133
Th	0
U	0
Sc	28
Cr	305
Co	34
Ni	400

FeO calculated assuming FeO = 0.66 FeO*
Method of calculation in text

andesite (Mt8787) represents a mixture of 50% early group

rhyodacite (Mt8786) and 50% basaltic magma (SiO_2 =

approximately 50 wt.%). These proportions were chosen

because basaltic magma cannot realistically mix with a

larger proportion of silicic magma (Sparks and Marshall,

1986), and they produce a primary magma with a reasonable

SiO_2 content (58.5%) and Mg# (67) before removal of olivine (see

below). The andesite sample was chosen because it is the

stratigraphically lowest mafic lava in the Egan Range

volcanic complex and therefore it may have been less

affected by processes such as magma chamber recharge; it

is the only olivine-bearing lava in the early group; and

it has extensive petrographic evidence for mixing between

silicic and mafic endmembers. The Ni concentration (42

ppm) and Mg# ($Mg/Mg+Fe^{2+}$; 58) of this calculated parent

are, however, lower then expected for a basaltic magma in

equilibrium with the mantle and, therefore, olivine was

added to this composition until a magma with 400 ppm Ni

was derived. A partition coefficient of 10 was used for

the distribution of Ni between basaltic liquid and olivine

(Leeman, 1976). This method requires fractionation of

approximately 22% olivine from the primary basalt to

produce the parental basalt. Olivine was the only

crystalline phase considered to have been removed because

the andesite has a high concentration of Cr suggesting

that pyroxene had not yet begun to fractionate. The
resulting primary basalt (Table 10) has a Mg# of 67
(assuming $Fe^{2+}O$ = 0.66 FeO*) which is close to the Mg-
value estimated by Green et al. (1974) for primary magmas
forming from mantle peridiotites (Mg# = approximately 70).

In Figure 38a-c, possible evolution paths for the
early and middle group magmas originating at this model
composition are given by solid lines; possible evolution
paths followed by the late group magmas are drawn as
dashed lines. I will focus on the late group lavas
because they constitute the largest volume of volcanic
rocks in the Egan Range volcanic complex. As discussed in
the previous section, the textures and compositional
trends of the evolved late group magmas indicate that they
evolved largely by crystal fractionation paired with
crustal assimilation. This suggests that the late group
andesites may be related to the primary magma by an AFC
process. To test this premise the assemblage 50% pyroxene
+ 25% olivine + 24% plagioclase + 1% magnetite was removed
from the primary magma (assuming Rayleigh fractionation)
concurrent with assimilation of a rhyodacitic composition
(Mt8765) in the ratio r = 0.3 (r = mass assimilated/mass
fractionated; DePaolo, 1981). In the three cases
illustrated (Figures 38a-c), the calculated trends closely
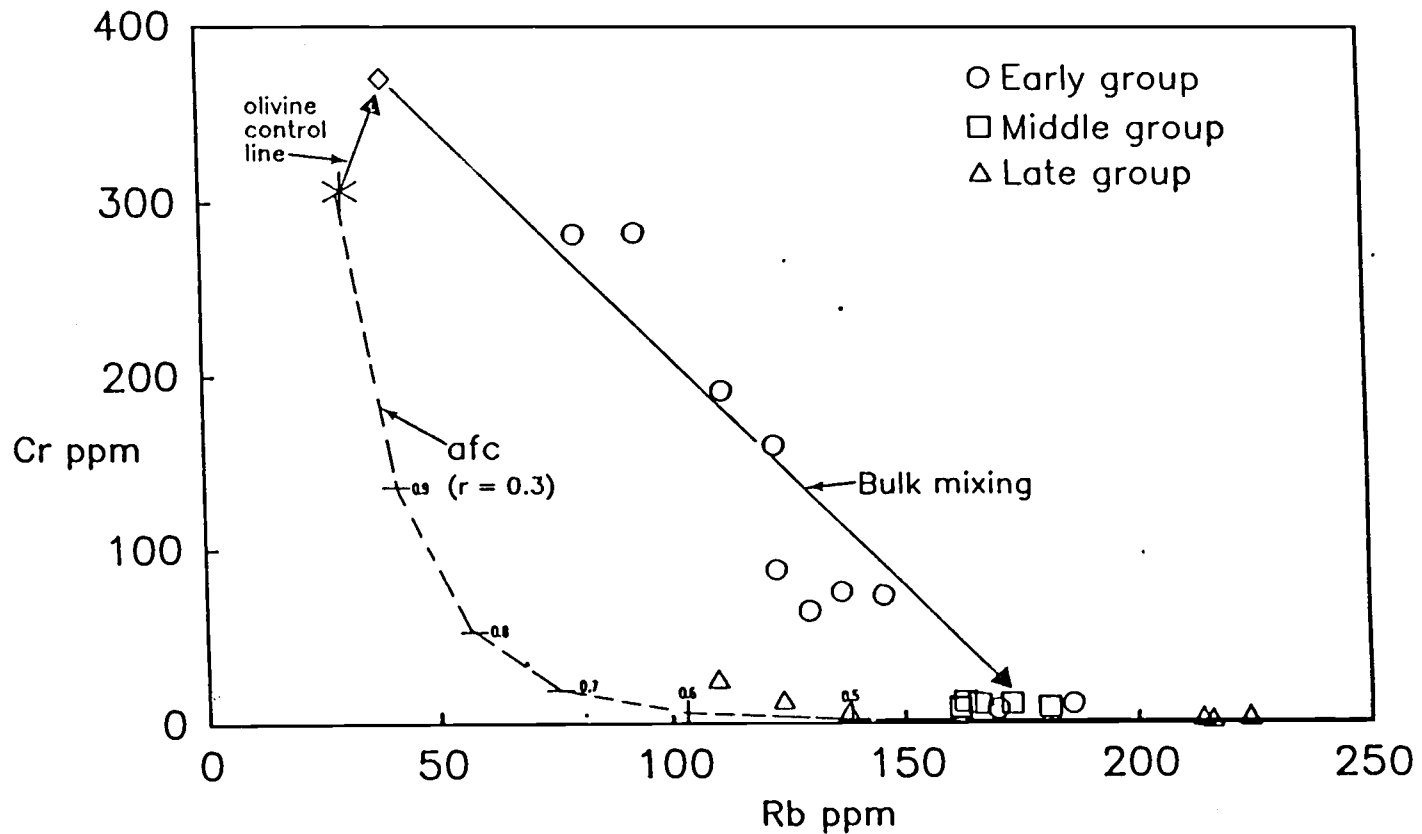
Figure 38a. Cr versus Rb model for Egan Range volcanic complex magmas. The star is the composition of the model primary basalt (Table 10). Dashed curve is assimilation fractional crystallization (AFC) model for late group magmas. In AFC, r, the rate of assimilation versus the rate of crystallization, equals 0.3 for the interval basalt to andesite, and 0.2 for interval andesite to rhyodacite. Tic marks are at 10% intervals of F. The crystallizing assemblage over each interval is given in Figure 38b. The Diamond is the basalt composition calculated assuming sample Mt8787 represents a mixture of 50% rhyodacite and 50% basalt. See text.
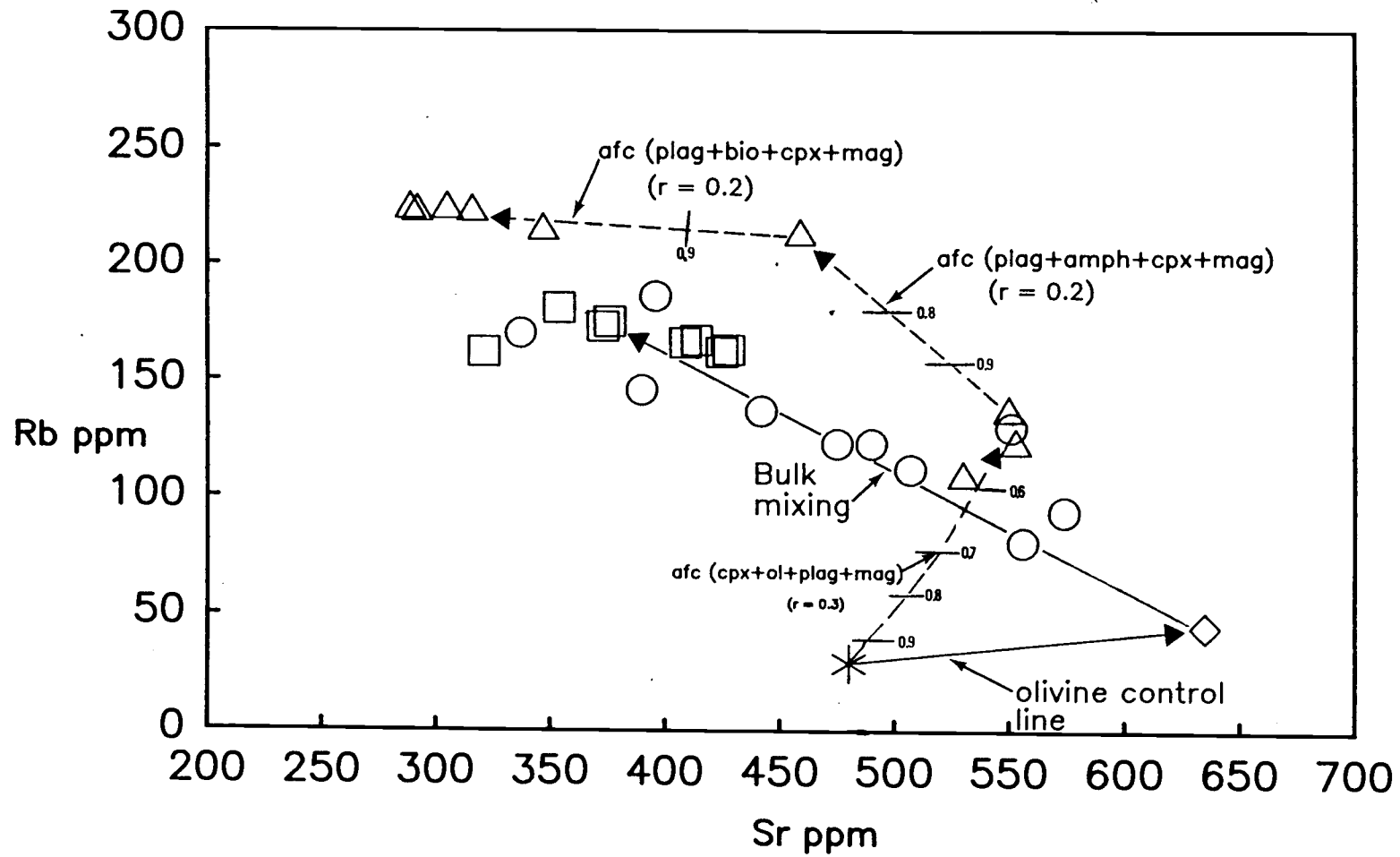
Figure 38b. Rb versus Sr model for Egan Range volcanic complex magmas. Symbols are the same as in Figure 38a.
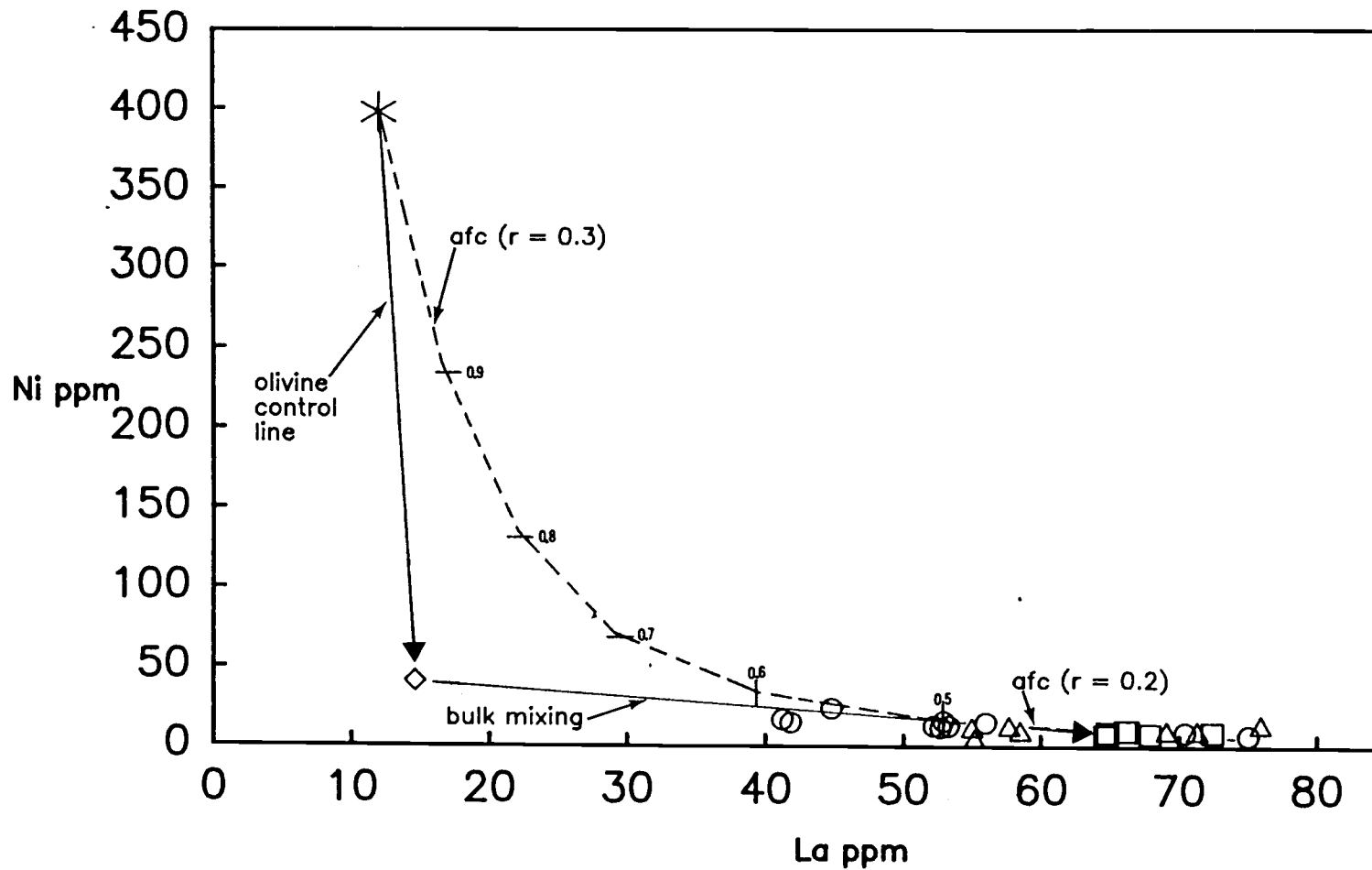
Figure 38c. Ni versus La model for Egan Range volcanic complex magmas. Symbols are the same as in Figure 38a.

reproduce the andesite compositions near F = 0.5 (F = mass of magma/ mass of original magma; DePaolo, 1981).

Using Tvl_3 rhyodacites as a silicic endmember in the AFC process a rough estimate of the volume of new mantle-derived magma added to the crust is calculated as follows. The volume of the late group magmas is approximately 35 km^3, of which two thirds (23.3 km^3) are estimated to be Tvl_3 rhyodacites. For the interval dacite to rhyodacite Figure 3b indicates that F is approximately 0.8:

$$F = M_m/M^o_m = 0.8$$

Therefore: $M^o_m = 23.3$ km^3 /0.8

and $M^o_m = 29.1$ km^3

For the interval andesite to dacite Figure 28b indicates F is approximately 0.7:

Therefore: $M^o_m = 29.1$ $km^3/0.7$

and $M^o_m = 41.6$ km^3

Using this volume of andesite to calculate the volume of basalt in the system yields the result:

$$M^o_m = 41.6 \ km^3/0.5$$

$$= 83.1 \ km^3$$

Since Tvl_3 rhyodacites are conservatively estimated to crop out over an area of 100 km^2,

$$83.1 \ km^3/100 \ km^2 = 0.83 \ km$$

Assuming an intrusive to extrusive ratio of 10:1 (Smith, 1979), I estimate that approximately 8.3 km of new magma

were added to the crust during eruption of the late group.
This value represents a maximum value in that these magmas
were erupted during crustal extension; the intrusive to
extrusive ratio in such a setting may be somewhat smaller
owing to continuous bleeding of subcrustal reservoirs
along surface faults. Nonetheless, the data indicate that
a substantial amount of new mass was added to the crust
during extension.

The calculated volume of new mantle magma added to
the crust critically relies on the interpretation that the
late group rhyodacites are products of an AFC process as
opposed to largely anatectic melts. Farmer and DePaolo
(1983) and Lee and Christiansen (1983) took the apparent
absence of mafic igneous rocks and high Sr-isotopic ratios
as permissive evidence against involvement of mantle-
derived magmas to produce broadly coeval granitic rocks in
east-central Nevada. These granitic rocks have Sr-isotope
ratios that are very similar to the late group rhyodacites
and may represent their deep seated equivalents. The
discovery of basaltic andesite magmatic inclusions and
olivine-phyric andesites in this study, however,
invalidates the assumption that mantle-derived magmas were
absent during generation of the silicic magmas.
Furthermore, the isotopic composition of the early mafic
rocks suggests that the isotopic composition of the mid-

Tertiary mantle in east-central Nevada may have been more enriched then previously assumed. For example, an early olivine-bearing andesite in the White Pine Range (WP1; Gans et al., 1989) has a initial $^{87}Sr/^{86}Sr$ ratio of 0.70837. Assuming that this rock was produced exclusively by mixing of 63% primary mantle-derived basalt and 37% early group rhyodacite (Mt8786; $^{87}Sr/^{86}Sr_i$ = 0.71235) indicates that the basaltic endmember has an initial $^{87}Sr/^{86}Sr$ ratio of 0.707. The mixing proportions were determined for a primary basalt with a SiO_2 wt.% of 45%. It must be emphasized that the calculated $^{87}Sr/^{86}Sr_i$ ratio of the primary basalt is a minimum value because if the evolution of the andesite involved any degree of crystal fractionation as opposed to magma mixing, or if the primary basalt had a higher SiO_2 content, the Sr isotope composition of the basaltic endmember must be more radiogenic.

In conclusion, the geochemical characteristics of the Egan Range volcanic complex magmas support the hypothesis of Miller et al. (1983) and Gans (1987) that large volumes of new mantle magmas were added to the crust during mid-Tertiary extension in east-central Nevada. Geochemical modeling suggests that the crust recieved up to 8.3 km of new material. This amount is similar to the amount (5 km) derived independently by Gans (1987) from structural

considerations. The volume of mafic magma involved in the genesis of the Egan Range volcanic complex is underrepresented by the rocks exposed at the surface today because of the large silicic system suppressing the amount of mafic magma to actually reach the surface.

Bibliography

Anderson, A.T., 1976, Magma mixing: Petrological process and volcanological tool: Jour. Volcanol. Geotherm. Res., 1:3-33.

Armstrong, R.L., 1970, Geochronology of Tertiary igneous rocks, eastern Basin and Range Province, western Utah, eastern Nevada and vicinity, USA: Geochim. et Cosmochim. Acta., 34:203-232.

--------------, 1972, Low-angle (denudational) faults, hinterland of the Sevier orogenic belt, eastern Nevada and western Utah: Geol. Soc. America Bull., 83:1720-1754.

Arth, J.G., 1976, Behavior of trace elements during magmatic process - A summary of theoretical models and their applications: Jour. U.S. Geol. Survey, 4:41-47.

Arth, J.G., and F. Barker, 1976, Rare-earth partitioning between hornblende and dacitic liquid and implications for the genesis of trondhjemitic-tonalitic magmas: Geology, 4:534-536.

Bacon, C.R., 1986, Magmatic inclusions in silicic and intermediate volcanic rocks: Jour. Geophys. Res., 91:6091-6112.

Bacon, C.R., and J. Metz, 1984, Magmatic inclusions in rhyolites, contaminated basalts, and compositional zonation beneath the Coso volcanic field, California: Contrib. Mineral. Petrol., 85: 346-365.

Bartley, J.M., and B.P. Wernicke, 1984, The Snake Range decollement interpreted as a major extensional shearzone: Tectonics, 3:647-657.

------------------------, 1985, Reply to "Comment on the Snake Range decollement interpreted as a major extensional shear zone" by P.B. Gans and E.L. Miller: Tectonics, 4:411-415.

Bence, A.E., and A.L. Albee, 1968, Empirical
correction factors for the electron
microanalysis of silicates and oxides:
Jour. Geol., 76:382-402.

Bender, J.F., F.N. Hodges, and A.E. Bence, 1978,
Petrogenesis of basalts from the project FAMOUS
area: Experimental study from 0 to 15 kbars:
Earth Planet. Sci. Lett., 17:277-302.

Blake, M.C., Jr., R.K. Hose, and E.H. McKee, 1969,
Tertiary volcanic stratigraphy of White Pine
County, Nevada: Geol. Soc. America Rocky
Mountain Sec., 22 Ann. Mtg., Salt Lake City,
Utah, Abs. Prog., pt. 5, p.8.

Blake, S., and Ivey, G.N., 1986, Magma-mixing and the
dynamics of withdrawl from stratified
reservoirs: Jour. Volcanol. Geotherm. Res.,
27:153-178.

Campbell, I.H., and J.S. Turner, 1984, The fluid
dynamics of fountains in magma chambers: in:
Dungan, M.A., T.L. Grove, and E.W. Hildreth,
eds., Proceedings of the Conference on Open
Magmatic Systems, Institute for Study of Earth
and Man, Southern Methodist Univ., Dallas, Tex.

Christiansen, E.H., M.G. Best, and B.J. Kowallis,
1988, Geochemistry of Oligocene calc-alkaline
volcanic rocks of the Needles Range Group,
Indian Peak volcanic field, Utah and Nevada:
Geol. Soc. America Abs. Prog. v. 20, n.7, p.
A315.

Christiansen, R.L., and P.W. Lipman, 1972, Cenozoic
volcanism and plate tectonic evolution of the
western United States: II. Late Cenozoic: in: A
Discussion on Volcanism and the Structure of the
Earth: Philos. Trans. R. Soc. London., ser. A,
217:249-284.

Coney, P.J., 1974, Structural analysis of the Snake
Range decollement, east-central Nevada: Geol.
Soc. America Bull., 85:973-978.

Crandell, D.R., 1971, Postglacial lahars from Mount

Rainier Volcano, Washington: U.S. Geol. Sur. Prof. Paper 677, 75 p.

Crawford, A.J., T.J. Falloon, and S. Eggins, 1987, The origin of island arc high-alumina basalts: Contrib. Mineral. Petrol., 97:417-430.

Crittenden, M.D., Jr., P.J. Coney, and G.H. Davis, eds., 1980, Cordilleran Metamorphic Core Complexes: Mem. Geol. Soc. America, 153, 490 pp.

DeBari, S., and R.G. Coleman, 1989, Examination of the deep levels of an island arc, evidence from Tonsina ultramafic-mafic assemblage, Tonsina, Alaska: EOS, v. 70, p. 144.

Deer, W.A., R.A. Howie, and J. Zussman, 1963, An Introduction to the rock forming minerals, Langman Group Limited, Harlow, England.

DePaolo, D.J., 1981, Trace element and isotopic effects of combined wallrock assimilation and fractional crystallization: Earth Planet. Sci. Lett., 53:189-202.

Douglass, W.B., Jr., 1960, Geology of the southern Butte Mountains, White Pine County, Nevada: Intermountain Association of Petroleum Geologists, 11th Annual Field Conference Guidebook, p. 181-185.

Dungan, M.A., 1987, Open system magmatic evolution of the Taos Plateau volcanic field, northern New Mexico. II: The genesis of cryptic hybrids: J. Petrology, 28:955-977.

Dungan, M.A., and J.M. Rhodes, 1978, Residual glasses and melt inclusions in basalts from DSDP Legs 45 and 46: Evidence for magma mixing: Contrib. Mineral. Petrol., 67:417-431.

Eichelberger, J.C., 1975, Origin of andesite and dacite: Evidence of mixing at Glass Mountain in California and other circum-Pacific volcanos: Geol. Soc. America Bull., 86:1381-1391.

----------------, 1980, Vesiculation of mafic magma during replenishment of silicic magma chambers: Nature, 288: 446-450.

Eichelberger, J.C., and R. Gooley, 1977, Evolution of
    silicic magma chambers and their relationships to
    basaltic volcanism: Geophys. Monograph, Am.
    Geophys. Union, v. 20, p.57-77.

Epstein, S., and H.P. Taylor, Jr., 1967, Variation of
    O^{18}/O^{16} in minerals and rocks: in: P.H. Abelson,
    ed., Researches in Geochemistry, 2:29-62, John
    Wiley, New York, 663 p.

Farmer, G.L., and D.J. DePaolo, 1983, Origin of
    Mesozoic and Tertiary granite in the western
    United States and implications for pre-crustal
    structure: 1. Nd and Sr isotopic studies in the
    geocline of the northern Great Basin: Jour.
    Geophys. Res., 88:3379-3401.

Feeley, T.C., and Morris, E.M., 1986, Petrologic
    similarities of Eocene quartz-olivine basaltic
    andesites, Oregon and Montana: Geol. Soc.
    America Abs. Prog., v. 18, n. 6, p. 599.

Feeley, T.C., A.L., Grunder, and P.B. Gans, 1988,
    Hybridization of crust and mantle melts during
    early stages of mid-Tertiary extension in eastern
    Nevada: Evidence from the Egan Range: Geol.
    Soc. America Abs. Prog., v. 20, n. 8, p. A314.

Fisher, R.V., and H-.U. Schmincke, 1984, Pyroclastic
    Rocks: New York, Springer-Verlag, 472 p.

Fritz, W.H., 1960, Structure and stratigraphy of the
    northern Egan Range, White Pine County, Nevada:
    unpub. Ph.D. Thesis, Univ. of Washington,
    Seattle, Wa.

Gans, P.B., 1982, Mid-Tertiary magmatism and
    extensional faulting in the Hunter District,
    White Pine County, Nevada: unpub. M.S. Thesis,
    Stanford Univ., Stanford, Ca.

----------, 1987, An open-system, two-layer crustal
    stretching model for the eastern Great Basin:
    Tectonics, 6:1-12.

Gans, P.B., and G.A. Mahood, 1989, The interplay
    between Cenozoic extension and magmatism in the

Basin and Range Province: in: New Mexico Bureau of Mines and Geology Bulletin 131:101; M.A. Dungan, ed..

Gans, P.B., G. Mahood, and E.R. Schermer, 1989, Syn-extensional magmatism in the Basin and Range Province: A case study from the eastern Great Basin: Geol. Soc. America Spec. Paper 233, 53 pp.

Gans, P.B., and E.L. Miller, 1983, Style of mid-Tertiary extension in east-central Nevada: in: Utah Geological and Mineral Survey Special Studies 59; Guidebook part I, GSA Rocky Mtn. and Cordill. Sec. Mtg., Salt Lake City.

------------------------, 1985, Comment on "The Snake Range decollement interpreted as a major extensional shear zone" by J.M. Bartley and B.P. Wernicke: Tectonics, 4:411-415.

Gans, P.B., E.L. Miller, T. McCarthy, and M.L. Ouldcott, 1985, Tertiary extensional faulting and evolving ductile-brittle transition zones in the northern Snake Range and vicinity: New insights from seismic data: Geology, 13:189-193.

Garcia, M.O., and S.S. Jacobson, 1979, Crystal clots, amphibole fractionation, and the evolution of calc-alkaline magmas: Contrib. Mineral. Petrol., 69:319-327.

Gill, J.B., 1978, Role of trace element partition coefficients in models of andesite genesis: Geochim. et Cosmochim. Acta, 42:709-724.

Glazner, A.F., W. Ussler, III, and J.W. Mies, 1988, Fate of granitic minerals in mafic magmas: EOS, v. 69, n. 44, p. 1504.

Green, D.H., D. Edgar, P. Beasley, E. Kiss, and N.G. Ware, 1974, Upper mantle source for some hawaiites, mugearites and benmoreites: Contrib. Mineral. Petrol., 48:33-43.

Green, T.H., and N.J., Pearson, 1985a, Rare earth element partitioning between clinopyroxene and silicate liquid at moderate to high pressure: Contrib. Mineral. Petrol., 91:24-36.

------------------------, 1985b., Experimental determination of REE partition coefficients

between amphibole and basaltic to andesitic
liquids at high pressure: Geochim. et Cosmochim.
Acta, 49:1465-1478.

Griffiths, J.H.E., J. Owen, and I.M. Ward, 1954,
Paramagnetic resonance in neutron irradiated
diamond and quartz: Nature, 173:439-440.

Gromet, L.P., and L.T. Silver, 1983, Rare earth
element distributions among minerals in a
granodiorite and their petrogenetic
implications: Geochim. et Cosmochim. Acta,
34:331-376.

Grove, T.L., and J.M. Donnelly-Nolan, 1986, The
evolution of silicic lavas at Medicine Lake
Volcano, California: Implications for the
origin of compositional gaps in calc-alkaline
series lavas: Contrib. Mineral. Petrol.,
92:281-302.

Grove, T.L., D.C. Gerlach, and T.W. Sando, 1982,
Origin of calc-alkaline series lavas Medicine
Lake Volcano by fractionation, assimilation, and
mixing: Contrib. Mineral. Petrol., 80:160-182.

Grunder, A.L., 1986, The Calabozos caldera complex:
Geology, petrology, and geochemistry of a major
silicic volcanic center and hydrothermal system
in the southern Andes: unpub. Ph.D. Thesis,
Stanford University, Stanford, Ca.

-------------, 1987, Low $\delta^{18}O$ silicic volcanic rocks
of the Calabozos caldera complex, southern
Andes: Contrib. Mineral. Petrol., 95:71-81.

Grunder, A.L., and T.C. Feeley, 1989, Evidence for
crustal and mantle sources of Tertiary,
extension related volcanism in east-central
Nevada: in: New Mexico Bureau of Mines and Geology
Bulletion 131:116, M.A. Dungan, ed..

Grunder, A.L., and G.A. Mahood, 1988, Physical and
chemical models of zoned silicic magmas: The
Loma Seca Tuff and the Calabozos Caldera,
Southern Andes: Jour. Petrol., 29:831-867.

Grunder, A.L., P.B. Gans, and E.R., Schermer, 1987,
Time-composition trends of volcanic rocks associated
with mid-Tertiary extension in east-central Nevada

and adjacent Utah: Geol. Soc. America
Abs. Prog., 19:384.

Helz, R.T., 1976, Phase relations of basalts in their
melting range at P_{H2O} = 5 kb. Part II. Melt
compositions: Jour. Petrol., 17:139-193.

Hildreth, W., 1981, Gradients in silicic magma
chambers: Implications for lithospheric
magmatism: Jour. Geophys. Res., 86:10,153-
10192.

Hose, R.K., and M.C. Blake, Jr., 1976, Geology and
mineral resources of White Pine County, Nevada:
Part I, Geology: Nevada Bureau of Mines and
Geology, Bulletin 85, 105 p.

Huppert, H.E., and R.S.J. Sparks, 1988, The
generation of granitic magmas by intrusion of
basalt into continental crust: Jour. Petrol.,
29:599-624.

Irvine, T.N., and W.R.A. Baragar, 1971, A guide to
the chemical classification of the common
volcanic rocks: Can. J. Earth Sci., 8:523-548.

Irving, A.J., and F.A. Frey, 1984, Trace element
abundances in megacrysts and their host basalts:
Constraints on partition coefficients and
megacryst genesis: Geochim. Cosmochim. Acta,
48:1201-1221.

Janda, R.D., K.M. Scott, K.M. Nolan, and H.A.
Mortinson, 1981, Lahar movement effects, and
deposits: in: Lipman, P.W., and D.R.
Mullineaux, eds., the 1980 eruptions of Mount
St. Helens, Washington: U.S. Geol. Sur. Prof.
Paper 1250, p. 461-478.

Johnson, C.M., and P.W. Lipman, 1988, Origin of
metaluminous and alkaline volcanic rocks of the
Latir volcanic field, northern Rio Grande rift,
New Mexico: Contrib. Mineral. Petrol., 100:107-
18.

Kleinhampl, F.J., and J.I. Zioney, 1985, Geology of
northern Nye County, Nevada: Nevada Bureau of
Mines and Geology Bulletin 99A, 172 p.

Koyaguchi, T., 1985, Magma mixing in a conduit:
    Jour. Volcanol. Geotherm. Res., 25:365-369.

------------, 1986, Textural and compositional
    evidence for magma mixing and its mechanism, Abu
    volcano group, southwestern Japan: Contrib.
    Mineral. Petrol., 93:33-45.

Kuno, H., 1950, Petrology of Hakano volcano and the
    adjacent areas: Geol. Soc. America Bull.,
    61:957-1020.

Langmuir, C.H., R.D. Vocke, Jr., G.H. Hanson, and
    S.R. Hart, 1978, A general mixing equation with
    applications to Icelandic basalts, Earth Planet.
    Sci. Lett., 37:380-392.

Leake, B.E., 1978, Nomenclature of amphiboles: Am.
    Mineral., 63:1023-1052.

Leeman, W.P., 1976, Petrogenesis of Mckinney (Snake
    River) olivine tholeiite in light of rare-earth
    element and Cr/Ni distributions: Geol. soc.
    America Bull., 87:1582-1586.

Lindsley, D.H., 1983, Pyroxene thermometry: Am.
    Mineral., 68:477-493.

Lofgren, G.E., 1974, An experimental study of
    plagioclase crystal morphology: Isothermal
    crystallization: Am. Jour. Sci., 274:243-273.

Luhr, J.F., and I.S.E. Carmichael, 1980, the Colima
    volcanic complex, Mexico: I. Post-caldera
    andesites from Volcan Colima: Contrib. Mineral.
    Petrol., 71:343-372.

Mathis, A.C., 1988, Programmed cooling experiments:
    Morphological and compositional changes for
    plagioclase and olivine crystals in a basaltic
    melt: Honors Essay, Dept. of Geology, Univ. of
    North Carolina, Chapel Hill, 36 p.

McKee, E.H., A.L. Tarshis, and R.F. Marvin, 1976,
    Summary of radiometric ages of Tertiary volcanic
    and selected plutonic rocks in Nevada. Part V:
    Northeastern Nevada: Isochron West, 16:15-27.

McMillan, N.J., and M.A. Dungan, 1984, Magma mixing
    in the Taos Plateau magmatic system: in:

Dungan, M.A., T.L. Grove, and E.W. Hildreth, eds., Proceedings of the Conference on Open Magmatic Systems, Institute for study of Earth and Man, Southern Methodist Univ., Dallas, Tex.

------------------------------, 1986, Magma mixing as a petrogenetic process in the development of the Taos Plateau volcanic field, New Mexico: Jour. Geophys. Res., 91:6029-6045.

------------------------------, 1988, Open system magmatic evolution of the Taos Plateau volcanic field, northern New Mexico: 3. Petrology and Geochemistry of andesite and dacite: Jour. Petrol., 29:527-557.

Miller, E.L., P.G. Gans, and J. Garing, 1983, The Snake Range decollement: An exhumed mid-Tertiary ductile-brittle transition: Tectonics, 2:239-263.

Misch, P., 1960, Regional structural reconnaissance in central-northeast Nevada and some adjacent areas: Observations and interpretations: Intermountain Association of Petroleum Geologists, 11th Annual Field Conference Guidebook, p. 17-44.

Musselwhite, D.S., D.J. DePaolo, and M. McCurry, 1989, the evolution of a silicic magma system: isotopic and chemical evidence from the Woods Mountains volcanic center, eastern California: Contrib. Mineral. Petrol., 101:19-29.

Nagasawa, H., 1970, Rare earth concentrations in zircon and apatite and their host dacites and granites: Earth Planet. Sci. Lett., 9:359-364.

Nagasawa, H., and C.C. Schnetzler, 1971, Partitioning of rare earth, alkali and alkaline earth elements between phenocrysts and acidic igneous magma: Geochim. et Cosmochim. Acta, 35:953-967.

Nassau, K., and B.E. Prescott, 1975, A reinterpretation of smokey quartz: Phys. Stat. Sol., 29:659-663.

------------------------------, 1977, Smokey, blue, greenish yellow, and other irradiation-related colors in quartz: Mineral. Mag., 41:301-312.

Nicholls, J., I.S.E. Carmichael, and J.C. Stormer, Jr., 1971, Silica activity and Ptotal in igneous rocks: Contrib. Mineral. Petrol., 33:1-20.

Nielsen, R.L., 1988, A model for the simulation of combined major and trace element liquid lines of descent: Geochim. et Cosmochim. Acta, 52:27-38.

Nielsen, R.L., and M.A. Dungan, 1985, The petrology and geochemistry of the Ocate volcanic field, north-central New Mexico: Geol. Soc. America Bull., 96:296-312.

O'Hara, M.J., and R.E. Mathews, 1981, Geochemical evolution in an advancing, periodically replenished, periodically tapped, continuously fractionating magma chamber: Jour. Geol. Soc. Lond., 138:237-277.

Peacock, M.A., 1932, Classification of igneous rock series: Jour. Geol., 39:54-67.

Pearce, J.A., and M.J. Norry, 1979, Petrogenetic implications of Ti, Zr, Y, and Nb variations in volcanic rocks: Contrib. Mineral. Petrol., 69:33-47.

Sato, H., 1975, Diffusion coronas around quartz xenocrysts in andesite and basalt from Tertiary volcanic region in northeastern Shikoku, Japan: Contrib. Mineral. Petrol., 50:49-64.

--------, 1977, Nickel content in basaltic magmas: Identification of primary magmas and a measure of the degree of olivine fractionation: Lithos, 10:113-120.

Schermer, E.R., and P.B. Gans, 1985, Isotope and trace element geochemistry of syn-extensional volcanic rocks, east-central Nevada: EOS, 66:1138.

Sheridan, M.F., 1981, Emplacement of pyroclastic flows: A review: in: Ash Flow Tuffs, Chapin, C.E., and W.E. Elston, eds., Geol. Soc. America Spec. Pap. 180, p. 125-134.

Smith, G.A., 1986, Coarse-grained nonmarine volcaniclastic sediment: Terminology and

depositional process: Geol. Soc. America Bull.,
97:1-10.

Sonder, L.J., P.C. England, B.P. Wernicke, and R.L.
Christiansen, 1987, A physical model for Cenozoic
extension of western North America: in: Dewey,
J., and M. Coward, eds., Continental Extensional
Tectonics, Jour. Soc. London, 143:187-201.

Sparks, R.S.J., and L.A. Marshall, 1986, Thermal and
mechanical constraints on mixing between mafic
and silicic magmas: Jour. Volcan. Geotherm.
Res., 29:99-124.

Sparks, R.S.J., P. Meyer, and H. Sigurdsson, 1980,
Density variation amongst mid-ocean ridge
basalts: Implications for magma mixing and the
scarcity of primitive lavas: Earth Planet. Sci.
Lett., 46:419-430.

Spear, F.S., and K.L. Kimball, 1984, RECAMP- A
Fortran IV program for estimating Fe^{3+} contents
in amphiboles: Computers and Geosciences,
10:317-325.

Stewart, D.C., 1975a, Crystal clots in calc-alkaline
andesites as breakdown products of high-Al
amphiboles: Contrib. Mineral. Petrol., 53:195-
204.

--------------, 1975b, Crystal clots in calc-alkaline
andesites as breakdown products of high-Al
amphiboles: unpub. M.S. Thesis, Pennsylvania
State Univ., 47 pp.

Stewart, J.H., 1980, Geology of Nevada: A discussion
to accompany the Geologic Map of Nevada: Nevada
Bureau of Mines and Geology Special Publication
4, 136 p.

Stewart, J.H., and T.E. Carlson, 1978, Geologic Map
of Nevada: U.S. Geological Survey, 1:500,000.

Stewart, J.H., and F.G. Poole, 1974, Lower Paleozoic
and uppermost Preccambrian strata of the
Cordilleran Miogeocline, Great Basin, western
United States: in: Tectonic and sedimentation,
Dickinson, W.R., ed., Society of Economic
Paleontologists and Mineralogists Special
Publication, 22:28-57.

Taylor, H.P., Jr., 1968, The oxygen isotope
    geochemistry of igneous rocks: Contrib. Mineral.
    Petrol., 19:1-71.

-----------------., 1980, The effects of assimilation
    of country rocks by magmas on $^{18}O/^{16}O$ and $^{87}Sr/^{86}Sr$
    systematics in igneous rocks: Earth Planet. Sci.
    Lett., 47:243-254.

Thompson, R.A., M.A. Dungan, and P.W. Lipman, 1986,
    Multiple differentiation processes in early-rift
    calc-alkaline volcanics, northern Rio Grande
    rift, New Mexico: Jour. Geophys. Res., 91:6040-
    6058.

Ussler, W., III, and A.F. Glazner, 1987, Origin of
    augite coronas around quartz xenocrysts in
    basalts and andesites: Geol. Soc. America Abs.
    Prog., v. 19, n. 7.

------------------------------------, in press, Phase
    equilibria along a basalt-rhyolite mixing line:
    Implications for the origin of calc-alkaline
    intermediate magmas: Contrib. Mineral. Petrol.

Watson, E.B., 1982, Basalt contamination by
    continental crust: Some experiments and models:
    Contrib. Mineral. Petrol., 80:73-87.

Wernicke, B.P., R.L. Christiansen, P.C. England, and
    L.J. Sonder, 1987, Tectonomagmatic evolution of
    Cenozoic extension in the North American
    Cordillera: in: Dewey, J., and M. Coward, eds.,
    Continental Extensional Tectonics, Jour. Geol.
    Soc. London, 143:203-221.

Winfrey, W.M., Jr., 1958, Stratigraphy, correlation,
    and oil potential of the Sheep Pass Formation,
    east-central Nevada: Am. Ass. Petrol. Geol.,
    Rocky Mountain Sec., Geological Record, p. 77-82.

Woodward, L.A., 1962, Structure and stratigraphy of
    the central northern Egan Range, White Pine
    County, Nevada: unpub., Ph.D. Thesis, Univ. of
    Washington Seattle, Wa.

Young, J.C., 1960, Structure and stratigraphy in the
    north central Schell Creek Range, eastern Nevada:

unpub. Ph.D. Thesis, Princeton Univ., Princeton, N.J.

Zoback, M.L., R.E. Anderson, and G.A. Thompson, 1981, Cainozoic evolution of the state of stress and style of tectonism of the Basin and Range Province of the western United States: Phil. Trans. R. Soc. Lond. ser. A, 300:407-434.

APPENDICES

Appendix I: Sample Locations and Petrographic
Descriptions

Sample locations and petrographic descriptions
of analyzed rocks are summarized here. Samples are
grouped according to map unit and are described in
ascending stratigraphic order. Silica contents are
given for each sample. Where multiple analyses were
preformed for a single map unit, descriptions may be
summarized. Locations are given by Township, Range,
1/4 section, and elevation and are indicated on Plate
1.

Early Group Rocks

Lower Clastic and Pyroclastic Unit (map unit Tves and Tvesa)

Mt8787, Mt8789: Seriate-glomeroporphyritic, olivine-, quartz-, and amphibole-bearing two-pyroxene andesite. Clasts from upper exposed section of debris flow. Mt8787: T.18N., R.62E., SE 1/4 sec. 5, elevation 7840 feet. Silica content = 59.5%. Mt8789: T.18N., R.62E., NW 1/4 sec. 9, elevation 7885 feet. Silica content = 59.9%. Clinopyroxene (12%, average 0.7 mm across, Wo39-41, En47-54, Fs7-14) occurs as individual phenocrysts and glomerocrysts with Fe-Ti oxides. Crystals are subhedral to anhedral and may have foggy or ragged rims. Also occurs as acicular laths (up to 0.2 mm) radiating outward in reaction coronas surrounding quartz xenocrysts. Plagioclase phenocrysts (5.8%) form three groups: phenocrysts up to 5.0 mm across with sieved calcic cores (An80) and fresh, slightly zoned overgrowths (An78), phenocrysts up to 5.0 mm across with fresh sodic cores (An34) and foggy, reversely zoned rims (An40), and as microphenocrysts (up to 0.2 mm; An60) in groundmass. Orthopyroxene (6%, up to 0.6 mm across, Wo5-3, En70-66, Fs25-31) forms individual grains and glomerocrysts with plagioclase. Fe-Ti oxides (3%) are dispersed as microphenocrysts in the groundmass, as individual phenocrysts, in glomerocrysts with clinopyroxene, and as reaction rims surrounding amphibole. Olivine (1.4%, 0.3-0.7 mm) are anhedral and largely altered to bowlingite. Quartz xenocrysts (0.6%; polycrystalline clots up to 1.2 cm across) are rounded, embayed and may have extensive reaction coronas of clinopyroxene. Amphibole (trace amounts, oxyhornblende, up to 3 mm across) is rimmed by opacite and granular clinopyroxene. Accessory grains of zircon and apatite.

Mt8816: Hypocrystalline, biotite- bearing rhyolite. T.18N., R.62E., SW 1/4 sec. 4, elevation 7721 feet. Silica content = . Clast from lower exposed section of debris flow. Phenocrysts: plagioclase (22.0%), sanidine (2.8%), biotite (2.8%), quartz (1.8%), Fe-Ti oxides (trace), plus accessory allanite, zircon and apatite. Plagioclase is the main phryic phase (up to 2.5 mm across) and occurs as euhedral, clear crystals (An35) some which may show minor oscillatory zoning (An25). Quartz (up to 3.0 mm across, average = 0.9mm

across) and sanidine (up to 2.6 mm across, average = 1.3 mm across) occur as anhedral to subhedral, commonly resorbed or broken phyric grains. Biotite is very fresh and occurs in euhedral books up to 1.0 mm across. A single xenolith of porphyritic granite is present in the section and is comprised of plagioclase, quartz, and alkali feldspar. Quartz and alkali feldspar are in graphic intergrowth. The xenolith is rounded, although its interior contains no interstitial glass. The wholerock groundmass is composed of partially devitrified glass.

Mt8735: Uhalde tuff (map unit Tvesa). Biotite rhyodacite lapilli ash-flow tuff. T. 19N., R.61E., SE 1/4 sec. 29, elevation 6880 feet. Silica content of pumice = 70.1%. Pumice analyzed from ash-flow tuff is white in salmon colored tuff-matrix and is slightly elongated. Phenocrysts in whole-rock are quartz (9.5%, up to 4.5 mm across), plagioclase (7.6%, An23 unzoned, up to 3 mm across), sanidine (3.1% up to 2.8 mm across), biotite (2.2%, up to 1.7 mm across), Fe-Ti oxides (trace), amphibole (trace), orthopyroxene (trace) and accessory phases allanite (up to 0.8 mm across) and zircon (up to 0.2 mm across). Phenocrysts observed in pumice: plagioclase, quartz, sanidine, biotite, orthopyroxene, zircon. Phenocrysts are euhedral to subhedral and are commonly broken.

Early Magmatic Inclusion-Bearing Lavas (map unit Tve$_1$)

·Mt8749, Mt879: Vesicular, microcrystalline, intergranular with minor diktytaxitic voids, two-pyroxene, amphibole basaltic andesite magmatic inclusions. Mt8749: T.19N., R.62E., SE 1/4 sec. 20, elevation 7310 feet. Silica content = 54.0%. Mt879: T.19N., R.62E., SW 1/4 sec. 16, elevation 2275 meters. Silica content = 56.9%. Phenocrysts: clinopyroxene, orthopyroxene (combined 39%; opx > cpx), plagioclase (35.1%), amphibole (6.1%), vesicles (14.4%). Mt879 contains xenocrysts of quartz (2.1%) biotite (1.5%), and large (up to 6 mm across) plagioclase (An20-An45) with cloudy, sieved rims. Clinopyroxene occurs as acicular phenocrysts up to 1.1 mm across, as strongly zoned equant phenocrysts (Wo37 En55 Fs7 core to Wo32 En39 Fs29 rim), and as reaction coronas surrounding xenocrystic quartz.

Orthopyroxene occurs as acicular laths (average size 0.2 mm) often with skeletal edges and in groups forming radiating fan splays. Plagioclase occurs as skeletal, acicular laths (up to 0.4 mm; An70 core to An65 rim) commonly in groups forming radiating fan splays, and in sample Mt879 as larger (up to 6.0 mm across) equant xenocrysts (core: An20 to An45) rarely with inclusions of biotite. Amphibole is present as small microphenocrysts as a few larger crystals (up to 2.0 mm across) of basaltic hornblende with opacite rims. Edges of opx, amphibole, and biotite are altered to Fe oxides imparting a red color to inclusions. Quartz xenocrysts (up to 5 mm across) are rounded and embayed and are commonly rimmed by clinopyroxene reaction coronas.

Mt8760: Glomeroporphyritic, seriate, two-pyroxene, biotite, amphibole andesite. T.19N., R.62E., SW 1/4 sec. 21, elevation 7575 feet. Silica content = 61.4%. Rock is extensively oxidized and devitrified. Phenocrysts: Plagioclase (15.6%), clinopyroxene (5.7%), orthopyroxene (4.1%), biotite (3.4%), amphibole (3.4), quartz (1.0%), sanidine (trace), Fe-Ti oxides (trace), plus accessory zircon and apatite. Plagioclase occurs as phenocrysts with sieved, sodic cores (An41) that are strongly reversely zoned and mantled by fresh calic overgrowths (An80), and as clear, unzoned (An36) phenocrysts. Clinopyroxene occurs as phyric grains (up to 0.9 mm across) which display a continuous range of grain sizes to microphenocrysts, as reaction rims surrounding amphibole phyric grains, and as acicular laths surrounding quartz xenocrysts. Amphibole crystals (up to 0.5 mm across) may be altered to biotite, Fe-oxides, or rimmed by cpx. Biotite is altered to Fe-oxides. Quartz xenocrysts (up to 1.0 mm across) anhedral, rounded, embayed and may be surrounded by rare cpx reaction coronas. The rock has a characteristic lack of primary Fe-Ti oxides. Glomerocrysts consist of plagioclase + amphibole, or plagioclase + clinopyroxene + orthopyroxene. The groundmass is composed of small plagioclase microlites (An 45).

Mt8763: Glomeroporphyritic, seriate, amphibole- and biotite-bearing orthopyroxne, quartz, clinopyroxene andesite. T.19N., R.62E., NE 1/4 sec. 29, elevation 7270 feet. Silica content = 63.2%. Phenocrysts:

plagioclase (7.9%), orthopyroxene (4.3%), quartz (4.1%), clinopyroxene (3.4%), amphibole (1.9%), Fe-Ti oxides (0.7%), biotite (0.3%), and accessory zircon and apatite. Plagioclase occurs as subhedral to euhedral crystals up to 3.0 mm across with sieved cores containing abundant melt inclusions (An70) and as fresh, euhedral smaller unzoned crystals (An40). Orthopyroxene occurs as acicular laths (up to 0.9 mm across) and as subhedral to euhedral polyhedra. Acicular crystals may be surrounded by clinopyroxene jackets. Quartz occurs as rounded, embayed crystals up to 3.6 mm across. Clinopyroxene reaction coronas are absent. Clinopyroxene occurs as subhedral polyhedra up to 0.6 mm across, commonly in glomerocrysts with other clinopyroxene crystals or with orthopyroxene, and as smaller acicular laths. Amphibole occurs as acicular laths up to 1.2 mm across, and as smaller subhedral to euhedral polyhedra that may be embayed. All amphibole phenocrysts have thick opacite reaction rims. Biotite occurs as a single euhedral crystal 1.5 mm across. Groundmass microphenocrysts consist of plagioclase + Fe-Ti oxides + orthopyroxene.

Mt872, Mt8711: Glomeroporphyritic, seriate, two-pyroxene-bearing amphibole (biotite) dacite. Mt872: T.19N., R.62E., NE 1/4 sec. 21, elevation 2240 meters. Silica content = 65.8 %. Mt8711: T.19N., R.62E., Nw 1/4 sec. 9, elevation 7885 feet. Silica content =   . Phenocrysts: plagioclase (20.1%), amphibole (3.7%), quartz (3.2%), clinopyroxene (2.1%), orthopyroxene (1.7%), plus accessory zircon and apatite. Mt8711 is more oxidized and contains slightly more amphibole in addition to biotite (approximately 2.0%). Plagioclase phenocrysts form two groups: fresh euhedral megacrysts (up to 2 cm in handspeciman) that are unzoned (An34) and as smaller grains with sieved cores containing abundant melt inclusions (An46) which are surrounded by fresh, reverse, oscillatory zoned overgrowths (An66). Plagioclase also occurs as lath shaped microlites (average approximately 0.2 mm across). Amphibole occurs as oxidized lath shaped phenocrysts (up to 3.0 mm across) which may be pseudomorphing biotite, and as equant grains with hopper crystal morphology, and opacite rims. Clinopyroxene occurs as acicular lath shaped subhedral-anhedral phenocrysts averaging about 0.6 mm across, as subequant crystals (Wo36 En39 Fs29 core to Wo39 En51 Fs10 rim) which may be in crystal

clots with orthopyroxene and plagioclase, as groundmass microlites averaging about 0.2 mm across, as parallel intergrowths with orthopyroxene, and as small acicular crystals in rare reaction coronas surrounding quartz xenocrysts. Orthopyroxene occurs as acicular laths (Wo3 En62 Fs35) up to 1.2 mm across, or as parallel intergrowths with clinopyroxene. Quartz occurs as rounded, embayed xenocrysts rarely surrounded by clinopyroxene reaction coronas.

Mt8786: Vitrophyric, biotite, amphibole rhyodacite. T.18N., R.62E., NE 1/4 sec. 5, elevation 7805 feet. Silica content = 68.1%. Phenocrysts: plagioclase (17.7%), biotite (5.6%), amphibole (4.9%), quartz (2.7%), sanidine (1.4%), orthopyroxene (trace), clinopyroxene (xenocrystic ?), Fe-Ti oxides (< 1.0%) and accessory sphene (up to 0.75 mm), zircon, and apatite. Plagioclase phenocrysts form two groups: as large (up to 2.9 mm across) phenocrysts with calcic (An80) sieved cores containing abundant melt inclusions and which are surrounded by strongly normally zoned, fresh subhedral rims (An56), and as smaller (up to 1.7 mm across) euhedral to subhedral grains with fresh sodic cores (An33) surrounded by oscillatory normally zoned rims (An27). Biotite occurs as bent or broken, euhedral-subhedral books (up to 6.0 mm long) rarely with apatite inclusions, as rare inclusions in plagioclase. Amphibole occurs as large (up to 4.5 mm across) brown (ppl) phenocrysts commonly rimmed by opacite. Biotite and amphibole may occur together in crystal clots. Quartz phenocrysts are rounded and fractured and are not surrounded by clinopyroxene reaction coronas. Sanidine is present as andedral to subhedral unzoned (An0.5 Ab24 Or76) phenocrysts which may contain inclusions of sodic plagioclase (An33). Orthopyroxene (Wo2.7 En63 Fs34) occurs as small (0.7 mm across) lath shaped phenocrysts which may be in glomerocrysts with Fe-Ti oxides. The groundmass is composed of glass and spherulites which commonly radiate from a crystal which forms a common nucleus.

Mt876: Glomeroporphyritic, seriate, amphibole-, orthopyroxene-bearing biotite rhyodacite. T.19N., R.62E., SE 1/4 sec. 16, elevation 2180 meters. Silica content = 70.9%. Phenocrysts: plagioclase (21.6%), biotite (4.3%), amphibole (2.8%), sanidine (2.5%), orthopyroxene (2.1%), quartz (1.3%), clinopyroxene (xenocrystic; 0.9%), Fe-Ti oxides

(<1.0%), and accessory zircon and apatite. Plagioclase phenocrysts form two groups: as large (up to 6 mm across) subhedral grains with calcic (An80-An75) sieved cores containing abundant melt inclusions which are surrounded by fresh, intermediate (An65-An48) normally zoned rims, and as smaller crystals with fresh, sodic cores (An31) and unzoned to slightly reversely zoned rims (An34). Sanidine (Ab21 Or79) phenocrysts are subhedral and range up to 5.0 mm across. Often sanidine crystals contain inclusions of smaller sanidine crystals or inclusions of zircon. Biotite occurs as euhedral books up to 1.9 mm across, and as smaller inclusions in plagioclase. Quartz crystals are extremely rounded, average 1.2 mm across, and are free of clinopyroxene reaction rims. A large (approximately 8.0 mm across) gabbroic xenolith in the center of the investigated thin section consists of plagioclase > orthopyroxene > amphibole > clinopyroxene. Plagioclase crystals in this inclusion are similar in morphology to large plagioclase crystals elsewhere in the section; cores are calcic (An80) and sieved with abundant melt inclusions, and are surrounded by more sodic (An65), clear rims. Amphibole in inclusions are subhedral, up to 2.4 mm across, and extensively oxidized and rimmed by opacite. Clinopyroxene (Wo39 En50 Fs11 core to Wo39 En52 Fs9 rim) in inclusions is anhedral, up to 1.3 mm across, and mainly occurs as a glomerocrystic clot at the center of the inclusion. Clinopyroxene is a rare phenocryst phase outside of the inclusion. The whole rock groundmass is composed of small plagioclase and pyroxene microlites in extensively devitrified glass. Extensive oxidation has imparted a red color to this sample.

Middle Group Rocks

Autoclastic Dacites (map unit Tvml)

__Mt871a__: Vitrophyric, glomeroporphyritic, clinopyroxene-bearing, amphibole, hypersthene, biotite dacite. Clast from block and ash flow. T.19N., R.62E., SE 1/4 sec. 16, elevation 2215 meters. Silica content = 65.7%. Phenocrysts: plagioclase (20.5%), amphibole (3.8%), hypersthene (3.7%), biotite (3.5%), clinopyroxene (1.6%), Fe-Ti oxides (1.2%), quartz (trace), plus accessory apatite and zircon. Plagioclase phenocrysts range up to 3 mm across (average = 0.8 mm) and occur in two groups:

sieved (most common) with rounded edges and as fresh
euhedral grains. Most phenocrysts are present as
broken fragments probably broken during flowage.
Amphibole (largest = 1.0 mm across, average 0.6 mm)
is present in two occurrences: (1) as anhedral
overgrowths on pyroxene (less common), and (2) as
subhedral-euhedral phenocrysts. Phenocrysts are
fresh and commonly contain opaque inclusions. Some
grains may be pitted or skeletal. Most grains are
broken. Hypersthene (largest = 1.0 mm, average 0.7
mm) commonly contains opaque inclusions, and occurs
in glomerocrysts with plagioclase + opaques ±
amphibole. Phenocrysts are subhedral with rounded
edges, and are commonly lath shaped. Biotite
(average = 0.9 mm long) occurs as lath shaped books
with euhedral outlines, although they are commonly
pitted and skeletal. Clinopyroxene (largest = 0.7
mm, average = 0.2 mm) occurs as clusters of small
phenocrysts, rarely with opaques, as isolated
phenocrysts, and as overgrowths on hypersthene.
Opaques usually occur as inclusions in amphibole,
hypersthene, or as isolated crystals.

Mt8712: Vitrophyric, glomeroporphyritic,
hypersthene-, clinopyroxene-bearing, biotite,
amphibole dacite. T.19N., R.62E., NW 1/4 sec. 21,
elevation 2310 meters. Silica content 66.3%.
Phenocrysts: plagioclase (19.6%), biotite (6.4%),
amphibole (4.3%), hypersthene (2.3%), clinopyroxene
(0.7%), Fe-Ti oxides (1.0%), quartz (trace), plus
accessory zircon and apatite. Two populations of
plagioclase: sieved grains with abundant glass
inclusions (An81 core to An64 rim), and fresh
euhedral phenocrysts (An41 core to An60 core).
Biotite occurs as lath shaped, often skeletal, books
and as inclusions in plagioclase. Amphibole is
extremely fresh and commonly forms glomerocrysts with
plagioclase. Hypersthene commonly contains opaque
inclusions and occurs in glomerocrysts with
plagioclase ± amphibole.

Mt8715: Vitrophyric, glomeroporphyritic, biotite-,
amphibole-, two-pyroxene-bearing dacite. T.19N.,
R.62E., NE 1/4 sec. 20, elevation 2225 meters.
Silica content = . Phenocrysts: plagioclase
(15.9%), biotite (2.8%), amphibole (1.6%),
hypersthene (1.5%), Fe-Ti oxides (1.0%), quartz

(trace), clinopyroxene (trace), plus accessory zircon and apatite. Plagioclase phenocrysts (largest = 3.3 mm, average = 1.1 mm) are either extensively sieved (most common) or euhedral and clear. Biotite (largest = 1.7 mm, average = 0.7 mm long) occurs as lath shaped books, commonly with skeletal morphology. Green amphibole (largest = 1.0 mm across, average = 0.6 mm) occurs as euhedral isolated phenocrysts, and as overgrowths on hypersthene phenocrysts. Hypersthene (largest = 1.0 mm across, average = 0.4 mm across) usually occurs as acicular laths, although a few subhedral polyhedra are present. Hypersthene may also occur as inclusions in clear plagioclase phenocrysts.

Mt8717, Mt8734: Vitroclastic, glomeroporphyritic, amphibole-, biotite-, clinopyroxene-bearing, hypersthene dacite. Mt8717: T.19N., R.62E., SE 1/4 sec. 20, elevation 7180 feet. Silica content = 65.7%. Mt8734: T.19N., R.62E., NE 1/4 sec. 20, elevation 2280 meters. Silica content = 66.2%. Phenocrysts: plagioclase (24.8%), hypersthene (3.4%), biotite (2.9%), amphibole (2.9%), clinopyroxene (1.2%), Fe-Ti oxides (1.2%), quartz (trace), plus accessory zircon and apatite. Plagioclase (largest = 4.0 mm across, average =0.3 mm across) commonly occurs as anhedral phenocrysts with extensively sieved cores filled with brown glass inclusions. A smaller population of grains have fresh cores, although the edges of the crystals may be rounded. Hypersthene (largest = 0.7 mm, average = 0.2 mm) usually occurs in glomerocrysts with plagioclase and clinopyroxene. Commonly phenocrysts contain opaque inclusions. In glomerocrysts hypersthene is anhedral. A few lath shaped, isolated phenocrysts are also present. Hypersthene may also be surrounding clinopyroxene phenocrysts. Green amphibole (largest = 2.0 mm, average 0.2 mm) occurs as broken subhedral to anhedral phenocrysts often replaced by minute grains of Fe-Ti oxides. Many crystals are rounded laths; some are embayed or pitted. Biotite phenocrysts are crudely flow aligned and are often pitted and altered to opaques. Opaques mainly occur in glomerocrysts with hypersthene and plagioclase, or as inclusions in hypersthene.

Smokey Quartz-Bearing Rhyodacites (map unit Tvm2)

Mt8720: Hypocrystalline, two-pyroxene-bearing, amphibole, biotite rhyodacite. T.19N., R.62E., NE 1/4

sec. 20, elevation 2260 meters. Silica content 68.5%. Phenocrysts: plagioclase (11.8%), biotite (4.7%), amphibole (3.2%), hypersthene (2.5%), clinopyroxene (0.5%), quartz (0.2%), sanidine (trace), plus accessory zircon and apatite. This rock is extensively oxidized; biotite and amphibole are completely altered to Fe-oxides. In addition, the matrix contain abundant carbonates. Plagioclase occurs as phenocrysts with sieved cores and complex, reverse oscillatory zoning (An20 core to An35 rim), and as a smaller subset of clear, unzoned (An35) subhedral phenocrysts. Some fresh phenocrysts contain inclusions of apatite. Glomerocrysts with amphibole are common. Hypersthene occurs as small (average = 0.2 mm across) isolated phenocrysts, and as replacement rims surrounding rare clinopyroxene phenocrysts. Quartz may be unusually large (as large as 5 mm across), abundant, and exceptionally dense black in color. Most grains are extensively rounded.

Glomeroporphyritic Dacites (map unit Tvm3)

Mt8743, Mt8737, Mt8778: Glomeroporphyritic, two-pyroxene-, biotite-, amphibole-bearing dacite. Mt8743: T.19N., R.62E., NW 1/4 sec. 20, elevation 2315 meters. Silica content = 67.2%. Mt8737: T.19N., R62E., NE 1/4 sec. 18, elevation 2050 meters. Silica content = 67.2%. Mt8778: T.19N., R.61E., NE 1/4 sec. 35, elevation 7480 feet. Silica content 67.7%. Phenocrysts: plagioclase (15.2%), hypersthene (2.1%), biotite (0.9%), amphibole (0.8%), Fe-Ti oxides (0.5%), clinopyroxene (0.2%), quartz (trace), plus accessory zircon and apatite. This lithology contains conspicuous and abundant glomerocrysts of opx + plagioclase + opaques, plus less common glomerocrysts of amphibole + plagioclase, and opx + cpx + plagioclase + opaques. Plagioclase occurs as phenocrysts (as large as 4.0 mm across, An50) with sieved cores containing abundant brown glass melt inclusions, or as clear, subhedral to euhedral and reversely zoned (An44 to An58) crystals. Biotite occurs as strongly oxidized lath shaped books as large as 1.0 mm across. Hypersthene phenocrysts (as large as 1.8 mm across) are commonly oxidized to Fe-oxides on rims, are euhedral, and may be enclosed by plagioclase. Amphibole occurs as large (up to 3.1

mm across) subhedral phenocrysts extensively oxidized to minute grains of opaque oxides. The groundmass consists of extensively devitrified glass, often spherulitic, and with minor microlites of plagioclase and orthopyroxene.

Late Group

Lower Dacites (map unit Tvl1)

Mt8814, Mt8810, Mt8781, Mt8812: Porphyritic, hyaloplilitic, two-pyroxene, amphibole-bearing dacite. Mt8714: T.18N., R.61E., NE 1/4 sec. 24, elevation 7725 feet. Silica content = . Mt8810: T.18N., R.61E., SW 1/4 sec. 13, elevation 8420 feet. Silica content = . Mt8781: T.18N., R.61E., NE 1/4 sec. 14, elevation 7845 feet. Silica content = 66.0%. Mt8812: T.18N., R.61E., SW 1/4 sec. 13, elevation 8520 feet. Silica content = . Phenocrysts: plagioclase (4.7%), biotite (1.3%), clinopyroxene (0.9%), Fe-Ti oxides (0.9%), amphibole (0.3%), orthopyroxene (0.3%), quartz (trace), plus accessory zircon. Plagioclase phenocrysts (largest = 2.2 mm across), are commonly clear and euhedral to subhedral, although a few sieved phenocrysts are present. Largest crystals are normally zoned An55 to An45. Biotite phenocrysts are in flow alignment and are oxidized to minute grains of Fe-oxides. The largest grains are up to 2.1 mm across. Clinopyroxene phenocrysts (0.3 to 0.4 mm across) have foggy rims and appear to be in reaction with the host liquid although they retain their euhedral outlines. Amphibole phenocrysts are as large as 0.4 mm across and have thick opacite rims. A few glomerocrysts (aggregate size = 1.0 mm across) of plagioclase + opaques + clinopyroxene are present. The groundmass consists of microlites of plagioclase + opaques in a glassy, partially devitrified matrix.

Aphyric Andesites (map unit Tvl2)

Mt8764, Tf872, Mt888: Sparsely porphyritic, pilotaxitic, two-pyroxene-bearing andesite. Mt8764: T.19N., R.62E., SW 1/4 sec. 33, elevation 7565 feet. Silica content = 58.0%. Tf872: T.18N., R.61E., SE 1/4 sec. 9, elevation 7485 feet. Silica content = 58.4%. Mt888: T.18N., R.61E., NE 1/4 sec. 26, elevation 7805 feet. Silica content = . Phenocrysts: plagioclase (0.4%), orthopyroxene

(0.1%), clinopyroxene (0.1%), olivine (trace), quartz (trace). Plagioclase (largest = 1.5 mm across) occurs as lath shaped, subhedral to euhedral phyric grains, although some crystals may have ragged or rounded edges. Another population of plagioclase crystals are extensively sieved. Clinopyroxene (average size = 0.2 mm across) occurs as subhedral polyhedra or as lath shaped phyric grains with rounded edges. Clinopyroxene may be in small crystal clots with other clinopyroxene crystals. Orthopyroxene (average size = 0.3 mm across) occurs as lath-shaped phenocrysts with rounded edges. Opaques are rarely present as phyric grains and are lath shaped. The groundmass is composed of pilotaxitic plagioclase microlites with abundant interstitial opaque microphenocrysts. Olivine occurs as rare, extremely rounded phenocrysts.

Mt8759: Vesicular, microcrystalline, intergranular with minor diktytaxitic voids, clinopyroxene-bearing, olivine andesite dike. T.19N., R.62E., SW 1/4 sec. 21, elevation 7505 feet. Silica content = 57.3%. Microphenocrysts: plagioclase (approximately 30%), olivine (approximately 15%), clinopyroxene (approximately 8%). The principle microphenocryst phase is plagioclase (An55) which occurs as highly elongate laths in flow alignment. Minor normal oscillatory zoning occurs in some grains. Olivine occurs as highly elongate laths and as less common grains only slightly elongated along C. The highly elongate laths are subhedral, and may be skeletal, but they do not appear to be resorbed; their lack of perfect form appears due to quick growth at the ends of the crystals. Most grains have cores altered to iddingsite. Augite occurs as rare phyric grains (0.7 mm across) and as a groundmass phase subordinate in volume to olivine, but there is not a continuous range of sizes between the two occurrences. Phyric grains are subhedral to euhedral. The groundmass clinopyroxene occurs as andedral grains.

Upper Rhyodacites (map unit Tvl3)

Mt8813: Porphyritic, hypohaline, amphibole-, two-pyroxene-, biotite-bearing rhyodacite. T.18N., R.62E., NW 1/4 sec. 19, elevation 7640 feet. Silica content = . Phenocrysts: plagioclase (8.8%),

amphibole (1.1%), clinopyroxene (0.9%), Fe-Ti oxides (0.8%), orthopyroxene (0.7%), biotite (0.3%), plus accessory apatite. Glomerocrysts of plagioclase + clinopyroxene + opaques (most common); plagioclase + orthopyroxene + opaques; and plagioclase + orthopyroxene + amphibole. Plagioclase is present in three occurrences: (1) as clear euhedral phyric grains (unzoned An55) up to 3 mm across (average = 1.2 mm); (2) as phenocrysts with sieved cores containing brown glass inclusions; and (3) as groundmass microlites. Amphibole occurs as subhedral to euhedral phenocrysts up to 1.8 mm across which are commonly replaced by a minute aggregate of Fe-Ti oxides. Clinopyroxene phyric grains (up to 1.0 mm across) are commonly euhedral to subhedral, although their rims are foggy and appear to be reacting with the host liquid. Biotite (up to 3.0 mm across, average = 0.9 mm across) commonly has a skeletal, embayed morphology, and is replaced by minute grains of Fe-Ti oxides. Apatite occurs as isolated microphenocrysts and as inclusions in plagioclase. The groundmass is composed of brown glass plus Fe-Ti oxides microphenocrysts plus plagioclase microlites.

<u>Mt8765</u>: Vitrophyric, two-pyroxene-bearing, biotite rhyodacite. Basal vitrophyre from thick section of Tv13. T.19N., R.62E., NW 1/4 sec. 33, elevation 7805 feet. Silica content = 69.6%. Phenocrysts: plagioclase (9.0%), biotite (3.8%), clinopyroxene (0.3%)., orthopyroxene (0.1%), Fe-Ti oxides (trace), plus accessory and rare zircon. Most plagioclase phyric grains are euhedral and clear (average size is 1.0 mm across) and may be strongly normally zoned (An74 core to An40 rim). A distinct population of plagioclase phyric grains are larger (up to 2.5 mm across) and have reversely zoned, sieved cores with abundant brown glass melt inclusions (An53 to An74) which are mantled by clear subhedral normally zoned, clear overgrowths (An44). Biotite occurs as euhedral books up to 2.9 mm across (average = 1.1 mm) which are often intergrown with plagioclase phenocrysts. Clinopyroxene occurs either as elongate prisms (up to 0.8 mm across) or as euhedral octahedrons. Glomerocrysts of plagioclase + clinopyroxene + Fe-Ti oxides and plagioclase + Fe-Ti oxides are present. The groundmass is composed of clear glass plus minor plagioclase + biotite + Fe-Ti oxide microlites.

<u>Mt8791b, Mt8791c, Mt8791d, Mt8775</u>: Porphyritic, pilotaxitic, two-pyroxene-bearing, biotite

rhyodacite. Mt8791b: T.18N., R.61E., SE 1/4 sec. 2, elevation 8045 feet. Silica content = 69.7%. Mt8791c: T.18N., R.61E., SE 1/4 sec. 2, elevation 8120 feet. Silica content 69.2%. Mt8791d: T.18N., R.61E., SE 1/4 sec. 2, elevation 8200 feet. Silica content = 69.0%. Mt8775: T.19N., R.61E., NE 1/4 sec. 35, elevation 7625 feet. Silica content + 68.3%. Phenocrysts: plagioclase (10.5%), biotite (4.7%), clinopyroxene (0.5%), Fe-Ti oxides (0.3%), orthopyroxene (trace), plus accessory apatite and zircon. Plagioclase phenocrysts (up to 2.5 mm across) occurs as fresh grains that are slightly normally zoned (An30 core to An 25 rim ?) and as phyric grains with oscillatory zoned, sieved calcic cores (An60) that as mantled by clear sodic overgrowths (An40 ?). The calcic cores are altered to minor sericite. Biotite occurs as euhedral books that are up to 2.4 mm across and which are variably altered to minute grains of Fe-Ti oxides. Clinopyroxene phenocrysts (up to 1.5 mm across) are subhedral and mainly occur in glomeroporphyritic clots with plagioclase + Fe-Ti oxides ± orthopyroxene. Clinopyroxene may be rimmed by orthopyroxene. Many clinopyroxene phyric grains have foggy rims and appear to be in reaction with the enclosing liquid. The groundmass is composed of extensively devitrified glass + plagioclase + Fe-Ti oxide microlites.

APPENDIX II: Magma Mixing and Crystal
Fractionation Calculations

This section contains the results of the best-fit
petrogenetic models for lavas of the Egan Range volcanic
complex. Trace-element contents were calculated using the
program MAGMA86. Major-element contents were calculated
using the Basic program IGPET II. In models requiring
crystal fractionation in addition to magma mixing,
crystals were removed from endmembers prior to mixing.
Distribution coefficients used in fractionation steps are
given in Table 9. Mineral compositions used were
determined by electron microprobe and are given in Tables
3-6. All fractionation models assume Rayleigh
fractionation.

Appendix II

Petrogenetic mixing models for Egan Range volcanic rocks

Table A: Early Group

Sample:	Mt879		Mt8787		Mt8789		Mt8760	
Mafic endmember:	Mt8749		Mt8749		Mt8749		Mt8749	
% in mixture:	83		65		65		60	
Silicic endmember:	Mt8786		Mt8786		Mt8786		Mt8786	
% in mixture:	17		35		35		40	
% cpx fractionated:	--		--		3.5		2.5	
% apatite fractionated:	--		0.65		--		--	
*F:	1.0		.9935		0.9650		0.9750	
	Observed	Estimated	Observed	Estimated	Observed	Estimated	Observed	Estimated
SiO2	56.6	56.5	59.6	58.9	59.9	59.3	61.4	61.4
Al2O3	15.4	15.4	15.0	15.4	16.0	15.8	15.8	15.8
FeO*	7.6	8.1	6.5	7.1	6.3	7.0	6.1	6.0
MgO	5.4	5.5	4.9	4.5	3.9	4.1	3.2	3.3
CaO	8.4	7.9	7.1	6.5	6.4	6.3	5.9	6.0
Na2O	2.1	2.2	2.3	2.3	2.5	2.4	2.7	2.5
K2O	2.9	3.1	3.4	3.2	3.6	3.5	3.7	3.7
TiO2	1.1	1.1	0.88	0.98	0.93	0.99	0.85	0.89
MnO	0.13	0.14	0.12	0.12	0.11	0.12	0.10	0.10
P2O5	0.31	0.38	0.28	0.13	0.30	0.35	0.36	0.35
SSR:		0.57		1.06		0.66		0.07
Rb	94	99	112	118	130	122	123	126
Sr	574	529	507	491	551	516	490	503
Ba	1328	1308	1237	1294	1299	1332	1242	1312
La	41.2	47.4	44.8	44.9	53.3	55.0	56.0	56.1
Ce	81	91	89	87	104	107	113	109
Nd	38	36	35	32	41	39	44	39
Sm	6.9	7.8	7.1	6.4	7.7	8.1	8.0	8.1
Eu	1.8	1.8	1.6	1.5	1.7	1.8	1.6	1.7
Tb	0.9	1.0	0.8	0.9	0.8	0.9	0.9	0.92
Yb	2.7	2.9	2.5	2.5	2.7	2.8	2.8	2.8
Lu	0.37	0.41	0.35	0.34	0.35	0.38	0.36	0.37
Hf	5.6	5.6	6.0	5.8	6.1	5.9	6.1	5.9
Th	11	13	14	17	17	18	21	19
Zr	210	206	202	211	225	215	223	214
Sc	21.5	22.5	20.3	19.1	15.5	14.8	14.6	14.6
Cr	283	236	192	187	64	69	88	83
Co	24	25	23	21	18	19	15	18

SSR is the sum of the square of the residuals

Composition of apatite from Deer et al. (1962)

*F = Mass magma/mass original magma

Table A: continued

Sample:	Mt8763		Mt8711	
Mafic endmember:	Mt879		Mt879	
% in mixture:	55		65	
Silicic endmember:	Mt8786		Mt8786	
% in mixture:	45		35	
% cpx fractionated:	--		2.5	
% apatite fractionated:	0.23		0.3	
F:	0.9977		0.9720	
	Observed	Estimated	Observed	Estimated
SiO2	63.2	62.0	63.6	60.8
Al2O3	15.1	15.4	15.7	15.7
FeO*	5.4	5.8	5.6	6.2
MgO	3.3	3.4	2.1	3.5
CaO	5.7	6.0	5.2	6.0
Na2O	2.6	2.5	2.8	2.4
K2O	3.5	3.8	3.8	3.6
TiO2	0.79	0.86	0.83	0.92
MnO	0.09	0.10	0.10	0.10
P2O5	0.25	0.19	0.26	0.14
SSR:		0.72		5.14
Rb	123	136	137	139
Sr	475	491	442	500
Ba	1167	1209	1079	1240
La	52.9	52.8	52.7	52.7
Ce	105	105	104	104
Nd	42	39	37	38
Sm	7.8	7.1	7.4	6.9
Eu	1.6	1.6	1.6	1.5
Tb	1.0	0.8	1.0	0.8
Yb	2.9	2.5	2.6	2.5
Lu	0.38	0.32	0.35	0.31
Hf	6.2	6.0	6.2	6.1
Th	19	20	18	21
Zr	212	220	226	221
Sc	14.9	14.8	13.1	12.0
Cr	160	160	75	77
Co	15	16	15	15

Appendix II
Table 8: Middle Group

	Ave. Tvm1*		Ave. Tvm3*		Mt8720	
Sample:						
Mafic endmember:	Mt8763		Mt871a		..	
% in mixture:	49		44		..	
Silicic endmember:	Mt8720		Mt8720		Mt8786	
% in mixture:	51		56		100	
% cpx fractionated:	4.0		..		1.7	
% plagioclase fractionated:	..		..		1.3	
% oxide fractionated:	..		..		0.1	
F:	0.96		1.0		0.986	
	Observed	Estimated	Observed	Estimated	Observed	Estimated
SiO2	66.1	66.3	67.1	67.1	68.5	68.6
Al2O3	16.0	15.8	15.7	15.7	15.5	15.5
FeO*	4.2	4.2	4.0	3.9	3.5	3.5
MgO	1.3	1.5	1.1	1.1	0.8	0.8
CaO	3.8	3.5	3.2	3.3	2.7	2.7
Na2O	3.1	3.0	3.3	3.1	3.3	3.1
K2O	4.5	4.3	4.8	4.8	4.8	4.9
TiO2	0.66	0.68	0.62	0.59	0.54	0.52
MnO	0.07	0.08	0.05	0.06	0.06	0.06
P2O5	0.22	0.23	0.21	0.20	0.20	0.23
SSR:		0.20		0.06		0.08
Rb	164	149	176	162	162	191
Sr	419	406	367	368	321	342
Ba	1223	1235	1268	1213	1217	1241
La	65.2	63.4	67.0	68.7	72.4	75.9
Ce	125	128	133	131	145	153
Nd	45	43	48	45	43	46
Sm	8.2	7.8	8.2	8.2	8.2	9.0
Eu	1.5	1.5	1.4	1.4	1.4	1.4
Tb	0.8	0.8	0.8	0.8	0.8	0.8
Yb	2.7	2.8	2.6	2.8	2.8	2.5
Lu	0.32	0.34	0.31	0.30	0.30	0.29
Hf	6.5	6.4	6.5	6.3	6.3	6.6
Th	28	29	30	33	37	33
Zr	227	234	231	226	230	236
Sc	8.6	8.9	7.3	6.7	5.6	3.2
Cr	11	11	10	10	8	3
Co	8.5	8.6	7.2	7.1	6.0	3.4

* is average composition of map units Tvm1 and Tvm3
Oxide composition from Grunder (1988).

Appendix II
Table C: Late Group

	Mt8759		Mt8781		Mt8775	
Sample:						
Mafic endmember:	Mt8749		Tf872		Mt8781	
% in mixture	..		..		..	
Silicic endmember:	..		..		..	
% in mixture	..		..		..	
% cpx fractionated:	10.0		3.6		1.4	
% plagioclase fractionated:	7.7		12.9		8.0	
% amphibole fractionated:	..		9.6		..	
% biotite fractionated:	..		..		3.6	
% oxide fractionated:	2.5		3.7		0.2	
% olivine fractionated:	3.5		..		..	
F:	0.763		0.702		0.868	
	Observed	Estimated	Observed	Estimated	Observed	Estimated
SiO_2	57.3	57.2	66.0	66.0	68.3	68.3
Al_2O_3	16.5	16.5	16.5	16.5	15.8	15.8
FeO^*	7.8	7.8	4.1	4.1	3.3	3.3
MgO	3.8	3.8	0.9	0.9	0.5	0.4
CaO	7.2	7.2	3.2	3.2	2.5	2.6
Na_2O	2.6	2.4	3.4	3.6	3.5	3.4
K_2O	3.1	3.4	5.1	5.0	5.3	5.4
TiO_2	1.18	1.18	0.70	0.70	0.51	0.63
MnO	0.11	0.11	0.04	0.04	0.07	0.07
SSR:		0.14		0.05		0.05
Rb	110	104	214	191	216	208
Sr	530	563	459	478	347	347
Ba	1219	1658	1520	1637	1346	1155
La	49.0	51.3	58.5	6.3	69.1	63.5
Ce	107	97	116	122	142	128
Nd	49	40	44	42	42	48
Sm	8.7	8.3	8.1	7.6	8.4	8.9
Eu	2.0	1.9	1.7	1.6	1.6	1.1
Tb	1.1	1.0	0.8	0.8	0.9	0.4
Yb	3.6	3.3	2.9	2.6	3.3	3.2
Lu	0.50	0.47	0.40	0.37	0.43	0.43
Hf	7.2	6.6	7.0	6.9	8.4	7.7
Th	13	12	23	19	30	26
Zr	273	273	251	252	290	274

Appendix II
Table C: Late Group continued

Sample:	Mt8775		Mt8791d	
Mafic endmember:	Mt8781		Mt8781	
% in mixture:	35.8		21.9	
Silicic endmember:	Mt8765		Mt8765	
% in mixture:	64.2		78.2	
% cpx fractionated:	..		..	
% plagioclase fractionated:	..		..	
% amphibole fractionated:	..		..	
% biotite fractionated:	..		..	
% oxide fractionated:	..		..	
% olivine fractionated:	..		..	
F:	1.0		1.0	
	Observed	Estimated	Observed	Estimated
SiO_2	68.3	68.3	69.0	69.0
Al_2O_3	15.8	15.8	15.6	15.6
FeO^*	3.3	3.3	3.2	3.2
MgO	0.5	0.6	0.5	0.6
CaO	2.5	2.6	2.3	2.4
Na_2O	3.5	3.2	3.4	3.1
K_2O	5.3	5.4	5.3	5.4
TiO_2	0.51	0.51	0.49	0.49
MnO	0.07	0.07	0.07	0.07
SSR:		0.14		0.14
Rb	216	220	224	221
Sr	347	351	316	328
Ba	1346	1351	1320	1314
La	69.1	69.7	71.3	72.1
Ce	142	137	143	142
Nd	42	46	54	47
Sm	8.4	8.9	8.9	9.1
Eu	1.6	1.5	1.5	1.5
Tb	0.9	0.9	1.0	1.0
Yb	3.3	3.5	3.5	3.6
Lu	0.43	0.43	0.47	0.44
Hf	8.4	7.8	8.4	8.0
Th	30	30	30	31
Zr	290	274	285	280

Appendix III: Supplemental Rare-Earth
Element Analyses

     This section contains rare-earth element analyses of
samples for which major-element analyses were unavailable
at the time of writing.

Appendix III

Sample #	Mt8816a	Mt8819a	Mt8819	Mt8826	Mt8832	Mt8814	Mt8810	Mt8812	Mt888	Mt8813
Strat. Unit	Tves	Tvel	Tvel	Tkt	Tkt	Tvl1	Tvl1	Tvl1	Tvl2	TVl3
Rock type	Rl	Mi	Al	Df	Df	Dl	Dl	Dl	Al	Dl
La	35.9	42.2	58.7	70.9	68.5	60.2	57.3	57.1	54.9	66.1
Ce	70	83	114	135	130	115	114	116	110	126
Nd	31	41	45	46	39	47	43	47	47	45
Sm	5.8	7.8	8.4	7.9	7.3	8.6	8.3	8.2	8.5	8.6
Eu	1.0	1.8	1.6	1.3	1.1	1.7	1.7	1.7	2.1	1.6
Tb	<0.2	1.0	<0.3	1.0	0.7	0.9	0.9	0.9	1.0	0.9
Yb	1.8	2.8	2.7	2.8	2.6	2.9	3.0	2.8	3.0	3.5
Lu	0.01	0.42	0.36	0.35	0.35	0.36	0.43	0.39	0.47	0.43

Rock types: Al = andesite lava, Dl = dacite lava, Rl = rhyolite lava, Df = dacite fiamme, Mi = magmatic inclusion